Characterization and paragenesis of nordite-group minerals from the Ilímaussaq alkaline complex, South Greenland

Emil Holtung Gulbransen

Master Thesis in Geosciences

Study programme: Mineralogy, Petrology and Geochemistry

60 credits

Natural History Museum

Department of Geosciences

Faculty of Mathematics and Natural Sciences

University of Oslo

15/06/2020

Supervisors: Henrik Friis (Natural History Museum, University of Oslo)

Muriel Marie Laure Erambert (Department of Geosciences, University of Oslo)

This work is published digitally through DUO – Digitale Utgivelser ved UiO

http://www.duo.uio.no

It is also catalogued in BIBSYS (https://www.bibsys.no/english)

Acknowledgment

First and foremost, I would like to express my deepest appreciation to my main supervisor Henrik Friis. Thank you for letting me have a peak into your world of mineralogy. Without your knowledge and support, this project would not have been possible. Ever since the mineralogy course during the bachelor you have shown me an area of expertise unlike any other. I am deeply grateful for your invaluable contribution to my thesis.

I would like to extend my gratitude to Muriel Marie Laure Erambert, for helping me with the chemical analysis of nordite and its accessory minerals. Furthermore, our discussions on the uncertainties and problems in the chemical data produced were valuable.

Tekna deserved a big thank you for granting me funding so I was able to go on the fieldtrip to Ilímaussaq Alkaline Complex, South Greenland. The thanks is extended to Salahalldin Akhavan for the making of thin sections and Magnus Kristoffersen for help on the ICPMS.

I would also like to thank Fabrice Dal Bo and Nanna Rosing-Schow for inspiration, help and laughs during the writing of this thesis. In addition, Nelia Castro and Hans Arne Nakrem deserves a thanks for the help along the way.

Moreover, I thank my friends and fellow students who I have met during these two years. Juan, thank you for the good times. Markus, thank you for all the long days at Økern and "Kursrommet". There have been discussions, frustrations, laughter and joy in these two years together, but we made it in the end, and I am grateful for all the moments we shared.

Last but not least, I would like to thank my mother and father for their support and motivation along the way. Thank you Ingrid for always being there for me, I appreciate you every day.

Abstract

This thesis uses chemical and X-ray data to explore the composition and crystal-structure of nordite-group minerals from the two localities Igdlutalik Island and Taseq slope in Ilímaussaq Alkaline Complex in South Greenland.

The nordite-group is a complex rare-earth silicate with the general formula of $A_2BXYZT_6O_{17}$ and consists of five approved species all of which have first been described from the alkaline complexes of the Kola Peninsula, Russia. From the Ilímaussaq Alkaline Complex, nordite-(Ce) has been described from a trachytic dyke on the island of Igdlutalik, and I suggest how nordite could have formed in this low alkaline system. The Igdlutalik nordite forms 20 µm - 100 µm euhedral crystals sparsely distributed in an aegirine and albite matrix. The mineral is homogeneous with the ideal formula of $Na_3SrCeZnSi_6O_{17}$. The crystal structure was refinement in *Pcca* to $R_1 = 0.0158$, with a unit cell of $a = 14.3891(2)$, $b = 5.1799(1)$, $c = 19.7554(2)$ Å and $V = 1472.44(3)$ Å^3.

At a new occurrence on the Taseq nordite is associated with ussingite, i.e. highly agpaitic conditions, as it is the case from most of the Kola occurrences. The Taseq nordite forms concentric circles growing from a chemical distinct Nd-rich core, forming clusters up to 5 mm in the ussingite matrix. The Taseq nordite is heterogeneous and displays sector zoning. The different zones are either Ba or Sr dominated, which has not previously been described in nordites. The ideal formula is $Na_3BaCeZnSi_6O_{17}$. The crystal structure was refinement in *Pcca* to $R_1 = 0.0246$, with a unit cell of $a = 14.5596(4)$, $b = 5.2213(1)$, $c = 19.8270(4)$ and $V = 1507.25(3)$ Å^3.

Overall, the *X*-site in the structure is dominated by Ba, which reflected in the chemical analysis. This means that the Taseq nordite is a new mineral to the world and the Ba-equivalent to nordite-(Ce) with the ideal formula of $Na_3BaCeZnSi_6O_{17}$.

Since the nordite-group already have a prefix and suffix determined by the *Z*-site and *Y*-site, respectively, a new root name is required. Illoq is the Greenlandic word for cousin and would describe the Ba-bearing nordites chemical relation to the other group members. Therefore, the new mineral from Taseq is suggested to be named illoqite-(Ce).

Glossary

NHM	Natural History Museum – Oslo, Norway
REE	Rare Earth Elements (Lanthanides)
LREE	Light Rare Earth Elements (La-Eu)
HREE	Heavy Rare Earth Elements (Gd-Lu)
HFSE	High Field Strength Elements
SXRD	Single Crystal Diffraction
PXRD	Powder X-ray Diffraction
SEM	Scanning Electron Microscope
EPMA	Electron Probe Micro-Analyzer
LA-ICP-MS	Laser Ablation Iductively Coupled Plasma Mass Spectrometry
Peralkaline	Rocks that are oversaturated with alkalies ($Na_2O + K_2O$), and thus undersaturated in respect to Al_2O_3. $Al_2O_3 < (Na_2O + K_2O)$.
Agpaitic	Peralkaline rocks with HFSE such as Zr and Ti that accommodates into complex minerals such as rinkite and eudialyte.
Hyperagpaitic	Highly alkaline minerals such as ussingite and naujakasite crystallize instead of feldspars and feldspathoids.
Miaskitic	Non-agpaitic peralkaline rocks, distinguished by HFSE entering less complex minerals such as titanite or zircon.

Table of content

1. List of minerals mentioned in the text

Mineral	Abbreviation	Chemical Formula	Reference
Tectosilicate			
Tugtupite	Tug	$Na_4BeAlSi_4O_{12}Cl$	1
Sodalite	Sod	$Na_8(Al_6Si_6O_{24})Cl_2$	1
Ussingite	Uss	$Na_2AlSi_3O_8OH$	1
Nepheline	Ne	$Na_3K(Al_4Si_4O_{16})$	1
Albite	Alb	$Na(AlSi_3O_8)$	1
Alkali feldspar	Afs	$(Na,K)AlSi_3O_8$	1
Analcime	Anl	Na(AlSi2O6)·H2O	1
Inoslilicate			
Nordite-group	Nor	$A_2BXYZT_6O_{17}$	2
Narsarsukite	Nar	$Na_4(Ti,Fe)_2(Si_8O_{20})(O,OH,F)_2$	1
Emeleusite	Eme	$Li_2Na_4Fe_2Si_{12}O_{30}$	1
Arvedsonite	Arf	$(Na)(Na_2)(Fe^{2+}{}_4Fe^{3+})Si_8O_{22}(OH)_2$	1
Aegerine	Aeg	$NaFe^{3+}Si_2O_6$	1
Riebeckite	Rie	$\square(Na_2)(Fe^{2+}{}_3Fe^{3+}{}_{2)}Si_8O_{22}(OH)_2$	1
Pectolite	Pec	$NaCa_2Si_3O_8(OH)$	1
Meieranite	Mei	$Na_2Sr_3MgSi_6O_{17}$	1
Lorenzenite	Lor	$Na_2Ti_2(Si_2O_6)O_3$	1
Chkalovite	Chk	$Na_2BeSi_2O_6$	1
Cyclosilicate			
Ilímaussite-(Ce)	Ilí	$(Na,K)_{7-8}(Ba,K)_{10}Ce_5(Nb,Ti)_6(Si_3O_9)_4(Si_9O_{18})O_6(O,OH)_{24}$	1
Lovozerite	Lov	$Na_2Ca(Zr,Ti)(Si_6O_{12})((OH)_4O_2)\cdot H_2O$	1
Steenstrupine-(Ce)	Ste	$Na_{14}Ce_6Mn_2Fe_2(Zr,\ Th)(PO_4)_7(Si_6O_{18})_2(OH)_{23}H_2O$	1
Eudialyte	Eud	$Na_{15}Ca_6(Fe^{2+},Mn^{2+})_3Zr_3(Si_{25}O_{73})(O,OH,H_2O)_3(OH,Cl)_2$	1
Taseqite	Tas	$Na_{12}Sr_3Ca_6Fe_3Zr_3NbSi_{25}O_{73}(O,OH,H_2O)_3Cl_2$	1
Phyllosilicate			
Natrosilite	Nat	$Na_2Si_2O_5$	1
Naujakasite	Nau	$(Na,K)_6(Fe^{2+},Mn^{2+},Ca)(Al,Fe)_4Si_8O_{26}$	1
Biotite	Bt	$K(Fe^{2+},Mg)_2(Al,Fe^{3+},Mg)(Si,Al)(Si_2O_{10})(OH,F)_2$	1
Lalondeite	Lal	$(Na,\ Ca)_6(Ca,\ Na)_3Si_{16}O_{38}(F,OH)_2\ 3H_2O$	1
Ussingite	Uss	$Na_2AlSi_3O_8OH$	1
Neptunite	Nep	$KNa_2LiFe^{2+}{}_2Ti_2Si_8O_{24}$	1
Polylithionite	Pol	$KLi_2AlSi_4O_{10}F_2$	1
Nesosilicate			

Zircon	Zrc	$Zr(SiO_4)$	1
Titanite	Tit	$CaTi(SiO_4)O$	1
Sorosilicates			
Epistolite	Epi	$Na_2(Nb,Ti)_2(Si_2O_7)O_2\ nH_2O$	1
REE			
Britholite-(Ce)	Brt	(Ca, Ce)5(SiO4, PO4)3(OH, F)	1
Ancylite-(Ce)	Anc	$CeSr(CO_3)_2(OH) \cdot H_2O$	1
Rinkite	Rnk	$Na_2Ca_4REE(Ti, Nb)(Si_2O_7)_2(O, F)_4$	1
Vitusite-(Ce)	Vit	$Na_3REE(PO_4)_2$	1
Monazite-group	Mon	MTO_4 , where M = REE, Th, Ca, Bi; T = P, As	1
Diversilite-(Ce)	Div	$Na_2Ba_6Ce_2Fe^{2+}Ti_3Si_{12}O_{36}(OH)_{10}\ nH_2O$	1
Oxide			
Lueshite	Lue	$NaNbO_3$	1
Hematite	Hem	Fe_2O_3	1
Uraninite	Ura	UO_2	1
Carbonate			
Calcite	Cal	$CaCO_3$	1
Dolomite	Dol	$CaMg(CO_3)_2$	1
Halides			
Villiaumite	Vil	NaF	1
Fluorite	Flu	CaF_2	1

1: Mindat (https://www.mindat.org/). 2:This study.

2. Introduction

In a world gradually becoming more dependent on the earth's natural resources, the search for alternative and unconventional occurrences becomes increasingly important. Rare Earth Elements (REE) are being used in modern technologies such as the LED-screens on smartphones, magnets for windmills and batteries for electric cars. These technologies fall under the Norwegian government's plan of a "Green shift", which is an ambition striving towards more environmental friendly and resource efficient technologies. Alkaline complexes, such as the Ilímaussaq complex in Southern Greenland, are some of the few places on earth you have deposits of REE.

China is the main producer of REE, both now and historically. Today they have an estimated global supply of 70% of the raw critical materials produced in the world (Gislev & Grohol, 2018). In addition, Kingsnorth (2016) and Mancheri *et al.* (2019) have reported that 40-50% of Chinas rare earth production is illegal. This is exemplified by Chinas reported export of REEs in 2011 to have been 16,860 tons, while trade partners reported a total import of 37,615 tons of REE from China.

The illegal industry is not the only issue with having China as the main REE producer. In 2015 the BBC reported: "it could be argued that Chinas dominance of the rare earth market is less about geology and far more about the country's willingness to take an environmental hit that other nations shy away from" (Maughan, 2015). Due to China's standards, or lack thereof, when it comes to the environmental aspect of REE production, the companies can produce at a lower cost and in larger quantities than other countries. This is mainly due to the fact that there is no direct involvement of a government-apparatus to oversee the emissions from this industry (Mancheri *et al.*, 2019).

These are some of the reasons why the search for new methods of extraction and new deposits, especially in the West, has been blossoming since 2009. In Norway, because of a growing desire to move away from the conventional petroleum industry, it is possible that the REE industry may be one of the industries that can be viable as an option alongside others to substitute for the oil and gas industries. It is therefore crucial that these resources are being researched for both method of extraction and potential feasible deposits as well as Norway to build up the knowledge for all parts of the value chain for REE.

2.1 Exploration and exploitation

One of the challenges related to exploit new REE deposits is that they generally occur in geological settings where a lot more research is required to fully understand their nature and paragenesis. REE are often incorporated in minerals that are deposited in localities that exhibit a complex genesis (i.e. pegmatites and hydrothermalites). Due to this, these new deposits can vary in mineralogy from locality to locality and knowledge may not be directly transferrable between deposits. Furthermore, both target minerals and gangue may be unique to the world, meaning all methods of extraction and processing need to be developed for just one deposit. Consequently, it is important to understand the complex mineralogy of these deposits on a detailed level. This is often ignored by exploration companies and investors, but may very well be the key to understanding the best way for extraction and finding new deposits.

Due to the high concentration of REE in the Ilímaussaq complex, the complex has drawn interest from mining companies. The main targeted mineral is eudialyte. As of now there are two mining companies with license of exploration in the area (Fig. 2.1). Greenland Minerals A/S has the license of the northern part on the complex, including the Taseq slope and Kvanfjeld. Meanwhile TANBREEZ Mining Greenland A/S (Rimbal Pty. Ltd.) has license on the southern part which includes the Kringlerne Mountains (Fig. 2.1).

Although the companies have had their exploration license for more than 10 years, this has not resulted in any exploitation of the resources. One of the reasons for this is that REE deposits such as the ones in Ilímaussaq require a more advanced extraction method than normal ore deposits. An example of this is that the U content of the rocks are often bound in minerals such as lovozerite. These minerals have crystals of 30-100 um, which would require a non-feasible amount of electrical power to extract.

Although the extraction process is a challenge, Greenland Mineral and Energy has managed to float steenstrupine-(Ce), monazite and xenotime, all which are potential REE bearing phosphates (Simpson, 2015). Another challenge for extracting REE from Kvanefjeld is that Greenland currently do not allow exploitation of ore with a U-content above 50 ppm, even as a side product.

There is no active REE-mine in Europe as of now. The most advanced project was in the alkaline complex Norra Kärr in Sweden, but this closed down due to local environment concerns. The Norra Kärr deposit is a metamorphic analogy to the Ilímaussaq complex, and

could potentially be used as an inspiration for the mining projects in Ilímaussaq. Similar to Ilímaussaq, the primary ore mineral of Norra Kärr is eudialyte (Sjöqvist *et al.*, 2013).

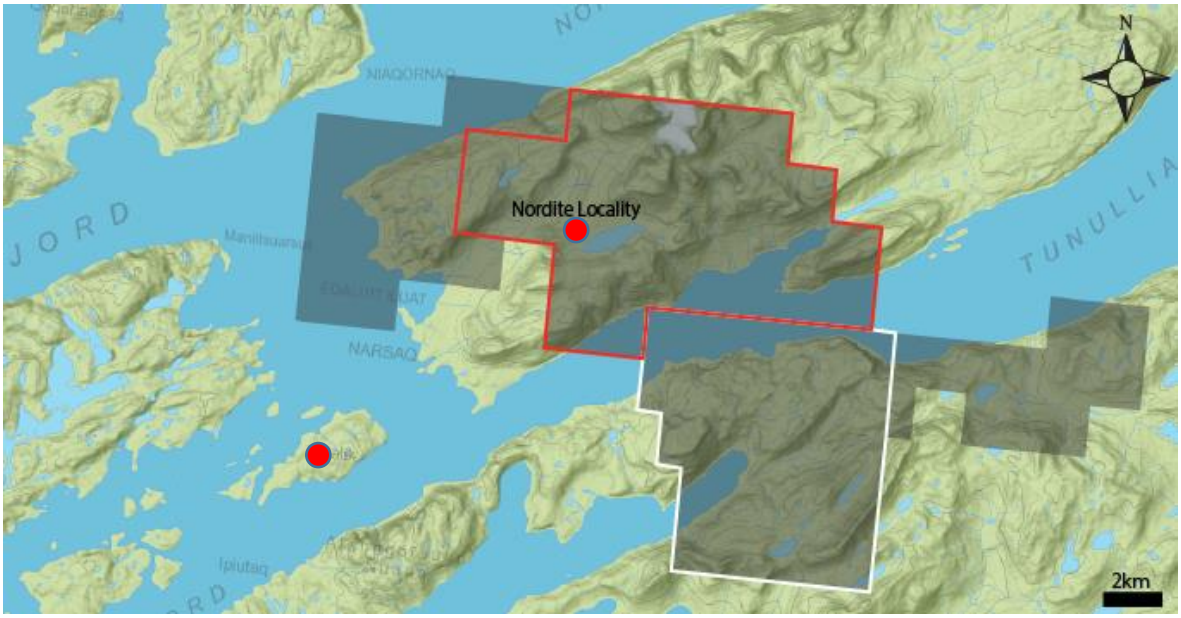

FIGURE 2.1: Map of the Ilímaussaq alkaline complex. Red area is under exploration license by Greenland Minerals A/S. White area is under exploration license by TANBREEZ Mining Greenland A/S. The not marked grey areas are other licenses outside of Ilímaussaq complex and will not be mentioned. Modified after published license data available on GEUS' web service Grønlandsportalen. The nordite localities are marked with a red dot.

2.2 Research Aims

The first description of the Greenlandic nordite is poor and microprobe data reported erroneous. The purpose of this study is to provide a full chemical and crystal structural characterization of material from the two localities Igdlutalik Island and the Taseq slope, in the Narsaq area of Southern Greenland.

2.3 Background

2.3.1 Alkaline rocks and complexes

2.3.1.1 Alkaline rocks

Alkaline rocks are by Daly (1910) described in two ways, firstly as rock that contain relatively high amounts of alkalis such as Na and K. Secondly, as rocks with relatively low amounts of alkalis, "yet carry essential amounts of minerals specially characteristic of alkali-rich eruptives, such as nephelite, leucite, analcite, etc". Alkaline rocks has since then been further defined when Ussing (1912) introduced the term "agpaitic". This term was used for alkaline rocks where the molar ration between (Na+K)/Al is equal or greater than 1.2. This was a purely geochemical classification and was redefined by Sørensen (1997) to include peralkaline rocks in which High Field Strength Elements (HFSE) such as Zr and Ti,

accommodates into complex minerals such as rinkite and eudialyte. With this modernization, the classification of agpatic rocks is based upon the minerals paragenesis, rather than just its chemical composition. This can be applied to the distinction between agpaitic and miaskitic rocks, where in the later the HFSE are incorporated into minerals such as zircon and titanite (Sørensen, 1997; Friis, 2015; Marks & Markl, 2017).

The concept of agpaitic rocks was further developed when (Khomyakov, 1995) introduced the term hyperagpaitic. This definition includes the most evolved nepheline syenites and was first used to describe pegmatites and hydrothermalites from the Khibina Massif in the Kola Peninsula, Russia. Khomyakov (1995) further subdivided the classification system of the nepheline syenites. This system bases its classification on an alkalinity modulus (K_{alk}) calculated from $K_{alk} = (x * 100) / (x + y + p)$ where *x*, *y* and *p* are compositional parameters in accessory silicate minerals with the general formula $A_xM_ySi_pO_q$ (A = Na, K, etc.; M = Ti, Nb, etc.). From this classification, five subgroups were determined, miaskitic (K_{alk} << 15%), low agpaitic (K_{alk} = 15-25%), medium agpaitic (K_{alk} = 25-35%), highly agpaitic (K_{alk} = 35-40%) and hyperagpaitic (K_{alk} = > 40%).

Hyperapgaitic rocks contain water soluble minerals such as natrosillite ($Na_2Si_2O_5$) and villiaumite (NaF) in addition they contain complex phosphosilicates such as steenstrupine-(Ce). The steenstrupine-(Ce) succeeds the eudialyte in the agpaitic rocks (Khomyakov, 1995; Andersen & Friis, 2015; Friis, 2015). In addition, feldspars (e.g. albite) and feldspathoids (e.g. nepheline, analcime) are less abundant and minerals such as ussingite ($Na_2AlSi_3O_8(OH)$) and naujakasite ($Na_6FeAl_4Si_8O_{26}$) crystallize instead (Andersen & Friis, 2015).

In their global review on agpaitic rocks Marks & Markl (2017) suggested a new classification of the nepheline syenites based upon its mineralogical composition (Table 2.1).

TABLE 2.1: Comparison of the classification scheme for nepheline syenites. Modified from Marks and Markl (2017).

Khomyakov (1995)	
Group	*Diagnostic minerals*
Miaskitic	Allanite, zircon, ilmenite, hastingsite
Low agpaitic	Eudialyte, låvenite, titanite, zircon, apatite, katophorite
Medium agpaitic	Apatite, titanite, nosean, arfvedsonite, etc.
Highly agpaitic	Eudialyte, lamprophyllite, aenigmatite, astrophyllite, Li-arfvedsonite, nepheline, analcime, sodalite, villiaumite, etc.
Hyperagpaitic	Zirsinalite, vuonnemite, vitusite, steenstrupine, chkalovite, Li-arfvedsonite, ussingite, natrosilite, villiaumite, etc.
Mark & Markl (2017)	
Modifier	*Diagnostic minerals, excluding postmagmatic and secondary minerals*
Miaskitic	Zircon/baddeleyite, perovskite/titanite
Transitional agpaitic	Minerals being typical for miasktic and agpaitic rocks[1]
Miaskitic	Zircon/baddeleyite, perovskite/titanite
Agpaitic	Minerals of the eudialyte-, rinkite-, and wöhlerite-groups and aenigmatite, astrophyllite, dalyite, elpidite,hilairite, lamprophyllite, lorenzite, lovozerite, parakeldyshite, vlasovite, wadeite[2]
Hyperagpaitic	Steenstrupine-(Ce)/voronkovite, naujakasite, lovozerite/zirsinalite, lomonosovite, natrophosphate, vitusite, natrosilite, ussingite and others[3]

[1]See details in Marks *et al.* (2011)
[2]See details in Marks & Markl (2017)
[3]See details in Sørensen (1997, 2001); Andersen & Sørensen (2005); Sørensen *et al.* (2011); Andersen & Friis (2015); Marks & Markl (2017)

2.3.1.2 Alkaline complexes

As the name indicates, alkaline complexes are geological complexes dominated by evolved rocks (e.g. miaskitic, agpaitic), rich in alkali metals like Na and K. Usually, these complexes are dominated by miaskitic intrusive units (e.g. Mt. Saint-Hilaire and Larvik Plutonic Complex), but in some cases (e.g. Ilímaussaq, Khibina and Lovozero) the agpaitic intrusions dominate the complex (Marks & Markl, 2017). An illustrative overview of the localities and their associated alkaline rock types are shown in Fig. 2.2.

The general setting where we find alkaline complexes includes, (I) continental rifts (e.g. Gardar Rift, East African Rift, Oslo Rift), (II) intraplate settings of oceanic (e.g. Ascension, Azores, Cape Verde) and continental (e.g. Monteregian Hills, Damaraland province, and Serra

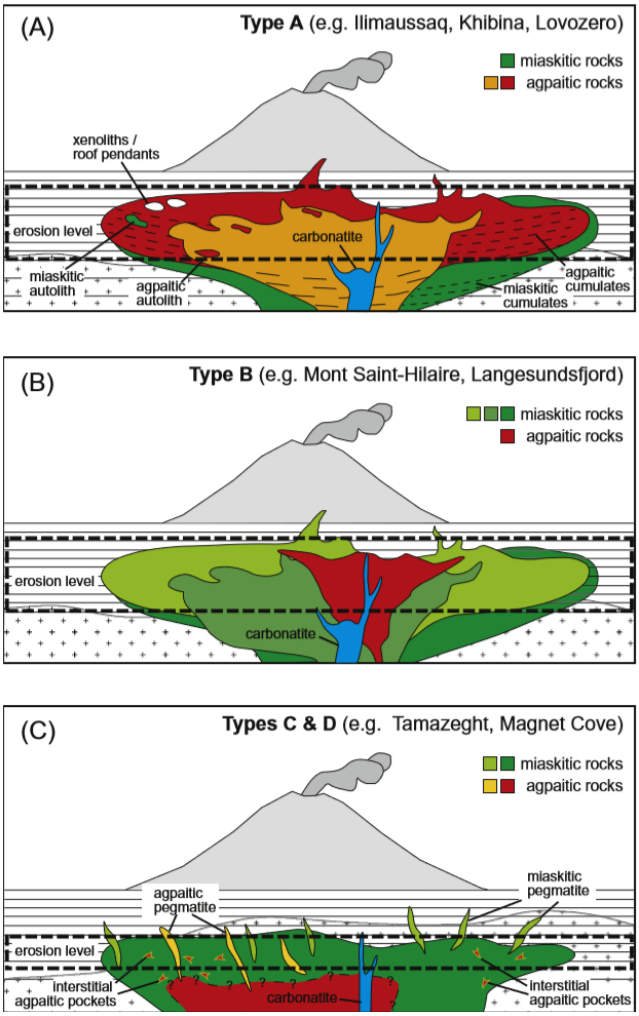

FIGURE 2.2: Illustration of alkaline complexes and their dominant alkaline rock type. Type A: predominantly agpaitic intrusions. Type B: predominantly miaskitic intrusions. Type C and D: Relation between miaskitic plutonic rocks and, agpaitic pockets and associated pegmatites. All types are somehow related to a carbonotite. From Marks & Markl (2017).

do Mar province) affinity, and (III) subduction-related settings (e.g. Trans-Pecos) (Sørensen, 1974; Fitton & Upton, 1987; Marks & Markl, 2017).

It is generally believed that the magmas which form the peralkaline systems derive from low-degree partial melting of mantle lithologies. Furthermore, the unique geochemical composition of agpaitic rocks is most likely related to differentiation at low oxygen fugacity (f_{O2}) and water activity (a_{H2O}) (Kogarko, 1974; Sørensen, 1974; Marks & Markl, 2017). These specific conditions allow for a Fe- and HFSE enrichment alongside an increase in peralkalinity and retention of halogens in the evolving magma. As a result of these processes we get a large diversity in the mineralogy of the agpaitic rocks (Marks & Markl, 2017). The rare occurrence of these agpaitic forming conditions is what makes complexes such as Ilímaussaq, Khibina and Lovozero a prime area for rare and diverse mineral occurrences.

The established levels of alkalinity (Khomyakov, 1995; Marks & Markl, 2017) is displayed in various complexes. Complexes such as the ones labeled type A in Fig. 2.2 (Ilímaussaq, Khibina and Lovozero) contain predominantly agpaitic to hyperagpaitic rocks. Whereas, the B type complexes (Mont Saint-Hilaire and LPC) are of a more miaskitic nature.

These complexes often show a transition between the different levels of alkalinity. This is well described by Andersen *et al.* (2017) for the Pilanesberg Complex, South Africa. Here the transition between miaskitic and agpaitic can be seen as the complex displays increasingly more alkaline intrusives. Through a sequence of concentric ring-dykes (Lurie, 2004), comprised of the lesser evolved red syenites, peralkaline nepheline syenites and agpaitic eudialyte-bearing

foyaite, the alkaline evolution is showcased. The transition from miaskitic to progressively more agpaitic can even be seen in-situ in the white nephline syenite (white foyaite) that occurs in the outermost ring of the complex. In this rock the mineral assemblage evolves from Ti-bearing minerals (i.e. titanite and ilmenite) to more agpaitic hosted Ti minerals (i.e. rinkite and lorenzenite). In addition to the alkaline sequence seen in the complex, there is also reported findings of minerals such as analcime, natrolite, bafertisite, jinshajiangite, fluorcaphite and barite. This would mean that the complex reaches hyperagpaitic compositions aswell (Andersen *et al.*, 2017).

2.3.2 Geological setting

The Ilímaussaq alkaline complex is exposed in a 136 km^2 large area that stretches across both the Tunulliarfik and Kangerluarsuk fjords in the Gardar Province of Southern Greenland (Fig. 2.3). The complex is host to over 230 different mineral species, being the type locality to 34 of those (Mindat[1]). It is one of the few complexes in the world where we find a large enrichment in REEs. The high concentrations of REE makes it an ideal place for many rare minerals to form, and it is considered an exotic place to visit for mineral collectors and enthusiasts from all over the world.

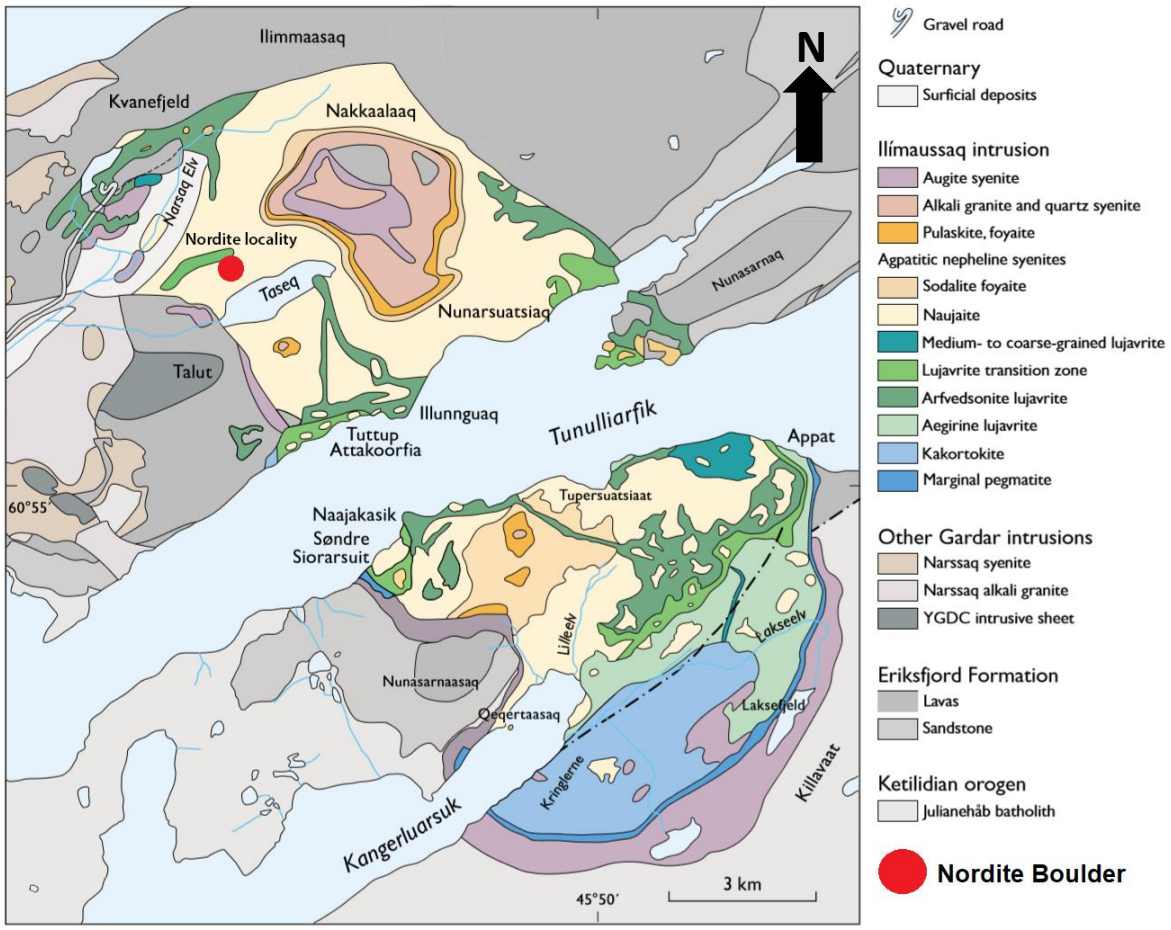

FIGURE 2.3: Geological map of the Ilímaussaq complex. Modified from Upton (2013), showing the nordite locality on the Taseq slope.

The geology of the Ilímaussaq complex is well described by the literature, e.g. (Ussing, 1912; Larsen & Sørensen, 1987; Sørensen & Larsen, 1987, 2001; Upton, 2013). The Gardar Province went through a series of continental rifts, alkaline magmatism and sedimentation 1300-1140 Ma ago. The province is often separated into the Older Gardar (1300-1163 Ma) and Younger Gardar (1163-1140 Ma). The Mesoproterozoic igneous Ilímaussaq complex was formed as a result of late magmatism along the southern rift zone and marks the end of the magmatism in the Gardar Province (Upton, 2013). The post-extensional complex has been dated by several authors (Table 2.2), and for this thesis it is assumed the latest dating at 1160 ± 2.3 Ma (Krumrei *et al.*, 2007). This makes it one of the youngest alkaline complexes in the region associated with the Gardar rifting (Upton, 2013).

The complex was for a long time considered to be formed by three successive intrusions, however Sørensen *et al.* (2006) argued there could be four or more intrusions that builds up the

complex. Because this subject is still under debate, for the case of simplicity it will be assumed that the complex is build up by three principal intrusions. The augite syenite represents the first phase and is only preserved as a partial marginal shell on the southern and western part as well as in the roof of the complex (Upton, 2013). The second phase is dominated by alkali granites and quartz syenites. These can be found in the roof and as fragments that has fallen down into the third intrusion (Sørensen, 2001). Thirdly, the last and arguably the most important phase consist of the agpaitic syenites. This intrusion occupies most of the complex and can be divided into a roof and floor zone (Fig. 2.4 and 2.5) (Sørensen, 2001; Upton, 2013).

The roof series consist of mainly naujaite, sodalite foyaite and pulaskite. In the floor series we find the kakortokite and the marginal pegmatite (Figs. 2.4 and 2.5). Lastly, the lujavrite intruded the other formations at a later stage, forming a sort of middle part of the complex. The mineralogy of the different rocks is somewhat similar, and can be easily confused if not familiar with the rocks or looked at in a hand specimen. The main difference between them is the texture and alkalinity.

TABLE 2.2: Radiometric age determination of the Ilímaussaq Alkaline Complex. Modified from Upton (2013).

Locality	Rock unit	Material	Age (Ma)	±(Ma)	Reference
Baddeleyite data					
Ilímaussaq	Agpaite cumulate	Baddeleyite	1160	5	Waight *et al.* (2002)
Ilímaussaq	Agpaite cumulate	Baddeleyite	1160	2.3	Krumrei *et al.* (2007)
Rb-Sr whole-rock and mineral age data					
Ilímaussaq, late dyke, Kvanefjeld	Monchiquite	Phlogopite	1134	17	Larsen (2006)
Ilímaussaq	Agpaites, syenites, granites	Whole-rock	1143	21	Blaxland & Upton (1978)
Ilímaussaq	Agpaite	Alkali feldspar, eudialyte	1160	2.3	Waight *et al.* (2002)

Errors are quoted at the 2σ level

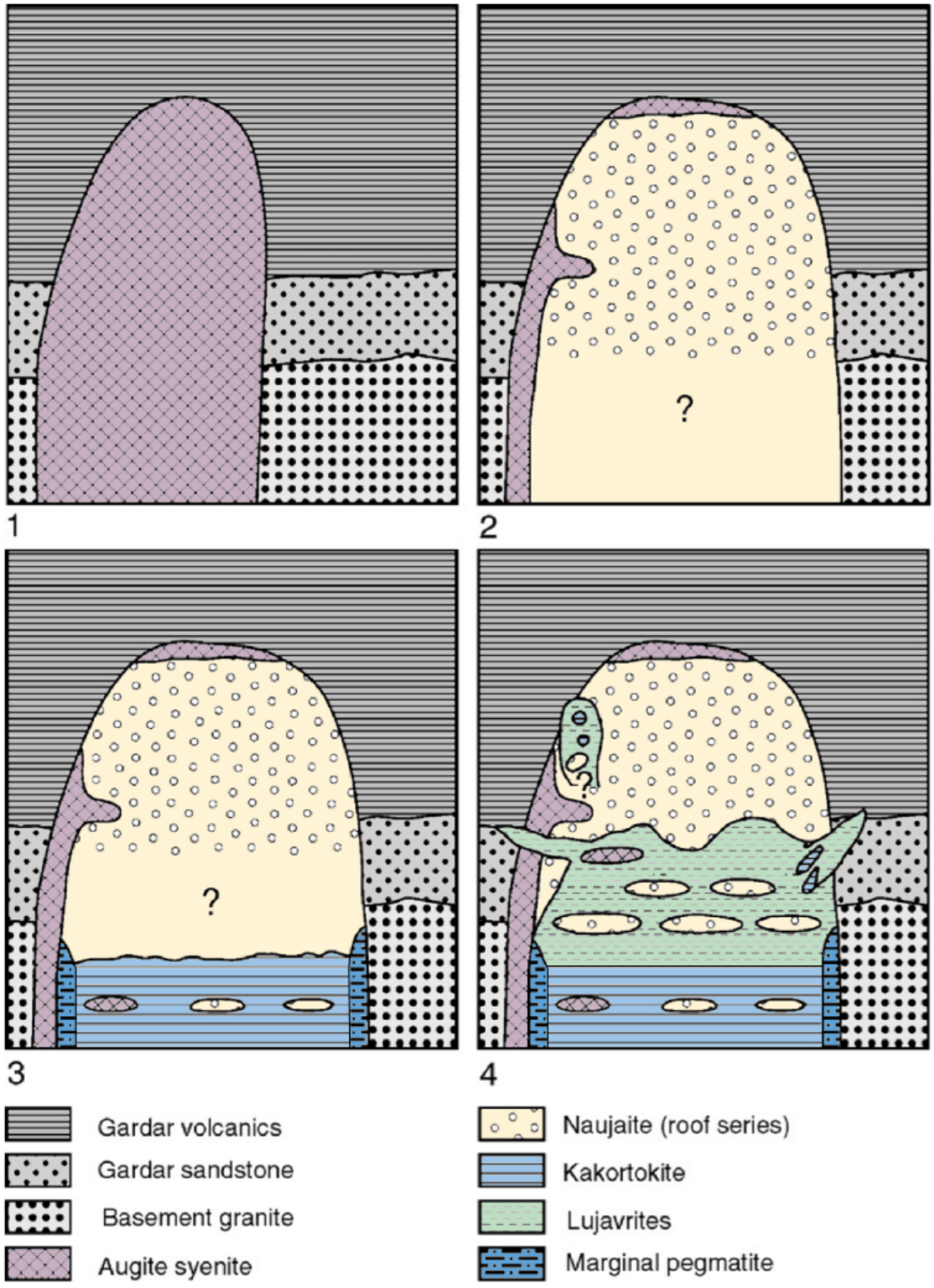

FIGURE 2.4: Evolution of the Ilímaussaq alkaline complex. Modified from Sørensen *et al*. (2006). 1: Augite syenite intrudes the Julianhaab batholite (Basement granite), Gardar sandstone and lavas (Eiriksjord fm.). 2: The forming of the roof series starting with the formation of the naujaite in a downward open magma system. 3: Formation of the marginal pegmatite and the kakortokite. 4: The intrusion of the lujavrite. The upper left lujavrite body, corresponding to the Kvanefjeld locality, still has an unknown source.

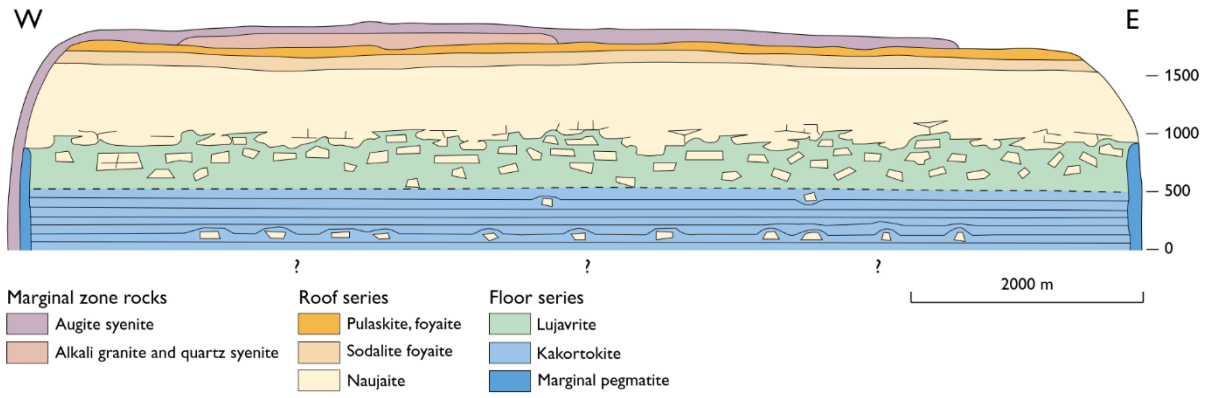

FIGURE 2.5: Section across the Ilímaussaq complex, illustrating geology of the complex. From Andersen *et al.* (1981) and Upton (2013).

Kakortokites

The magmatic layered kakortokite is a medium- to coarse-grained nepheline syenite. The rock has been divided into 29 units, where most units consist of three distinct layers. The thickest layer is the white top layer, rich in nepheline and alkali-feldspar. The middle layer is enriched in eudialyte and thereby red, while the lower most layer of the unit is a black horizon filled with arfvedsonite (Bohse *et al.*, 1971; Friis, 2015). The kakortokites are the least evolved rock of the three main apgaitic rocks: kakortokite, naujaite and lujaite. The rock can easily be observed (Fig. 2.6A) in the southern part of the complex, at the locality with the fitting name Kringlerne (Andersen *et al.*, 2006).

The cause of its rhythmic layering (Fig. 2.6 B) is highly debated and no single process seems to explain its formation. There have been several models proposed for the formation of the kakortokites ranging from gravitational sorting in the low viscosity melt (Bons *et al.*, 2015; Lindhuber *et al.*, 2015; Borst *et al.*, 2018) to periodic volatile releases or repeated melt influx (Pfaff *et al.*, 2008; Hunt *et al.*, 2017). The cyclicity of the kakortokite units and the geochemical trends is similar to that of other intrusions that we find in igneous complexes such as the Stillwater complex in Montana, USA and Bushfeld complex in South Africa (Jackson, 1970; Pfaff *et al.*, 2008).

An interesting observation is that although from distance it might look like a sharp boundary between the layers in the kakortokite units, the boundary is gradual (Fig. 2.6 C). Although the topic of kakortokite formation is very interesting, it is not relevant for this thesis and will not be discussed any further.

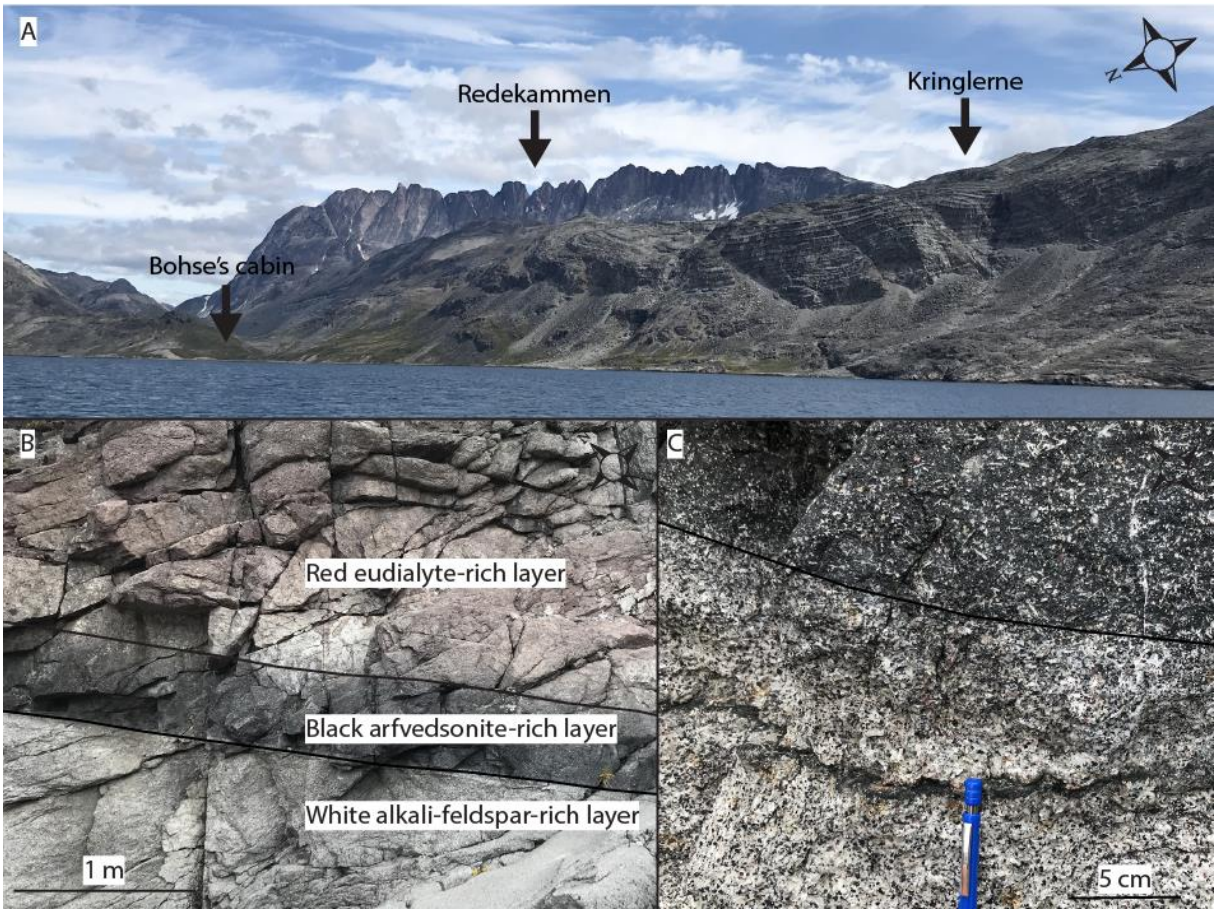

FIGURE 2.6: A) Overview of the Kanglerusuq fjord and Kringlerne. B) Picture showing unit 0 in the kakortokite series. C) Closeup of the transition between white and black kakortikite layers.

Naujaite

The naujaite is a cumulate rock consisting of greyish to greenish euhedral sodalite enclosed in alkali-feldspar, black to dark-green arfvedsonite and aegirine and red eudialyte. This poikilitic texture is due to the early formation of sodalite in the magma chamber that due to its low density, floated to the top of the magma. Sodalite is then included in by the other minerals as they crystallize. The eudialyte content can vary a lot as it does in the kakortokites, but the magmatic layering is not as pronounced in the naujaites. The Taseq slope is predominantly naujaite with different occurrences of pegmatites and hydrothermalites (Andersen *et al.*, 2006).

FIGURE 2.7: Boundary between the naujaite and lujavrite.

Lujavrite

Lastly, the most evolved rock in the complex is the lujavrite. This hyperagpaitic rock is the youngest of the nepheline syenites, forming a horizon between the naujaites and the kakortokites (Fig. 2.5). Contrary to the other rock types, the lujavrite is intruding the adjacent rocks, and does not form a single uniform unit. As with the other rocks, the lujavrite consists of the felsic minerals nepheline, albite, microcline and sodalite. There are several varieties of lujavrites in the complex, with both textural and mineralogical differences. However, the main two lujavrites can be separated by color based on which mafic mineral is present in the rock. The two most abundant lujavrites are the green lujavrites which predominantly contain aegerine, while in the black lujavrite arfvedsonite is the main mafic mineral (Andersen *et al.*, 2006; Upton, 2013; Friis, 2015). Figure 2.7 shows the rather sharp border between naujaite and lujavrite.

Because the lujavrite is not one uniform unit it is common to observe variation even on the meter scale when conducting fieldwork in Ilímaussaq. Due to this the lujavrite is the most

mineralogically diverse of the Ilímaussaq rocks. Despite this there have been very little detailed study of the mineralogy of the rock. Only a few publications on the petrology (Bailey *et al.*, 2006; Sørensen *et al.*, 2006) and the geochemistry (Sørensen *et al.*, 2011; Ratschbacher *et al.*, 2015) are available.

Pegmatites and hydrothermalites

There is an abundance of pegmatites in the Ilímaussaq complex. The diversity of the mineral assemblage in the pegmatites is extreme, and could possibly be divided into four main types:

1. Normal pegmatites with coarse feldspars as the matrix mineral.
2. White albite veins.
3. Zeolite rich pegmatites.
4. Ussingite veins (hydrothermalites).

The normal coarse grained feldspar pegmatites are characteristic of the southern part of the complex, at localities such as the Sørensen's Island in the fjord of Kangerluarsuk. This is where Steenstrup sampled the first eudialyte to see if Zr could be extracted.

The white albite veins occur in several different localities in the complex, but is maybe most abundant at the top of Kvanefjeld. This pegmatite is a common attraction for mineral collectors to visit due it being host to the much sought after tugtupite.

A second locality on top of Kvanefjeld hosts a zeolite rich pegmatite. This pegmatite contains large amounts of the zeolites natrolite and analcime that are often thought to be the alteration product of ussingite (Karup-Møller, 1978). However, due to the fact that we find large pockets of analcime in the lujavrite, such as the type locality of sørensenite, it might be that this is not an alteration product, but rather a result of immiscibility (Sørensen *et al.*, 2003).

Lastly, we have the ussingite pegmatites. There is an argument that many of these ussingite pegmatites can be classified as hydrothermalites. This is a term common among the Russian alkaline rocks specialists. Even though the concept of hydrothermalites has not been fully understood, it is believed to be a primary late stage alkaline rock forming process involving extreme alkaline hydrothermal fluids (Khomyakov, 1995). This would lead to the formation of ussingite as a rock forming mineral. Therefore, many of the pegmatites which consist of ussingite as the rock forming mineral are actually hydrothermalites.

With the introduction of hydrothermalites as a primary rock forming process, there would be a clear distinction from hydrothermal alteration, with the latter being a secondary rock forming process. For simplicity, pegmatite is the term mostly used throughout this study.

2.3.2.1 The Taseq slope

The town of Narsaq, situated just south west of the complex, is the main base for expeditions in the area. One of the more popular sites is the Kvanefjeld (NW part of the complex, Fig. 2.3) where the much sought after mineral tugtupite occurs. Kvanefjeld was in the 1950s discovered to be a potential U-deposit, and it was for exploration purposes drilled a 1km adit in 1980-81 (Sørensen, 2001). However, in 1983 the Kvanefjeld project was terminated for political reasons (Friis, 2016).

On the other side of the Narsaq river valley we find the Taseq slope location (Fig. 2.8). It is the type locality of three rare earth minerals such as ilímaussite-(Ce), and it is where most of the samples were collected for the thesis.

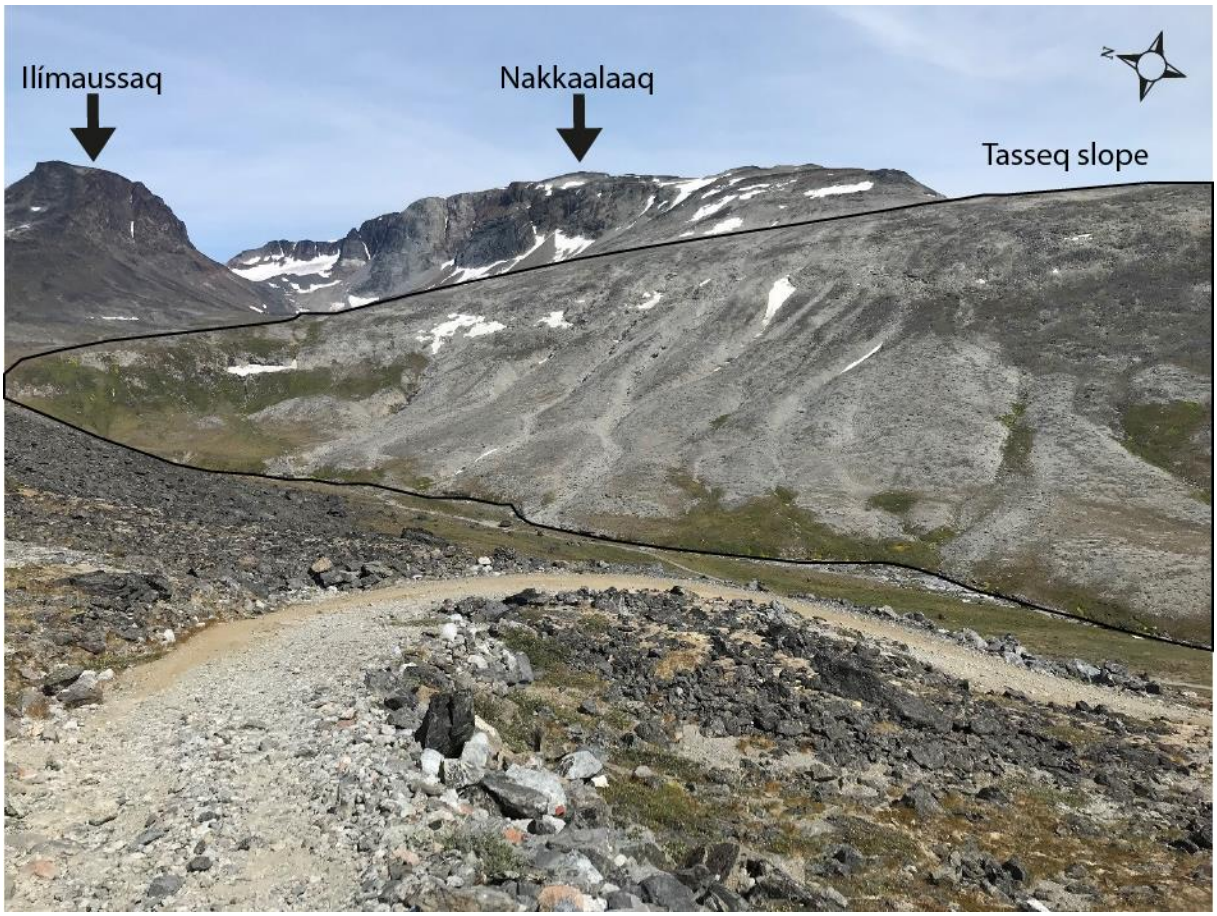

FIGURE 2.8: Overview of the Taseq Slope, Ilímaussaq complex. Picture taken from the road up to Kvanefjeld. The Taseq slope continues in S-SE direction from this picture.

The slope is partly covered with snow during most of the year, lying as a white belt in the upper part of the slope. During July, the snowbanks retreat and the outcrops of the slope becomes accessible. Due to its exotic mineralogy, many localities have been blasted by the locals looking for large occurrences of semiprecious and luminescent minerals such as the tugtupite and sodalite. These minerals are used as jewelry or sold online to mineral enthusiast collecting fluorescent minerals, however the blasting provides a unique chance to explore the mineralogy as rare minerals are usually left behind.

Contrary to Kvanefjeld, there has not been done any exploration for raw materials on the slope, except a beryllium mineralization study with a field beryllometer conducted by Greenland Geological survey (GGU) in 1971 (Engell *et al.*, 1971). However, this study produced some detailed maps over the slope's geology and mineralogy relevant for this study (Fig. 2.9 and 2.10).

Hydrothermalites are frequently occurring on the Taseq slope in particular, with both white and pink ussingite as the rock forming mineral. Figure 2.10 B shows the different occurrences mapped by Engell *et al.* (1971) with the addition of the boulder of hydrothermalite where the nordite subject for this thesis is occurring. In addition, this hydrothermalite also contain REE-rich minerals such as steenstrupine-(Ce), britholite-(Ce), ancylite-(Ce) and ilímaussite-(Ce) (Semenov & Tichonenkova, 1967).

FIGURE 2.9: Detailed overview over the Taseq slope. A: The inset is an overview of the Taseq slope, while the red box marks the more detailed map in the background. B: The red box on the main map marks the area of the detailed map on the next page. Resolution of the map is not that high due to that it's a scan of a non-A4 map. Modified from Engell *et al*. (1971).

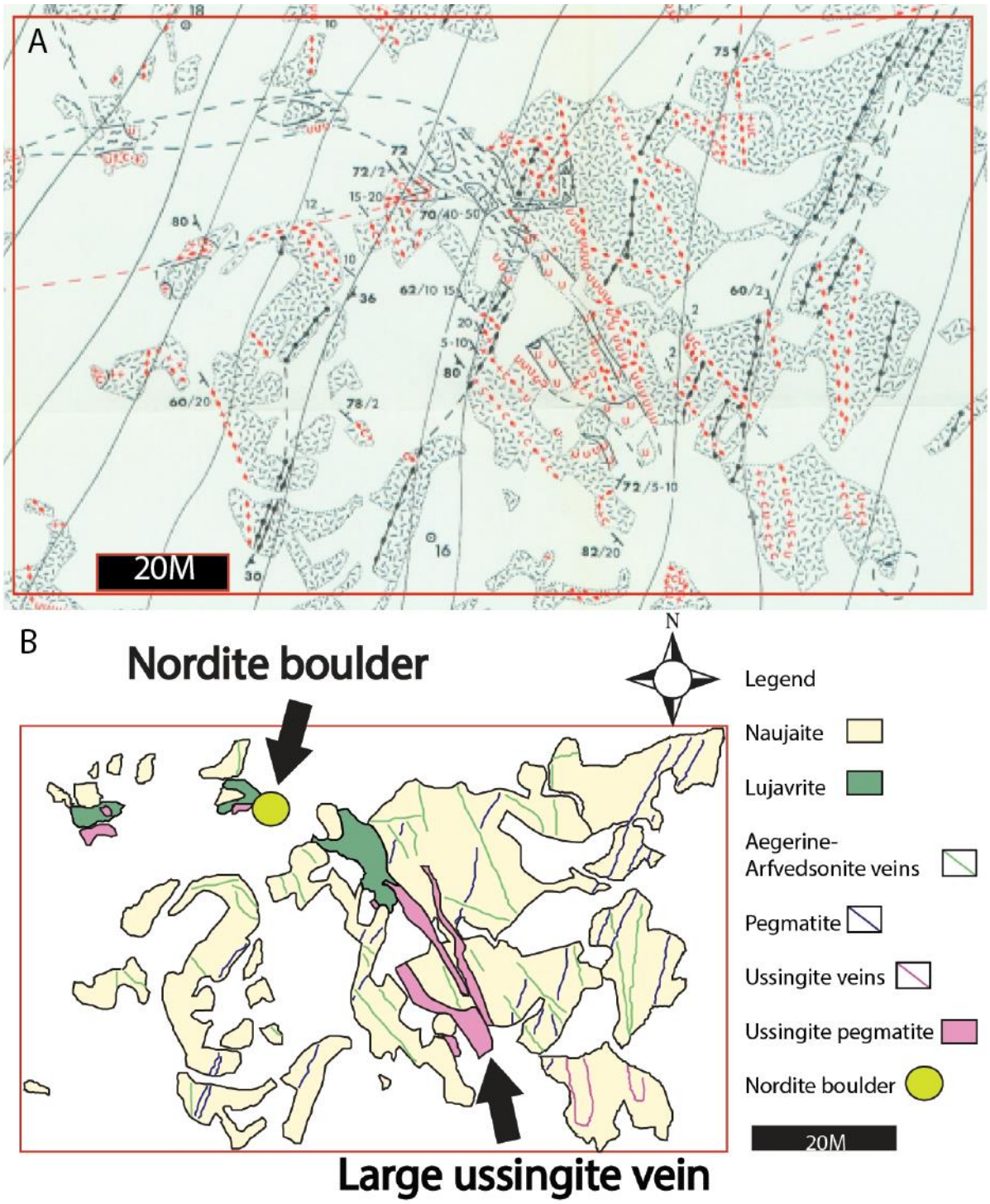

FIGURE 2.10: A) Closeup of the red box area from Figure 9B. B) Highlighted geological map of A. Including the location of the nordite boulder. Figure is sloping towards N-W.

2.3.2.2 The Igdlutalik Island

The Igdlutalik Island is situated outside of the Ilímaussaq alkaline complex. The Island is uninhabited and lies just S-SW of Narsaq town (Fig. 2.1). It is famous for being the type locality of emeleusite and hosts euhedral green narsarsukites (Upton *et al.*, 1976; Upton *et al.*, 1978). The narsarsukite-bearing dyke was discovered during 1:20 000 reconnaissance mapping of the Julianhaab area in the 1950-60s by the GGU. The outcrop is situated on a hill facing towards the NE at an altitude of around 180 m. The width of the outcrop is no more than 20 m and can only be traced a mere 30 m along the length of the dyke. The dyke is narsasukite bearing, in addition it hosts fine albite, aegirine, hematite, green biotite, opaque oxides, apatite, white mica, riebeckite, calcite, zircon, pectolite and nordite (Upton *et al.*, 1976). The swarm is believed to have intruded between 1150 and 1200 Ma ago.

There have been no other observations of similar outcrops along the same trachyte dyke, or any of the other dykes on the island (Upton *et al.*, 1976; Upton *et al.*, 1978). However, at an altitude of 50 m lies a comendite dyke with the same strike as the narsarsukite-dyke. It is therefore believed that these dykes are closely related and that the narsarsukite-dyke might represent a higher-level facies opposed to the comendite-dyke (Upton *et al.*, 1976).

2.4 Nordite

TABLE 2.3. The nordite-group. Occurrences and ideal chemistry.

Mineral	Ideal Formula	Locality		Reference
Nordite-(La)	$Na_3SrLaZnSi_6O_{17}$	Lovozero Massif, Kola peninsula, Russia	Chinglusuai River Valley	(Gerasimovsky, 1941)
		Lovozero Massif, Kola peninsula, Russia	Eveslogchorr Mt.	Pekov data, unpublished
			Kukisvumchorr Mt.	Kartashov data, unpublished
Nordite-(Ce)	$Na_3SrCeZnSi_6O_{17}$	Lovozero Massif, Kola peninsula, Russia	Alluaiv Mt.	(Pekov, 2000)
			Karnasurt Mt.	(Pekov, 2000)
			Kedykverpakhk Mt.	(Pekov, 2005)
			Sengischorr Mt.	(Pekov, 1998)
		Khibiny Massif, Kola peninsula	Eveslogchorr Mt.	(Yakovenchuk *et al.*, 2005)
		Québec, Canada	Mt. Saint-Hilaire	(Wight & Chao, 1995)
		Tien Shan Mt.,Tajikistan	Dara-i-Pioz	(Agakhanov *et al.*, 2017)
		Gardar Province, Southern Greenland	Igdlutalik Island	(Upton *et al.*, 1976)
Ferronordite-(La)	$Na_3SrLaFeSi_6O_{17}$	Lovozero Massif, Kola peninsula, Russia	Bolshoi Punkaruaiv Mt.	(Pekov *et al.*, 2001)
Ferronordite-(Ce)	$Na_3SrCeFeSi_6O_{17}$	Lovozero Massif, Kola peninsula, Russia	Bolshoi Punkaruaiv Mt.	(Pekov *et al.*, 2001)
			Chinglusuai River Valley	(Pekov, 1998)
			Karnasurt Mt.	(Pakhomovsky *et al.*, 2014)
			Kedykverpakhk Mt.	(Pekov, 2005)
			Malyi Punkaruaiv Mt.	(Yakovenchuk *et al.*, 2011)
Manganonordite-(Ce)	$Na_3SrCeMnSi_6O_{17}$	Lovozero Massif, Kola peninsula, Russia	Karnasurt Mt.	(Pekov, 1998)
			Kedykverpakhk Mt.	(Pekov, 1998)
			Malyi Punkaruaiv Mt.	(Yakovenchuk *et al.*, 2011)

The nordite-group consists of five known members and is an extremely rare mineral worldwide (Table 2.3)

The first description of the nordite mineral was done by Gerasimovsky in 1941. It was found six years earlier by the same man in the Lovozero alkaline massif of the Kola Peninsula, Russia (Gerasimovsky, 1941).

From this publication no good material was available for crystallographic structure, but by doing an x-ray study by the Laue method, the mineral was found to be orthorhombic. The estimated empirical formula of nordite solved to $2Na_2O_3(Sr, Ca, Mn, Mg)O_{0.7}TR_2O_{38}SiO_2$. The formula alongside structural parameters given in the publication is summarized in Table 2.3. It was not stated in the published article by which method of chemical analysis the formula was obtained. From the data gathered La was the dominant REE with 8.55 wt% to Ce 8.10 wt% (Table 2.4). This is then thought to be the first description of the nordite-(La) (Gerasimovsky, 1941). The nordite was discovered in a sodalite syenite pegmatite, composed of mainly ussingite, sodalite var. hackmanite and lomonsovite.

Semenov & Barinskii (1957) mentions a Ce dominant nordite in their paper about the composition characteristics of the rare earths in minerals. It is listed to have 55% occupancy of the REE position, while La has a percentage of 34. No other chemical data is published other than the REE occupancy. However, a couple of years later Semenov (1961) describes the nordite-(Ce) in more detail and reports the first occurrence on Zn in nordite (3.90 wt%). The mineral is described from the Motchisuai river valley (Sengischorr Mt., Lovozero) and was in fact the description of a new mineral at that time. In the same publication, the original nordite-(La) material from Gerasimovsky (1941) is reanalyzed, and discovered to contain 4.22 wt% ZnO (Semenov, 1961). This would mean that the original analysis by Gerasimovskii (1941) was wrong and that the first nordite is Zn-dominated rather than Mn-dominated as originally described.

The first structure solution of the nordite was when Bakakin *et al.* (1970) studied the crystal structure of nordite and its relationship to melilite and datolite-gadolinite. This was reported to be a nordite-(La) from the Lovozero massif. The method of calculation was by the three-dimensional Patterson function. The structural parameters from this publication is summarized in Table 2.5.

Six years after Bakakin *et al.* (1970) solved their structure the first occurrence from Greenland was described. Upton *et al.* (1976) discovered nordite on the island of Igdlutalik. The discovery

was a result of describing the narsarsukite from the locality. The discovery is somewhat intriguing given that nordite has never before been described or mentioned from a peralkaline rock. At Igdlutalik, it is mentioned as a minor phase alongside micas, apatite, quartz, pectolite and a thorium silicate.

TABLE 2.4: Published chemical data over the nordite-group minerals.

Reference	Gerasimovsky (1941)	Bakakin *et al.* (1970)	*Upton et al.* (1976)	Pekov *et al.* (1998)	Pekov *et al.* (1998)	Pekov *et al.* (2001)
n	-	-	8	-	-	-
Reported mineral	Nordite-(La)	Nordite-(La)	Nordite-(Ce)	Ferronordite-(Ce)	Manganonordite-(Ce)	Ferronordite-(La)
Weight percent oxides						
SiO_2	45.53	45.07	46.48	44.92	44.57	44.1(8)
Al_2O_3	-	-	-	0.09	0.01	0.14(4)
ZnO	-	3.90	9.74	2.28	2.45	2.3(4)
FeO	-	2.12	0.22*	3.71	2.09	3.7(6)
Fe_2O_3	1.84	1.15	-	-	-	-
MnO	6.04	3.29	-	2.22	3.70	2.5(6)
MgO	2.00	1.66	0.13	0.51	0.52	0.3(1)
La_2O_3	8.55	11.52**	8.48	8.79	8.64	11.4(7)
Ce_2O_3	8.10	9.38	-	10.64	10.56	8.2(8)
Nd_2O_3	1.85	-	1.35	0.90	1.06	0.9(3)
Pr_2O_3	1.60			0.56	0.43	1.0(2)
Sm_2O_3	-	-	-	0.06	-	-
CeO_2	-	-	11.37		-	-
ΣY_2O_3	0.95	-	-		-	-
SrO	7.40	7.11	9.73	12.64	13.24	12.7(4)
BaO	-	0.35	0.99***	0.31	0.38	0.36(4)
CaO	4.46	3.74	1.48	0.73	0.33	0.5(2)
Na_2O	11.70	11.20	11.15	11.34	11.48	11.2(5)
K_2O	0.08	-	-	-	-	-
ThO2	-	0.26	-	-	-	-
Total	100.10	100.75	101.12	99.70	99.46	99.31

*Both oxidized and reduced iron is reported as FeO. **From publication the value is given in Ln_2O_3. This is assumed to be wrong and corrected to La_2O_3. ***From publication the value is written as 8.99% Ba. This is assumed to be wrong and corrected to 0.99% Ba. Upton *et al.* (1976), Pekov *et al.* (1998) and Pekov *et al.* (2001) mention the use of electron microprobe. In Gerasimovsky (1941) and Bakakin *et al.* (1970) it is not mentioned which method of chemical analysis that was used.

The data published in this article was an important reference tool and were used frequently for comparison (Table 2.4). This was mainly due to the fact that several samples used and analyzed for the thesis were collected from the locality described by Upton.

Another first discovery was made when Wight & Chao (1995) mentions nordite-(Ce) as one of the discovered members from the Mont Saint-Hilaire locality in Canada. As with several of the Russian papers, nordite-(Ce) is only mentioned as an occurring mineral, and no data is published from either structure or chemical analysis. Only a short paragenic description is

written on nordite which says that it is forming "very tiny, radiating, silky white balls on lueshite in sodalite syenite xenoliths" (Wight & Chao, 1995).

Pekov *et al.* (1998) and Pekov *et al.* (2001) introduced three new nordites to the group. Ferronordite-(Ce) and manganonordite(-Ce) were both found in veins of pegmatitic ussingite-bearing rocks at the northern slope of Karnasurt Mount and in Karnasurt Mine of the Lovozero alkaline massif in Russia (Pekov et al., 1998). The ferronordite-(La) was discovered in the same massif, but at the Bol'shoi Punkaruaiv Mountain. It was found in ussingite cores within two hyperagpaitic pegmatites. Both chemical (Table 2.4) and structural data (Table 2.5) was published of the three minerals.

Pushcharovsky *et al.* (1999) published their paper on raite, mangannordite-(Ce), and ferronordite-(Ce) from the Lovozero Massif. In this paper they describe the structure of both mangannordite-(Ce) and ferronordite-(Ce). Both of these structures alongside the one Bakakin et al. (1970) solved were used for comparison to the structure solved during this project. The proposed empirical formula solved from their microprobe data was published (Table 2.5), but the actual microprobe data was not included in the publication.

More recently, nordite-(Ce) has been mentioned from the Dara-i-Pioz glacier in the Alai Range in Tajikistan. Again, it is only mention as a part of the odigitriaites paragenesis, and no structure or chemical data were published (Aghakhanov *et al.*, 2017). Alongside this, an interesting discovery of a non-REE mineral with all principle features of the nordite structural type was made from the Wessels Mine, Kalahari Manganese Fields of South Africa. The mineral, meieranite ($Na_2Sr_3MgSi_6O_{17}$) differs from nordite by substituting the nordites REE^{3+} and Na^+ sites with $2Sr^{2+}$ (Yang *et al.*, 2019).

TABLE 2.5: Published structural data over the nordite-group minerals. The proposed empirical formula by the respective author is also given.

Reference		*a (Å)*	*b (Å)*	*c (Å)*	Space group	*Z*	Proposed formula
Gerasimovsky (1941)	Nordite-(La)	-	-	-	-		$2Na_2O\ 3(Sr,Ca,Mn,Mg)O\ 0.7TR_2O_3\ 8SiO_2$
Semenov & Barinskii (1958)	Nordite-(Ce)	-	-	-	-		$Na_3Ce(Sr,Ca)(Mn,Fe)Si_6O_{17}$
Bakakin *et al.* (1970)	Nordite-(La)	14.27(3)	5.16(1)	19.4(6)	*Ortho. Pcca*	4	$Na_2(Na_{0.8}Mn_{0.2})(Sr_{2.1}Ca_{1.9})(La_{2.1}Ce_{1.7}Ca_{0.2})(Zn_{1.5}Mg_{1.3}Fe_{0.7}Mn_{0.5})(Si_{5.85}Fe_{0.15})O_{18}$
Upton *et al.* (1976)	Nordite-(Ce)	-	-	-	-		$Na_3Ce(Sr,Ca)(Mn,Mg,Fe,Zn)_2Si_6O_{18}$
Wight & Chao, (1995)	Nordite-(Ce)	-	-	-	-		$Na_2(Na,Mn)(Sr,Ca)(Ce,La)(Zn,Mg)Si_6O_{17}$
Pushcharovskii *et al.*** (1999)	Ferronordite-(Ce)	14.46 (1)	5.1947(3)	19.874(9)	*Ortho. Pcca*	4	$(Na_{2.91}Ca_{0.10})(Sr_{0.97}Ba_{0.02})(Ce_{0.52}La_{0.43}Nd_{0.04}Pr_{0.03})(Fe_{0.41}Mn_{0.25}Zn_{0.22}Mg_{0.10})Si_{5.97}O_{17}$
Pushcharovskii *et al.,*** (1999)	Manganonordite-(Ce)	14.44(2)	5.187(5)	19.82(1)	*Ortho. Pcca*	4	$(Na_{2.96}Ca_{0.05})(Sr^*_{1.02}Ba_{0.02})(Ce_{0.51}La_{0.42}Nd_{0.05}Pr_{0.02})(Mn_{0.42}Zn_{0.24}Fe_{0.23}Mg_{0.10})Si_{5.97}O_{17}$
Pekov *et al.* (2000)	Ferronordite-(La)	14.440(5)	5.191(2)	19.86(1)	*Ortho. Pcca*	4	$(Na_{2.92}Ca_{0.08})(Sr_{0.99}Ba_{0.02})(La_{0.57}Ce_{0.41}Pr_{0.05}Nd_{0.04})(Fe_{0.43}Mn_{0.29}Zn_{0.23}Mg_{0.06})Si_{5.94}O_{17}$

*In the publication it is written as Si. This is assumed to be wrong and corrected to Sr.

**These are the latest structural analysis on ferronordite-(Ce) and manganonordite-(Ce). Earlier structural analysis can be found in Pekov *et al.* (1998).

Because nordite is a rare mineral, no attempts to make a proper nomenclature has ever been carried out. Based on previous publications a general formula for nordite $A_2BXYZT_6O_{17}$ will be used throughout this study, where *A* and *B* are monovalent cation sites, with coordination number (CN) 8 and 6, respectively. *X* is a large 8-coordinated cation site. *Y* is the 8-coordinated REE-site and *Z* and is a small 4-coordinated divalent cation site. Lastly, the *T*-sites are silica-tetrahedral. As illustrated in Fig. 2.12, the *Z*-site and *T*-sites forms tetrahedral layers, and by adding the large cations to the structure, the nordite forms a sheet-like structure (Fig. 2.13). This resembles that of sheet-silicates with alternating tetrahedral and large cation layers. A graphical overview over all sites and its coordination is presented in Fig. 2.14.

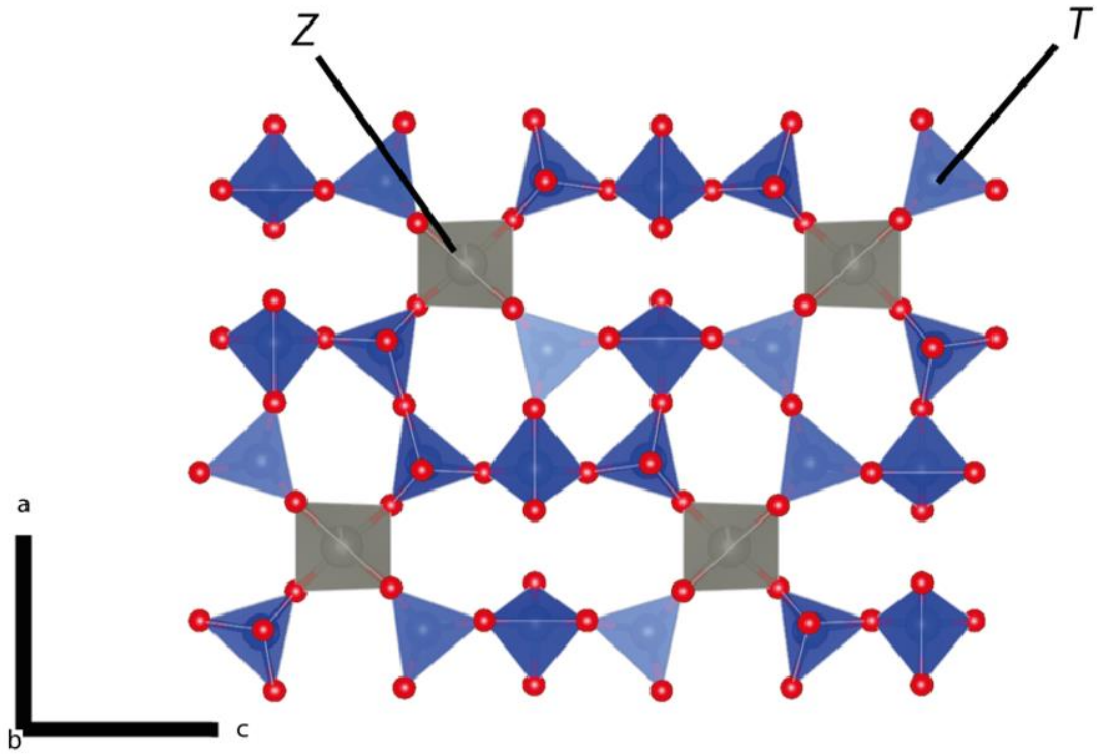

FIGURE 2.12: The tetrahedral-layer of the nordite structure, consisting of the small divalent cation *Z*-site and the tetrahedral *T*-site.

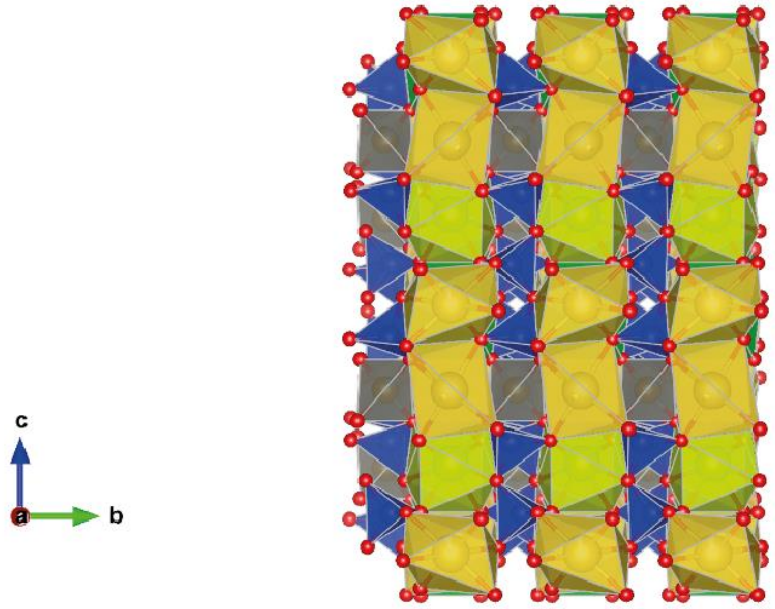

FIGURE 2.13: The full nordite structure as seen down the a-axis.

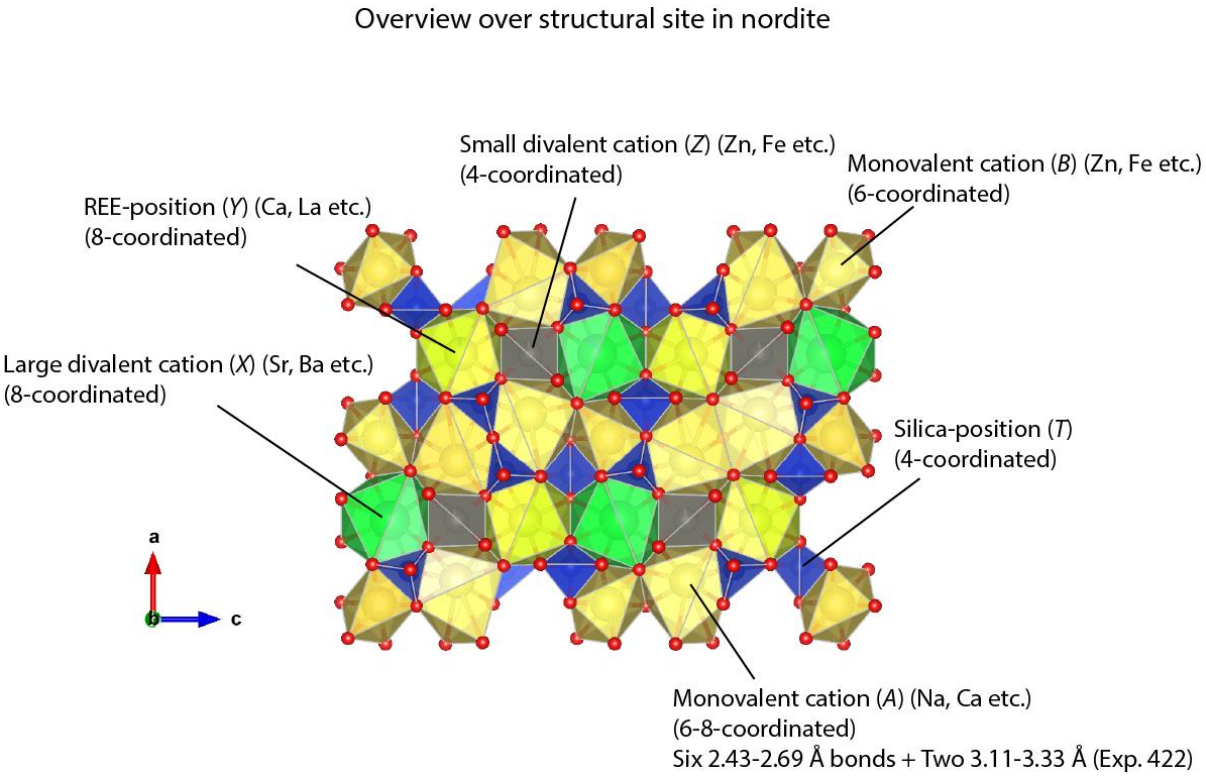

FIGURE 2.14: Overview over structural sites in nordite.

3. Methodology

3.1. Fieldwork

The Master project was not initially supposed to involve fieldwork, due to the inaccessibility of the locality and that there were already collected material from the areas in question. Henrik Friis collected the existing material from his trips to the Ilímaussaq complex. Due to time constraints, in regards to transporting the samples to Norway, the material gathered from the fieldtrip was only used as supporting material to the preexisting ones. All the material gathered from the fieldtrip is stored at the Økern facility, Natural History Museum. Only photographs and observations were directly used in this project. In addition, the money required to go on a fieldtrip would not be covered by the regular master project fund, given by the Department of Geosciences. However, with a successful application Tekna, enough funding was secured to finance a fieldtrip to Greenland during the summer of 2019.

Since nordite only has been found at the Igdlutalik Island and the Taseq slope (Fig. 2.1), these were the focal points for field studies. Despite of not expecting to find any nordite, the Kanglerusaq and Kriglerne area (Fig. 2.3) was also visited, due to the large amount of pegmatites present here and to give a deeper understanding of the geology of the entire alkaline complex.

3.2 Sample preparation

3.2.1 Thin section

In the hand samples, areas of interest were determined by examination with a LEICA MZ16A stereo binocular microscope. After this, the areas were marked with a permanent marker so it would be easier to cut the samples into sizeable pieces with the help of the diamond saw at NHM. After getting the desirable size, the prepared samples were marked again to show which side that was of interest, and where the thin sections should be made.

The thin sections were made externally with samples EHG 1 to EHG 10 made by Salahalldin Akhavan at the department of Geosciences at UiO. While samples EHG 10_2 to EHG 18 was sent to Vancouver Petrographics in Canada, to be processed with oil instead of the traditional water. The purpose for this was to retain any minerals that may be water-soluble. In this way, the two methods of making thin sections would complement each other.

In total, 18 polished thin sections were made with the standard thickness of 30 µm. These were to be used for SEM/EDS, EPMA and (ICP-MS).

TABLE 3.1: Sample names, localities and analysis done on each sample.

Samples	Localities	Analysis	Thin section
EHG 1	Igdlutalik	Optical + SEM	Scanned
EHG 2	Igdlutalik	Optical	Scanned
EHG 3	Igdlutalik	Optical	Scanned
EHG 4	Igdlutalik	Optical + SEM + EPMA + LA-ICP-MS + XRD + SXRD	Scanned
EHG 5	Igdlutalik	Optical + SEM	Scanned
EHG 6	Igdlutalik	Optical	Scanned
EHG 7	Taseq	Optical + SEM + EPMA + LA-ICP-MS + XRD	Scanned
EHG 8	Igdlutalik	Optical	Scanned
EHG 9	Taseq	Optical	Scanned
EHG 10	Taseq	Optical + SEM	Scanned
EHG 10_2	Taseq	Optical + SEM + EPMA + LA-ICP-MS	Scanned
EHG 11	Taseq	Optical + SEM	Scanned
EHG 12	Taseq	Optical	Scanned
EHG 13	Taseq	Optical + SEM + EPMA + LA-ICP-MS + SXRD	Scanned
EHG 14	Taseq	Optical	Scanned
EHG 15	Taseq	Optical + SEM + EPMA + LA-ICP-MS	Scanned
EHG 16	Taseq	Optical	Scanned
EHG 17	Taseq	Optical	Scanned
EHG 18	Taseq	Optical	Scanned
EHG EPOXY	Taseq	Optical + SEM + EPMA + LA-ICP-MS	

For scanning of the thinsection, a Nikon Super Coolscan 4000 scanner was used with the VueScan64 software. The scans of the thin sections can be found in Appendix 8.1 and 8.2.

The thin sections EHG 10_2 to EHG 18, which was processed and produced by Vancouver Petrographics were made on a thinner glass slide opposed to those made by Salahalldin Akhavan. Because of the fragileness of these thin section, extra care was taken when handling them. Unfortunately, one of the thin sections (EHG 10_2) was damaged during lab analysis, and sustained a major crack through half of the thin section. Luckily, this was after all analysis were complete and did not have any consequence for the data gathered.

3.2.2 Epoxy cast

From the existing material collected by Henrik Friis, two epoxy casts had previously been made EHG EPOXY and EHG EPOXY2. These were both from the Taseq slope locality. The purpose for using these was one of the samples in epoxy (EHG EPOXY) shows the altered surface of the rock. Only EHG EPOXY was used for further analysis.

3.3 Optical Microscopy

A LEICA DMCP petrographic microscope was used to study the thin sections. The camera used to take pictures in plane polarized light (PPL) and cross-polarized light (XPL), was a LEICA MC170HD digital camera. The software used was Leica Application Suite. Both of the microscopes mentioned in Sections 3.2 and 3.3 are located at the microscopy lab at the Natural History Museum in Oslo.

After thorough study of the 18 thin sections, only EHG 4, EHG 7, EHG 10_2, EHG 13, EHG 15 and EHG EPOXY was used for further analysis, as they exhibit the highest amount of observed nordite. For simplicity, EHG 10_2 will be referred to as EHG 10, as the original EHG 10 was not analyzed further.

3.4 Scanning Electron Microscope (SEM)

A Hitachi S-3600N low vacuum Scanning Electron Microscope equipped with a Dual Bruker XFlash5030 Energy Dispersive X-ray Spectroscopy (EDS) system. The characteristic x-ray lines on the energy spectrum obtained on the EDS system makes for rapid identification of the elements. It also requires minimal preparation of the sample before analysis. (Beane, 2004).

The purpose for using the SEM and EDS was to obtain semi-quantitative element data, which would be used for mineral identification and in preparation for the EPMA work. The internet sites Mindat (https://www.mindat.org/) and RRUFF (https://rruff.info/ima/) provided references for identifying the different spectrums.

Beam conditions used on SEM varied from an acceleration voltage of 15 kV with a spot size of ~150-200 nm. Carbon coating is common for both SEM and electron microprobe analysis, due to that a conductive layer of metal on the samples inhibits charging problems when analyzing in high vacuum. However, for the SEM analysis the thin sections were initially not carbon coated. Since the purpose of analysis was only to semi-quantitatively analyze the nordites and get a general idea of their positioning in the thin sections, running the samples in low-vacuum mode (variable P mode) was sufficient. Pressure used for the variable P mode was between 15-20 Pa.

However, when imaging nordite at a later stage in the project, the thin-sections were carbon coated and imaged at high-vacuum mode.

One of the EDS features is that it possesses the ability to create an element map of a rather large raster area. This is useful for getting an overview over the imaged area in regards to where the different elements are concentrated (Fig. 3.1).

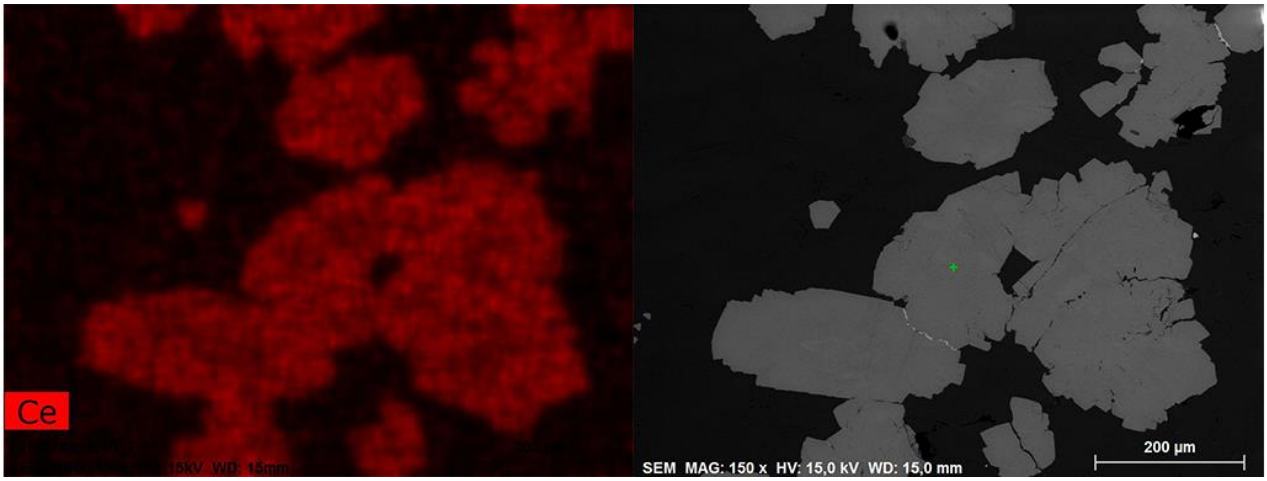

FIGURE 3.1: Backscatter image (BSE) on the right and EDS Ce elemental map on the left. Same scale on both, taken of sample EHG7.

Furthermore, mapping provides a good overview of the paragenesis and ensures that grains too small to be observed in optical microscope are not missed. The supporting software used for identification of the peaks in the spectrum was Bruker Quantax Esprit.

Although there are many advantages of using SEM and EDS there are some limitations aswell. The EDS detector cannot detect light elements such as B, Be, Li and H. Compared to a wavelength dispersive x-ray detector (WDS) such as in the EPMA instrument, the EDS is quicker but has both poorer energy resolution and detection limit. The poorer energy resolution of the EDS compared to WDS will lead potentially to more element overlaps. This in turn could impair analysis of minor elements if the element x-ray line of interest is too close to another x-ray line. For nordites large elemental overlaps are observed as seen from an example of a nordite EDS spectrum is given in Fig. 3.2.

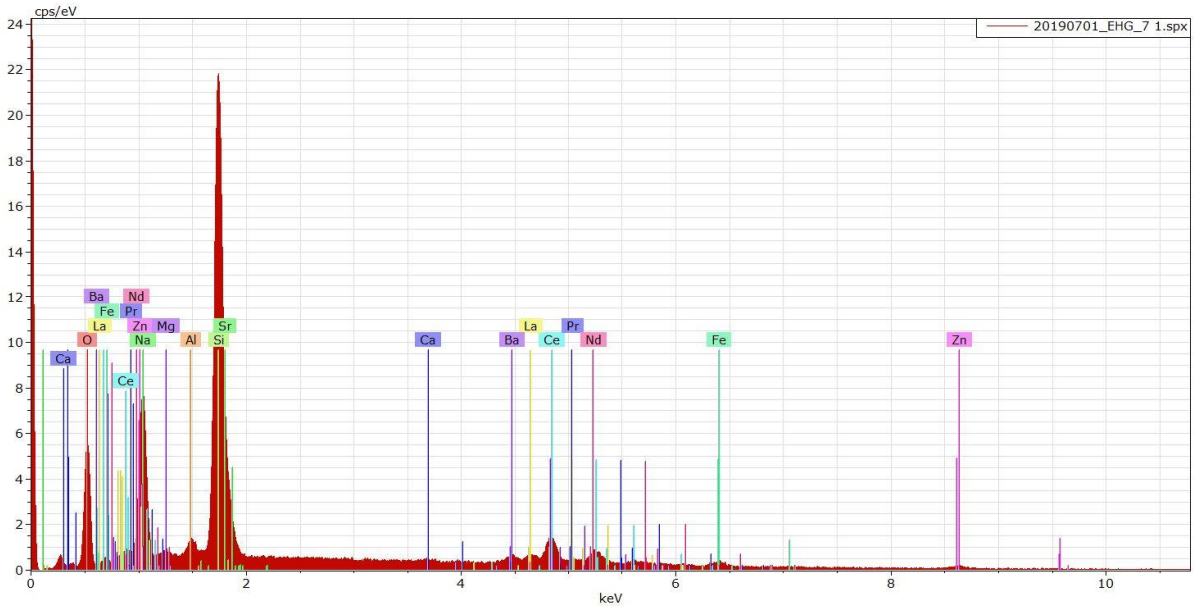

FIGURE 3.2: Energy spectrum of a nordite from sample EHG 7. Elemental lines are included to illustrate the difficulties with elemental overlap. Especially the Si/Sr, Fe/REE and the Na/Zn peaks have small degree of separation between them.

Problems

The instrument at the Natural History Museum aswell as SEM/EDS in general has some known problems associated with it. Firstly, the main issue as mentioned in the earlier paragraphs, are the elemental overlap. This was a major challenge moving forward with analysis of nordite in regards to both EDS and electron microprobe. Another issue that occurred several times, was that the sample kept drifting inside the chamber, making some analysis inaccurate. This is due to charging, but overall did not affect the semi-quantitive analysis done on nordite. Thirdly, due to the sample holder, some Al is recorded on the spectra (Fig. 3.2) even though most of the analyzed minerals do not contain this element. This is also an issue that occurs when using low-vacuum mode, but once again did not affect the observations made of nordite. Keeping these factors in mind, it signifies the use of EDS only for semi-qualitative use.

3.5 Electron Probe Micro-Analyzer (EPMA)

The EPMA offers high sensitivity quantitative chemical analysis through the WDS. At the Department of Geosciences, University of Oslo, the analyses were conducted using a Cameca SX100 fitted with five WDS spectrometers and a Bruker XFlash SDD EDS detector. An acceleration voltage of 15 kV and beam current of 15 nA was used. The diameter of the beam was 5.0 µm with a counting time of 10s on Na and Si, 30 s on Sr and Ca and 20 s on the rest of the elements. The low counting time on the Na was to prevent beam damage and element migration during the analyses. Na was analyzed first and matrix corrections were done using the PAP procedure implemented in the CAMECA software.

The purpose was to determine major and minor compositions of both nordites and other minerals in the paragenesis (aegirine, narsarsukite etc.). Thin sections from both Taseq and Igdlutalik as well as an epoxy cast from Taseq was analyzed (see Table 3.1).

Because of the numerous overlap between x-ray lines in nordite, this is not a routine analysis. Several WDS spectrums were taken on nordite, first a full spectrum then partial WDS around selected x-ray lines for analysis. These spectrums read and a possible background for each element could be determined.

The standards used for calibration were wollastonite (Si Kα, Ca Kα), Fe-metal (Fe Kα), albite (Na Kα), synthetic MgO (Mg Kα), pyrophanite (Mn Kα), ZnS (Zn Lα), $BaSO_4$ (Ba Lα), Sr-SiO glass (Sr Lα) and "synthetic REE orthophosphates" (La Lα, Ce Lβ, Pr Lβ, Nd Lβ) obtained from the Smithsonian Institution, Washington D.C. (Jarosewich & Boatner, 1991).

To prepare for the electron microprobe analysis, positioning images were taken on the EDS (such as left image in Fig. 3.1) so that it would be easy to locate in the WDS. In addition, the electron microprobe was fitted with its own EDS, which was used to qualitatively assure that the correct mineral was targeted.

Problems

During the analysis of both the nordites and the associated minerals (aegirine, arfvedsonite, ussingite, narsarsukite) there was difficulties in determining the right analytical conditions. When analyzing the nordites, especially the Ba-rich ones, the nordite bulk composition causes problems when it comes to separating the peaks used for identification. An example of this is the CeLα and BaLβ peaks that lie very close to each other, making them unable to be isolated on the LPET crystal typically used for identification of Ce.

Due to this issue, the CeLβ peak was chosen to quantify Ce. This peak was still of first order and is viable for identification of the Ce, however, several challenges was associated with this as well. Firstly, the problem with the Ba-overlap still persisted, although only in analysis with a high Ba amount. Secondly, another overlapping element, the NdLα peak had some slight interference with the CeLβ. The first program designed was based on Table 3.2.

The analysis was run on program 1 to test if the interference between the CeLβ1, NdLα1 and BaLβ2 peaks would cause an issue. The second program (Table 3.3) analyze the CeLβ on the LIFF crystal instead of the LPET crystal. This seemed to improve the accuracy of the Ce and was further used for analysis of nordite.

TABLE 3.2. Program 1 (CeLβ LPET)

Crystal	Peak			
PET	CaKα			
LTAP	NaKα	ZnLα	MgKα	
LPET	LaLα	BaLα	CeLβ	
LLIF	FeLα	MnKα	PrKα	NdLβ
TAP	SiKα	SrLα		

TABLE 3.3. Program 2 (CeLβ LIFF)

Crystal	Peak				
PET	CaKα				
LTAP	NaKα	ZnLα	MgKα		
LPET	LaLα	BaLα			
LLIF	FeKα	MnKα	PrKα	NdLβ	CeLβ
TAP	SiKα	SrLα			

Another problem related to the elemental overlap in the WDS, was overlap between Zn and Na. In the initial analysis of nordite (performed in august 2019) it was discovered that there is an interference of ZnLβ on NaKα (Fig. 3.3). The ZnLβ peak lies +282 from the NaKα, which means that some of counts of the tail peak of ZnLβ would be counted as NaKα. This leads to a slight overestimation of Na. This problem was corrected for when nordite was re-analyzed in October 2019, by using an analytical program on the Cameca software. The program includes an overlap correction for the ZnLβ and NaKα peaks, as well as only using -900 as backgroud for NaKα to avoid any tail peak interference from ZnLβ (Fig. 3.3). However, the analysis are still not satisfactory. In particular, ZnO is still underestimated if compared to Upton *et al.* (1976) results of the same material. Upton *et al.* (1976) reports ZnO of 9.74 wt% while the analysis of this study results in 8.60 wt% ZnO. This issues was not solved, and values used for this thesis were the results of the analysis done in October 2019. A possible solution could be to analyze Zn on the ZnKα x-ray line instead, which is something that could be done with further research.

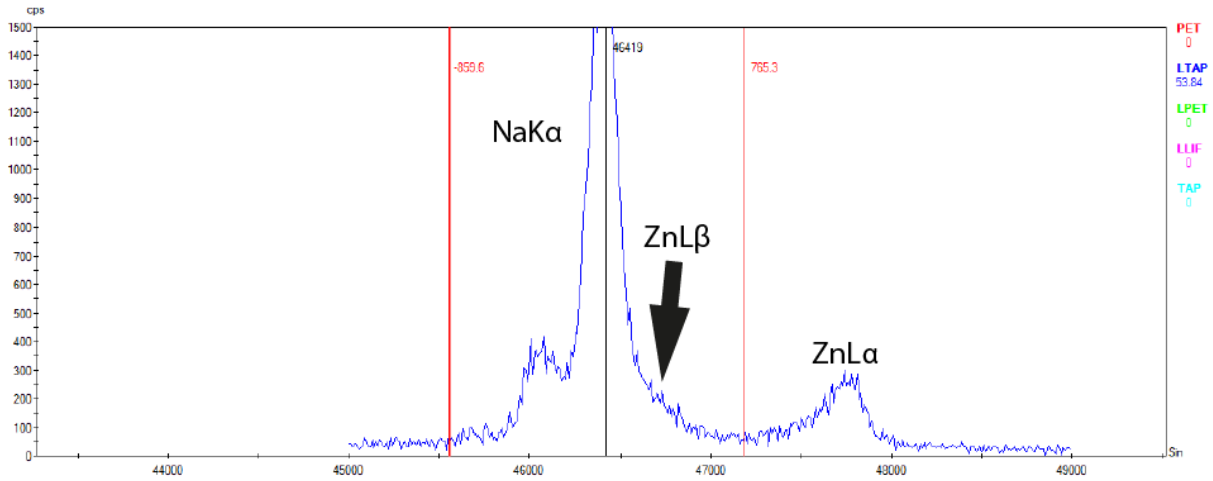

Figure 3.3: WDS spectrum of NaKa. Peak on the right is ZnLa. At NaKa + 282, ZnLb occurs.

3.6 Powder X-ray diffraction (PXRD)

Powder X-ray diffraction was used for preliminary analysis of the material. The instrument used was a Siemens D5005 X-ray Diffractometer, located at the Natural History Museum in Oslo. An acceleration voltage of 20.0 kV and current of 5.0 mA was used.

The sample is prepared by first breaking of a part of the targeted mineral, then crushed it in a mortar with ethanol. It is important to crush it well so that all crystal orientations are represented, and not just the preferred orientation of the crystal. A good grind also ensures a better signal to background ratio.

The structural data obtain from an XRD analysis can be used in combination with chemical data from the EDS to determine which mineral is present in your sample.

The use of PXRD for structural analysis is almost obsolete, due to the introduction of the SXRD. It still serves as a valuable tool for quick structural identification of minerals, but the data will not be used for describing minerals, unless no material suitable for SXRD is available. The data could be used to complement what is found in the structural analysis using the single crystal diffractometer.

3.7 Single Crystal Diffractometer (SXRD)

A Rikaku Oxford Diffraction XtaLAB Synergy-S single crystal diffractometer located at the Natural History museum was used for structure analysis of the nordite. The instrument is equipped with a Hybrid Photon Counting Detector (HyPix-6000HE) and two PhotonJet-S

microfocus sealed tube X-ray sources (Cu and Mo radiation). An acceleration voltage of 50.0 kV and current of 1.0 mA was used.

For the nordites, the Mo-radiation was used in the experiment to obtain data for crystal structure refinements. The Cu-radiation is mainly used for material containing lighter elements, very twinned or extremely small crystals. This method can still provide quality data for structure refinement, but was not used when experimenting on nordite.

Strengths of this method is that it provides unit cell dimensions, bond-lengths, bond-angles and site ordering information, making up a detailed crystal structure. In addition, powder patterns can also be produced using the Gandolfi method. This was the case when trying to identify a single crystal in a quick fashion. The Gandolfi method is an alternative to the standard analysis by PXRD. While standard XRD requires a significant amount of powdered material to produce results of good quality, the Gandolfi method only requires a single crystal of the selected mineral. With the unrestricted movement of the goniometer, the Gandolf method is able to simulate the powder phase of the single crystal. The data quality of the Gandolfi method opposed to standard PXRD can be worse as it is only a simulation and minute amount of material is used (down to 20 µm grains), but the speed of the analysis makes it a valid option when identifying minerals. In addition, if Gandolfi shows the sample is of interest, further analyses such as SXRD or EPMA can be carried out as it is non-destructive.

The software package that was used were CrysAlisPro. This package is split into two separate programs: (I) The “online” program used to control the operation of the diffractometer and for data collection and (II) the “red” program used for data reduction, processing and integration.

When handling the Igdlutalik samples (EHG 1 – EHG 6 see appendix 8.1 for pictures) careful examination and extraction of nordite crystals from the hand samples were required. Due to the size and the minerals color, considerable time was required in detecting and extracting specimens.

For extraction of a single crystal, needles, knifes and scalpels of different size and shapes were used. By putting the extracted material inside oildrops on a glass slide, the nordite crystals could be separated out from the rest of the extracted material. If necessary, the nordite specimen could be further reduced in size to make fragments that most likely resembles a single-crystal. For high-quality SXRD data of minerals with highly absorbent elements (i.e. Ba and REE) the preferred crystal size for analyses is <100µm.

Similar to the samples from Igdlutalik, the Taseq nordites also proved a challenge to extract. This was amplified by the fact that the matrix mineral (ussingite) is fairly similar in color, especially the purplish version of the mineral. Due to this, the most efficient way of extracting nordite was to break off a small part of the handsample and put it in a mortar. With a light crush of the material the different phases separated and could be further processed. By placing the mortar with the powder under the Zeiss Stemi 508 Stereo microscope, nordite crystals could be singled out and extracted by needles or similar equipment.

Data integration

Processing of the RAW-data produced from analysis starts with a data integration. In short, the software CrysAlisPro "red" scans through each frame taken of the mounted material, and generates a 3D-image of each reflection that is produced. By putting a box around this produced 3D-spot, the intensity of the reflection is calculated through summing up all the detector counts situated inside the 3D-box (Blake *et al.*, 2009). This 3D-box can for example be adjusted if there is apparent twinning in the sample to help differentiate the different phases.

The intensity of all *hkl* reflections is what it needed to solve a crystal structure. However, several data corrections must be made before the final *hkl*-list can be further used to solve the structure of the crystal. An important correction that must be made, is the absorption correction. The absorption is dependent on the crystal size and morphology and, the materials chemical composition. In general, the heavier the elements the larger the absorption, which makes it important to know what type of element composition you are analyzing. For the experiments regarding nordite, microprobe data (Appendix 8.3) acquired at an earlier stage of this research was used for correction. In addition, the size of the crystal in drawn in CrysAlisPro "red" (Fig 15.) to account for the path length of the X-rays. Lastly, the wavelength of the X-ray source is also a vital part of the absorption correction (Blake *et al.*, 2009). As mentioned earlier, Mo-radiation was used when analyzing nordite.

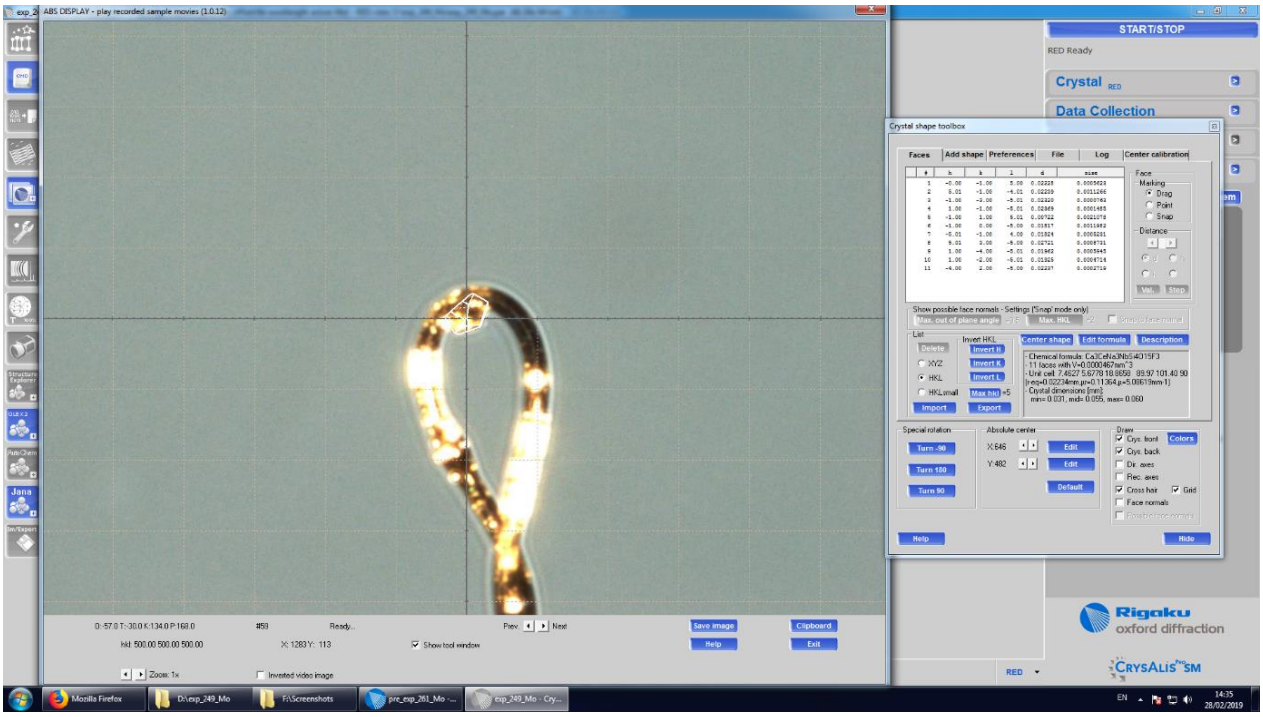

Figure 15: The user interface of CrysAlisPro and the crystal shape drawing tool used for face indexed absorption correction.

Structure solving and refinements

The structure solving and refinements were done by a combination of softwares. WinGx (Farrugia, 2013) was used as the interface-program controlling the refinements processed by the Shelx-package. The structures were solved by direct methods using ShelXS (Sheldrick, 2013) and refined by ShelXL (Sheldrick, 2015). The refinements were carried out by using neutral atom scattering factors. When all atoms were located, they were refined using anisotropic displacement factors. This did not lead to any problem. The occupancy for each site was slowely released and for some sites dual occupancy was refined, e.g. Sr and Ba in the X-site of the Taseq slope samples. Details of the experimental conditions can be found in appendix. 8.13. In addition, Vesta (Momma & Izumi, 2011) was used for modeling of the crystal structure during the refining, mainly to help get a visual aspect of the positioning of the different atoms in the crystal structure. Finally, Vesta was used for the structural figures in this thesis, with some slight modifications in Adobe Illustrator.

3.8 Laser Ablation Iductively Coupled Plasma Mass Spectrometry (LA-ICP-MS)

Thin sections EHG 4, EHG 13, EHG 7, EHG 10, EHG 15 as well as EHG EPOXY were all subject to analysis for trace elements at the Department of Geosciences, University of Oslo. Several minerals were targets for the analysis, including the nordite, aegerine, arfvedsonite and narsasukite.

A Q-ICPMS Bruker Aurora Elite M90 equipped with a Cetac LSX-213 G2+ laser was used for analyzing the samples. The isotopes for the trace elements include: ^{23}Na, ^{65}Zn, ^{85}Rb, ^{88}Sr, ^{89}Y, ^{91}Zr, ^{93}Nb, ^{133}Cs, ^{137}Ba, ^{139}La, ^{140}Ce, ^{141}Pr, ^{144}Nd, ^{150}Sm, ^{152}Eu, ^{157}Gd, ^{159}Tb, ^{162}Dy, ^{165}Ho, ^{167}Er, ^{169}Tm, ^{173}Yb, ^{175}Lu, ^{178}Hf, ^{181}Ta, ^{232}Th and ^{238}U. The Glitter software was used for isotope data calculations. For the internal standard, the silica data from the EPMA analysis was used. External standards “NIST610” and “BCR2G” were used to monitor the instrument while analyzing.

The settings used for analysis were: 40 μm spotsize, 10 % laser energy, 10 Hz laser shot frequency, 10 s shutter delay and 400 burst count. A slight moderation was made to the settings when doing standards, changing the spot size to 50 μm and the laser energy to 15 %.

Problems

Firstly, the accuracy of the point chosen on the software controlling the laser was not correctly calibrated. This meant that accurately hitting the wanted spot for analysis was difficult. Furthermore, the optical microscope on the instrument was not impressive, so even though pictures of the wanted areas had already been taken, it was hard to locate and hit targeted crystals. Thirdly, the spotsize required for getting satisfactory results was for some crystals to large. Fourthly, especially the nordite from Taseq showed zonation and were generally small, making it impossible to analyse chemically homogeneous areas. Finally, to avoid detector saturation of elements: Sr, Ba, Ce, La, Nd and Pr, an attenuation filter was applied.

4. Results

4.1 Field observations

The locality at Igdlutalik Island was visited once, while the locality on the Taseq Slope was visited twice during the three-week fieldtrip.

4.1.1. Igdlutalik

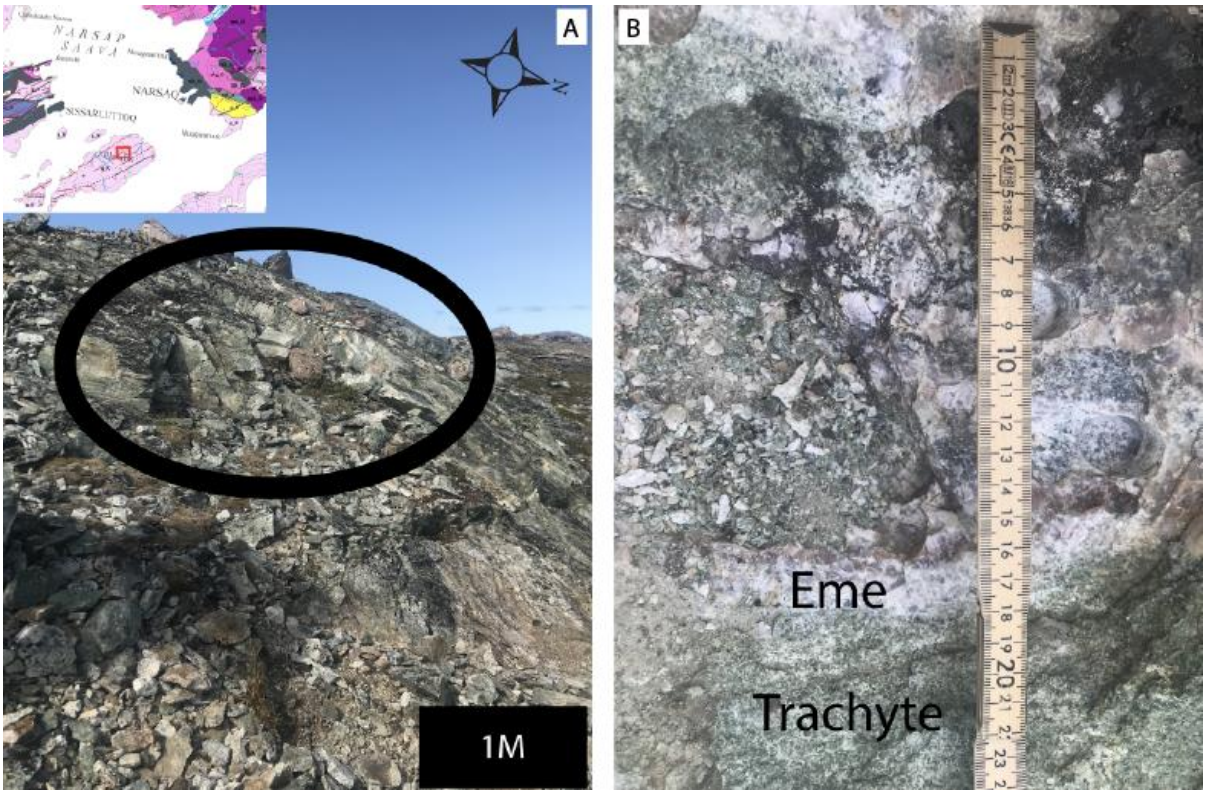

FIGURE 4.1: The Igdlutalik Island locality. A: The blasting site. B: Emeleusite (Eme) that has been blasted out. In the adjacent trachyte, is where the nordite has been found. The inset is from GEUS' "Grønlandsportalen", where the red box corresponds to the satellite image.

Due to some inaccurate GPS points, and dense fog, there were some trouble finding the locality on Igdlutalik Island. Fig. 4.1 A shows the overview of the locality. A closer look at the area where material was collected is seen in Fig. 4.1 B. In search for more occurrences of this particular paragenesis, the trachyte dyke was followed in a SW and NE direction. The dykes contact with the adjacent host rock was studied, but no similar occurrence was found. Several GPS points were taken along the dyke to get an overall direction and extent of the intrusion (Fig. 4.2).

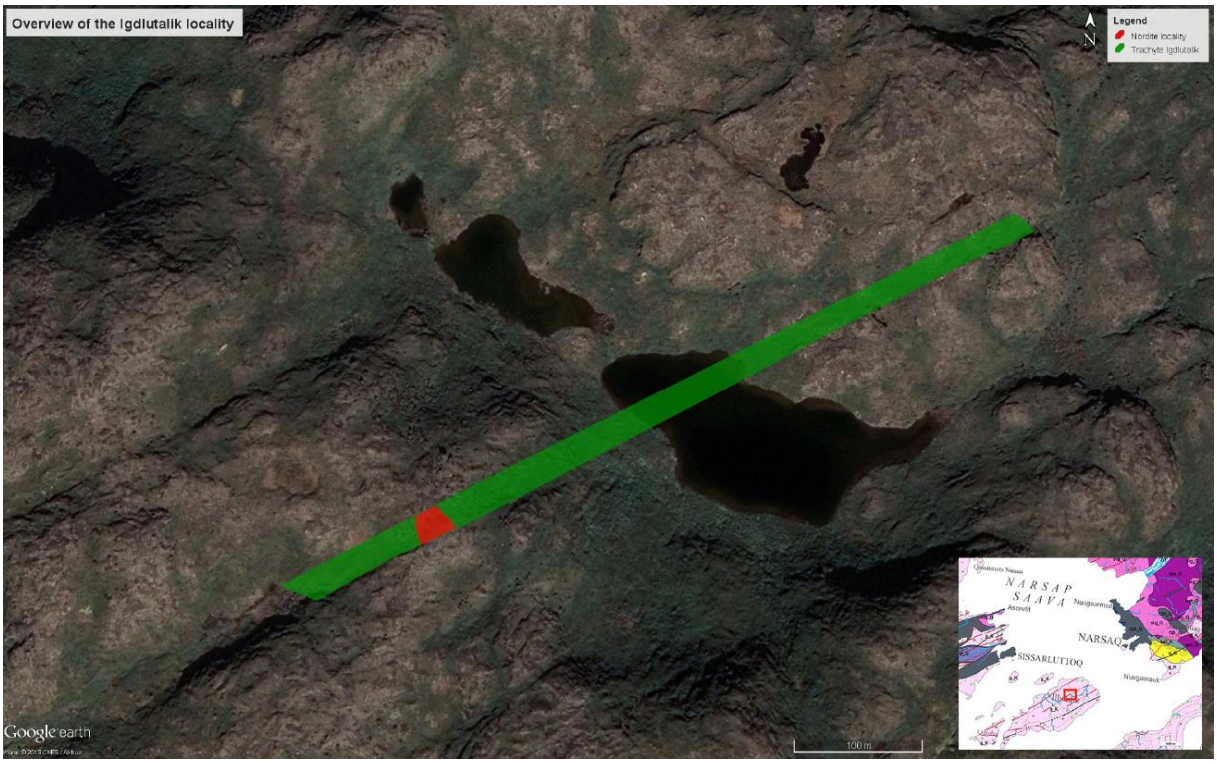

FIGURE 4.2: Map over the Igdlutalik locality, with the mapped trachyte dyke. Background picture from Google Earth. The inset is the same as in Fig. 14A, where the red box corresponds to the satelillite image

4.1.2 Taseq Slope

A GPS position previously saved by Henrik Friis was used to locate the nordite boulder. The boulder was situated in the SE part of the Taseq slope. It can be found 20-30 meters downhill from "the large ussingite-vein" (Fig. 4.3 A). In addition to the nordite boulder in Fig. 4.3 B, smaller samples of the same material were found while following a stream upwards to the large ussingite vein. Despite conducting a thorough investigation of the area, it was not discovered *in situ* nordite-bearing material on the Taseq Slope.

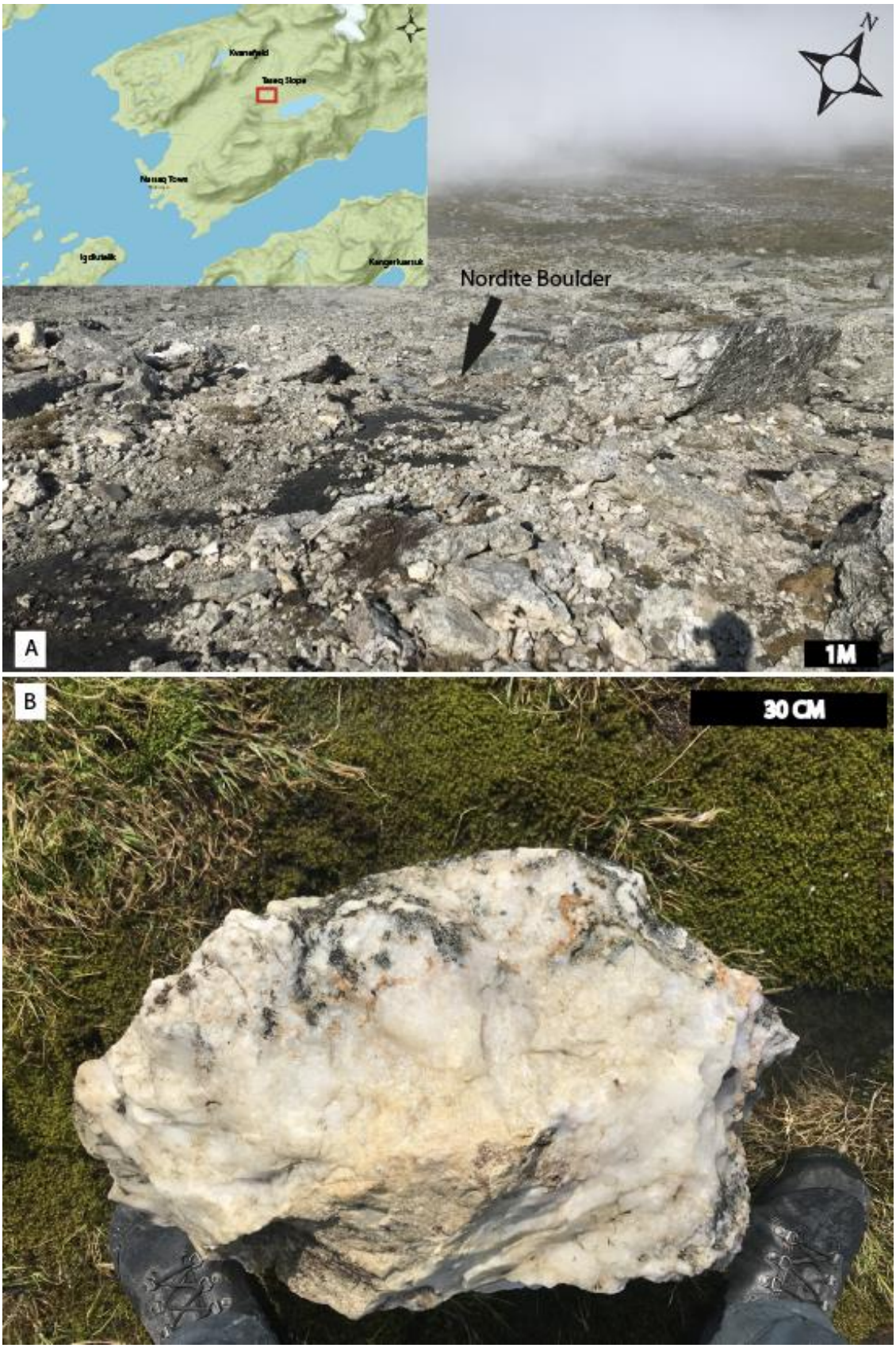

FIGURE 4.3: A: Looking down the Taseq slope from "the large ussingite vein" with the locality of the nordite boulder downstream. The inset is taken from GEUS' "Grøndlandsportalen" where the red box corresponds to where the picture was taken. B: The nordite boulder where most of material for this thesis is from.

4.2 Paragenesis and petrography

4.2.1 Optical

4.2.1.1 Igdlutalik Island

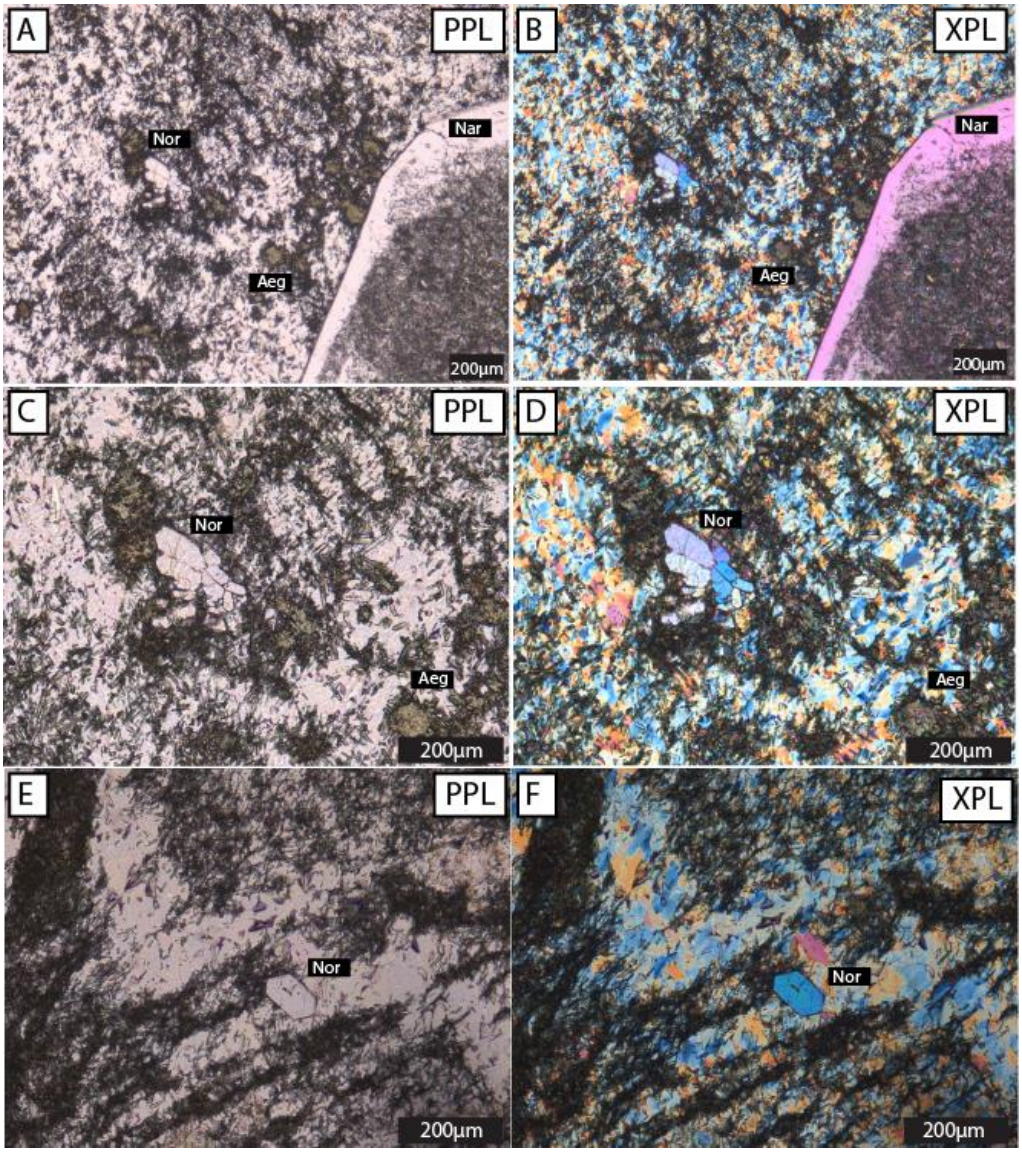

FIGURE 4.4: PPL and XPL view of selected area of the EHG4 sample from the Iglutalik Island.

The nordites shows a high birefringence interference color of up to third order blue as seen in the XPL view in Fig. 4.4 B, D and F. The nordite exhibits a rather high relief especially apparent in Fig. 4.4 E and F compared to the matrix minerals. The nordites show a homogeneity in the crystals apparent in the XPL (i.e. Fig. 4.4 B, D and F) view of the minerals. The size of the nordite crystals ranges from 20 µm -100 µm, and occur both as clusters (i.e. Fig. 4.4 A-D) and single crystals (i.e. Fig. 4.4 E-F). The narsarsukite crystal shows a homogeneity towards the rim of the crystal, while the core of the mineral consists of an assemblage of the matrix minerals. The green matrix mineral visible in Fig. 4.4 have crystal sizes up to 10 µm, and mostly occurs as clusters.

4.2.1.2 Taseq Slope

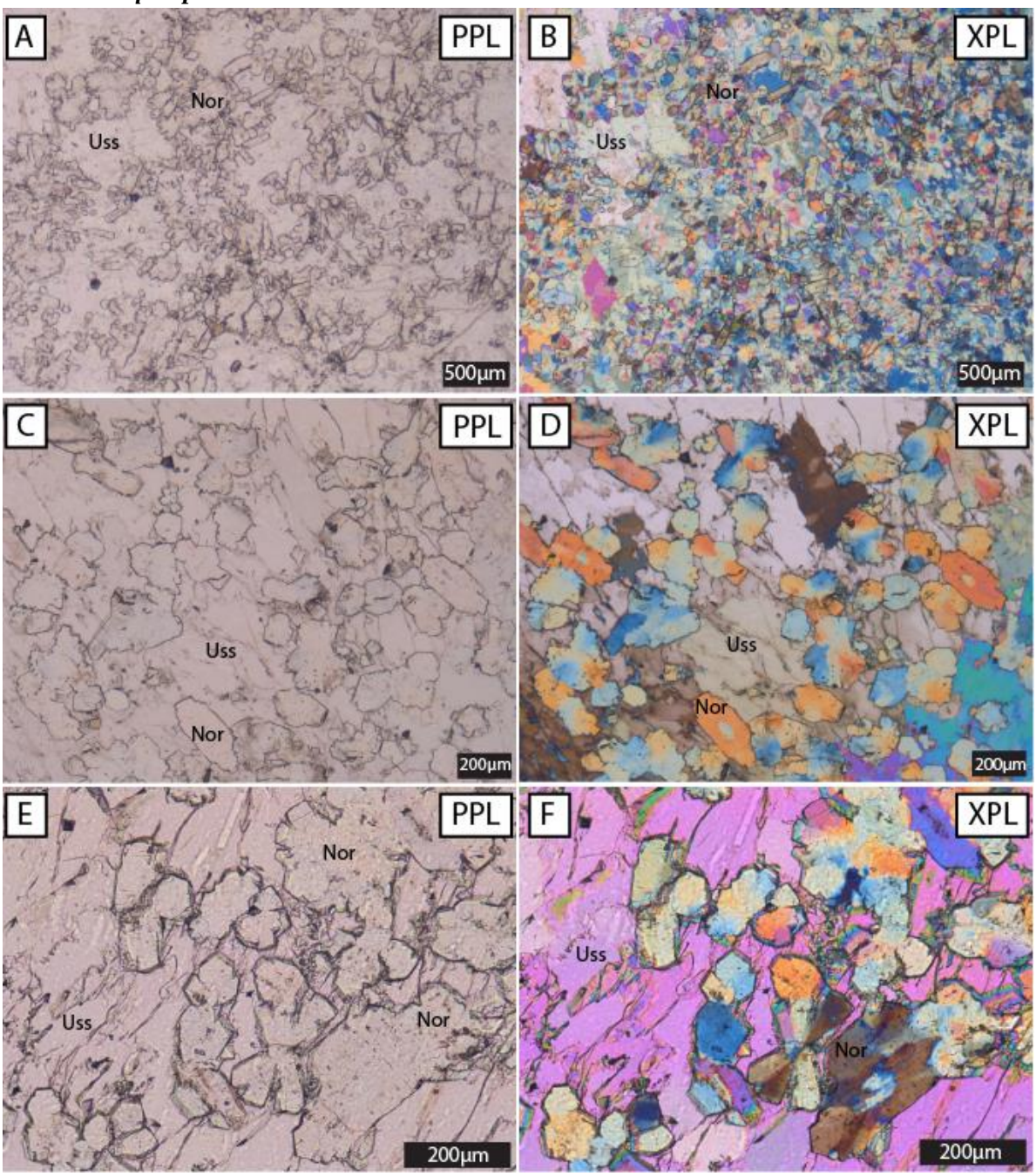

FIGURE 4.5: PPL and XPL view of selected area of the EHG 10 sample from the Taseq slope.

There are several large concentrations of nordite as seen in Fig. 4.5, which is typical for the Taseq occurrence. The nordites show a high interference color up to third order pink, and exhibits a higher relief than the matrix mineral ussingite. The intricate growth of the nordite crystal is visible in Fig. 4.5, especially in the close-up (Fig. 4.5 E-F). In addition, a core can easily be drawn out from the XPL view of the mineral (i.e. Fig. 4.5 D and F), due to the difference in interference colours. Almost no isolated single crystal can be seen in the thin sections. The size of the crystals ranges from 30 µm – 275 µm.

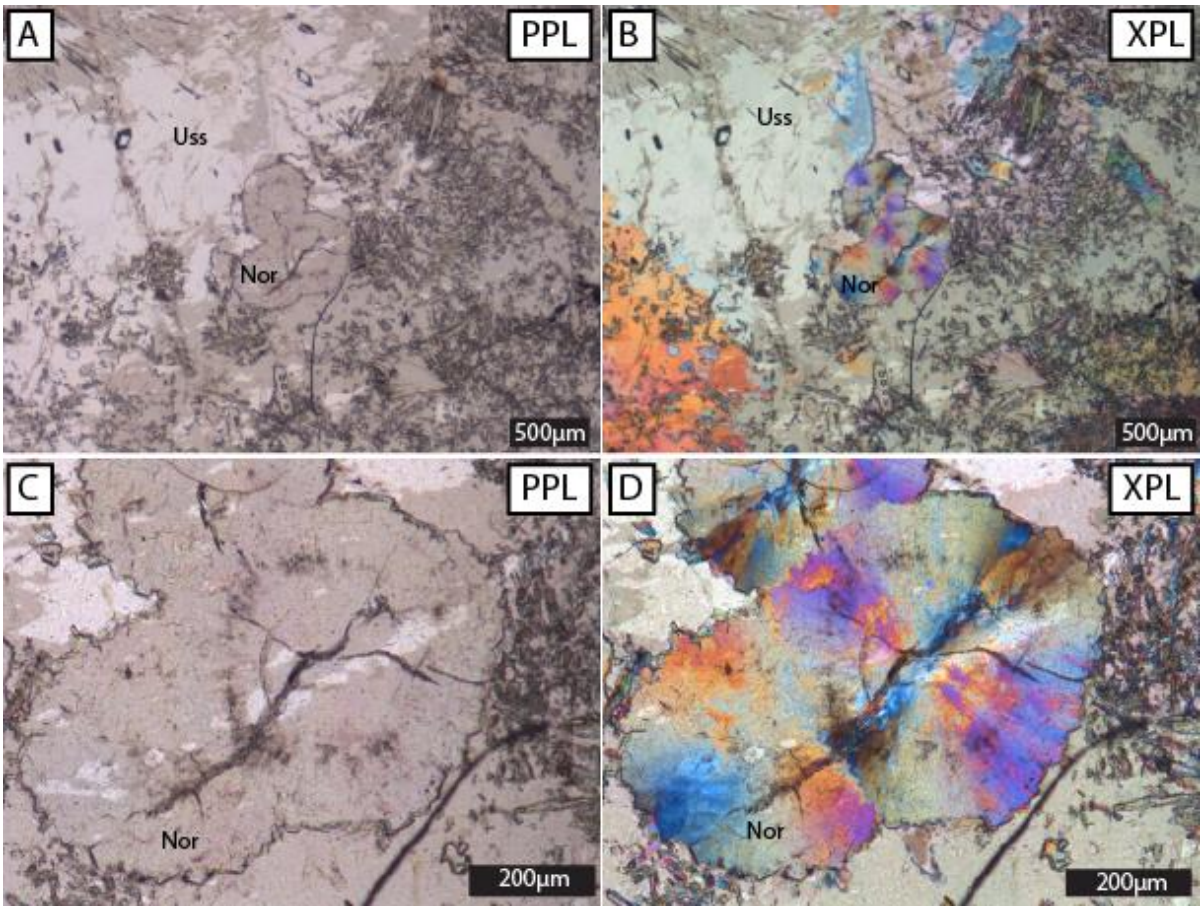

FIGURE 4.6: PPL and XPL view of selected area in sample EHG 10 from the Taseq Slope.

Figure 4.6 shows a large accumulation of nordite crystals. From the XPL view (i.e. Fig. 4.6 B and D) it is shown that at times the nordite forms fine-grained radiating aggregates up to 400 µm across. Figures 4.5 E and F shows a few coarser grained crystals growing in a similar way. The fine grained radiating growth results in a characteristic “bullseye” occurring when looking at the nordites in XPL.

4.2.2 SEM-EDS

4.2.2.1 Igdlutalik

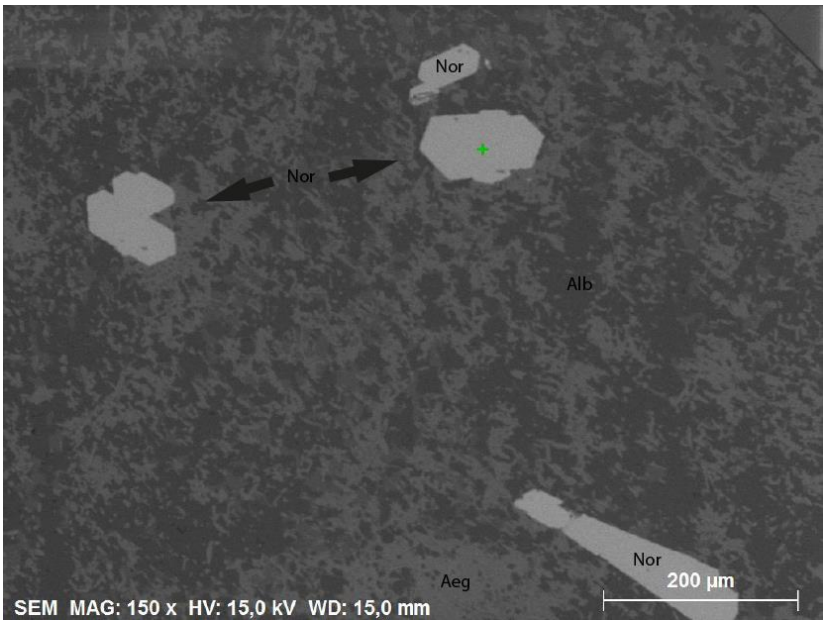

FIGURE 4.7: Backscatter image of nordites in EHG4. The matrix consists of a dark and bright mineral.

Figure 4.7 shows a backscatter image of nordites in EHG4. From the image there is a clear contrast between the nordites and the matrix minerals, with the nordites exhibiting a brighter color signifying a heavier elemental content. The homogeneity exhibited in the optical microscopy concurs with what seen in Fig. 4.7.

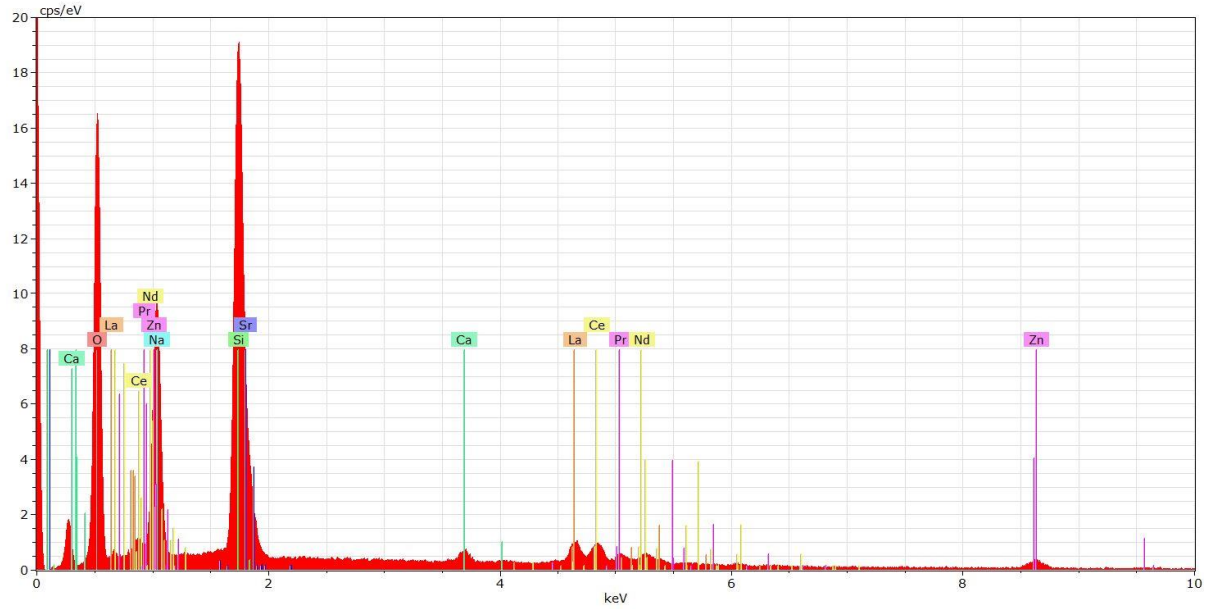

FIGURE 4.8: Representative EDS spectrum of the nordites in EHG4. Taken in the green point in Fig. 4.7.

Figure 4.8 illustrates challenges of elemental overlap for several of the elements during EDS analyses. Due to the overlap, ratios between the elements such as Si/Sr and Na/Zn are hard to interpret. This means that the quantification of the elements from the EDS analysis will yield skewed values and cannot be used comparing compositions. However, the results give indicators that help with the qualitative analysis conducted.

Because of the nordites homogeneity in EHG4, the EDS spectrum in Fig. 4.8 is representative for all the nordites in EHG4.

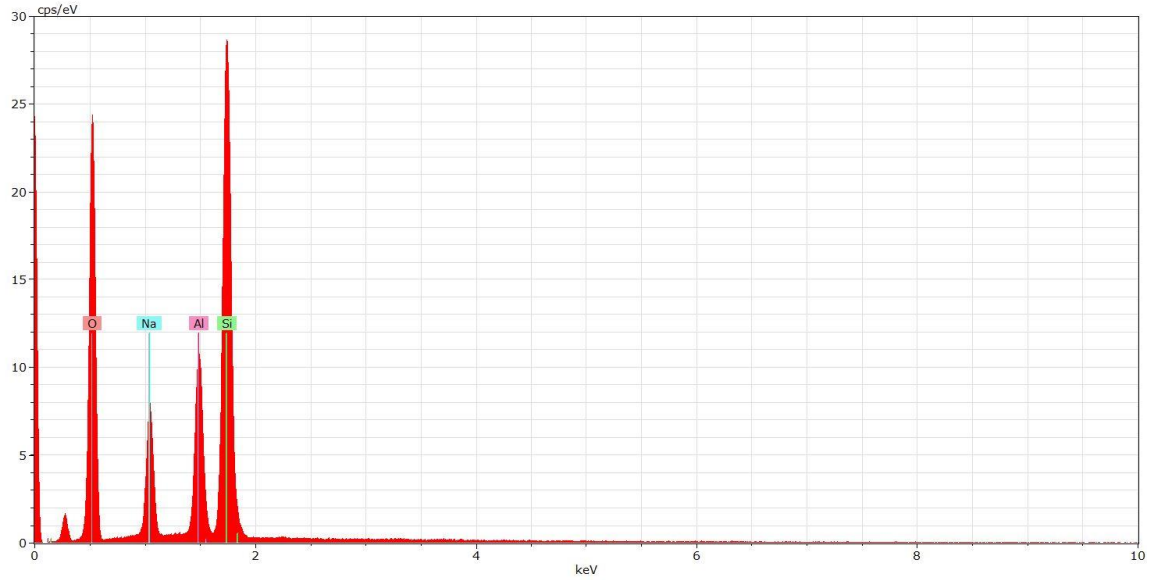

FIGURE 4.9: EDS spectrum of the dark matrix mineral seen in both Figs. 4.7 and 4.11 A.

Figure 4.9 shows the EDS of the darker mineral in the matrix, that has the elemental ratio between Na, Al and Si of approximately 1:1:3 which corresponds well with the ideal formula of albite. The slighty elevated Al content is related to the common issue with EDS analysis as mentioned in section 3.4.

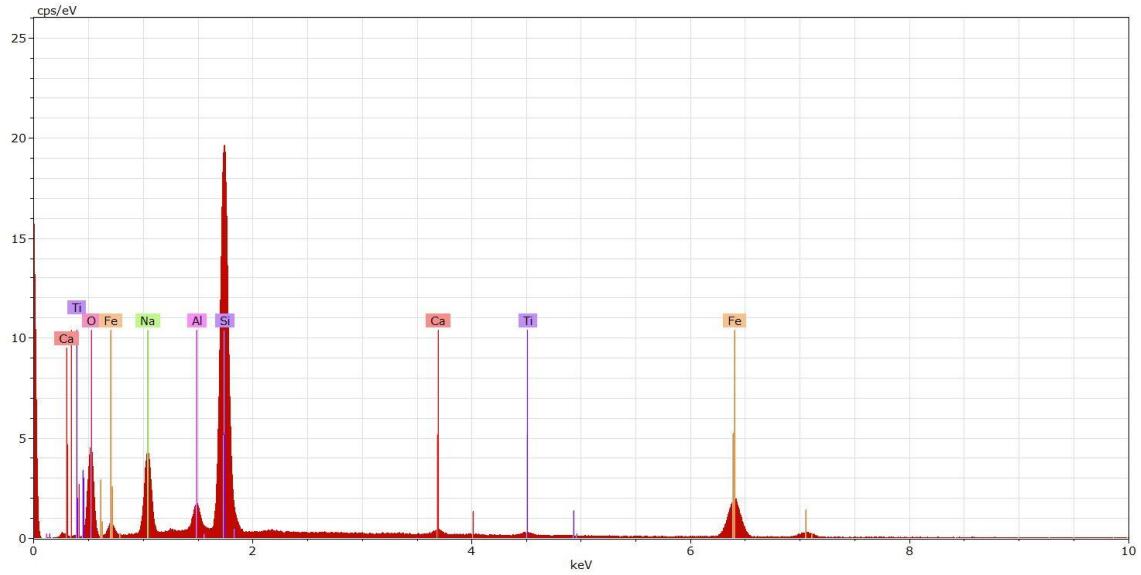

FIGURE 4.10: EDS spectrum of the brighter matrix mineral seen in Figs. 4.7 and 4.11 A.

Figure 4.10 shows the EDS of the medium grey mineral in the matrix of Figs. 4.7 and 4.11 A. The approximate 1:1 ratio between the elements Na/(Fe+Ti+Al) together with the Si content, would correspond to the ideal formula of aegirine.

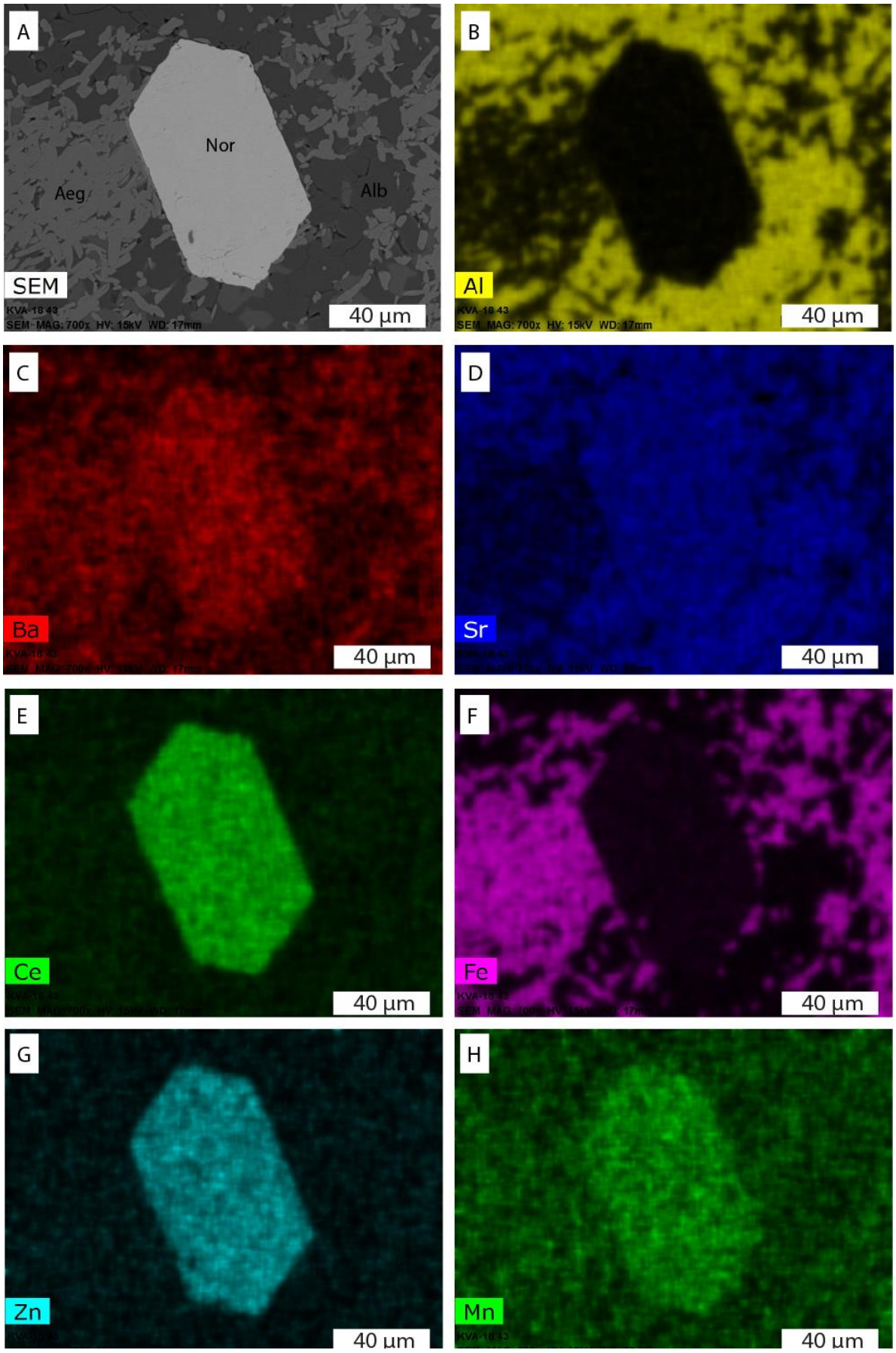

FIGURE 4.11: EDS mapping of elemental distribution in a nordite crystal from EHG4. A: EDS backscatter image. B: Al map. C: Ba map. D: Sr map. E: Ce map. F: Fe map. G: Zn. H: Mn

Figure 4.11 shows images of elemental mapping of the selected elements (Al, Ba, Sr, REE (represented by Ce), Fe, Zn and Mn) in a nordite from EHG4. These elements were selected based upon publications on the nordite minerals (Tables 2.3, 2.4 and 2.5). There is a clear Al deficiency in the nordite crystal evident by Fig. 4.11 B. In both the Ba and Sr map, one can make out the crystal shape of the nordite. However, more uncertainty is related to the Ba and Sr in the regards to that the primary Sr peak is closely related to Si peak, causing an interference between them (Fig. 4.8). Meanwhile the primary Ba peak has overlap with the primary La peak.

In Fig. 4.11 F you can see the clear difference in Fe concentration, with the aegirine having a relatively higher Fe concentration than the nordite. The overall distribution of Ce, Zn and Mn seems to be more or less equal throughout the nordite crystal.

4.2.2.2 Taseq Slope

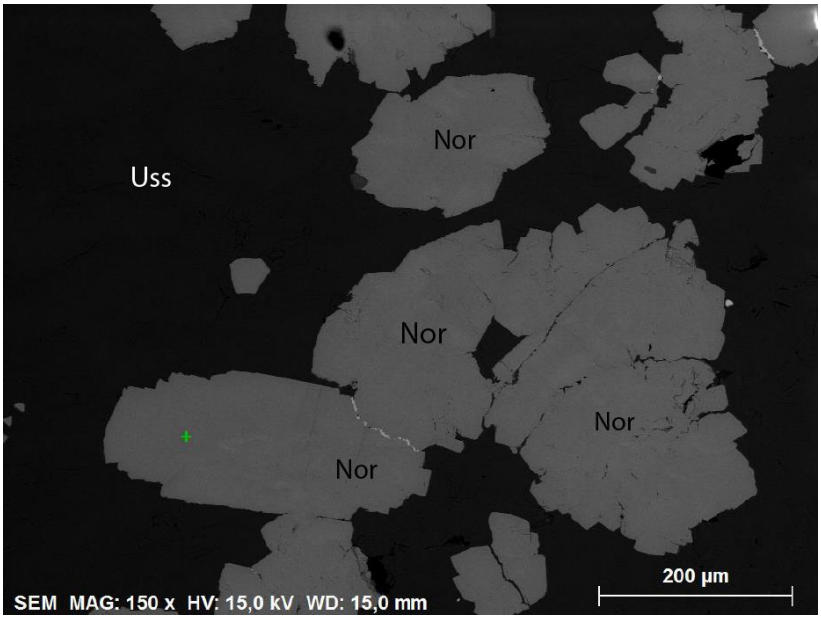

FIGURE 4.12: EDS backscatter image of nordites from Taseq in EHG7.

Figure 4.12 shows a backscatter image of nordites in EHG7. There is a clear contrast difference between the nordites and the matrix mineral ussingite. The contrast is so significant that the ussingite appears black. In addition, there is several brighter areas in the nordites. This would imply that contrary to the nordites of Igdlutalik (EHG4), which are more or less homogeneous, the nordites of Taseq are inhomogeneous. The green point in Fig. 4.12 is the target for the spectrum given in Fig. 4.13. Even though the quantification is not reliable, it is clear that there are several differences between the spectrums (Figs. 4.8 and 4.13)

of nordites in EHG4 and EHG7. Firstly, Fig. 4.13 shows that the EHG7 nordite contain Ba which is not something that we see in nordites in EHG4 (Fig. 4.8).

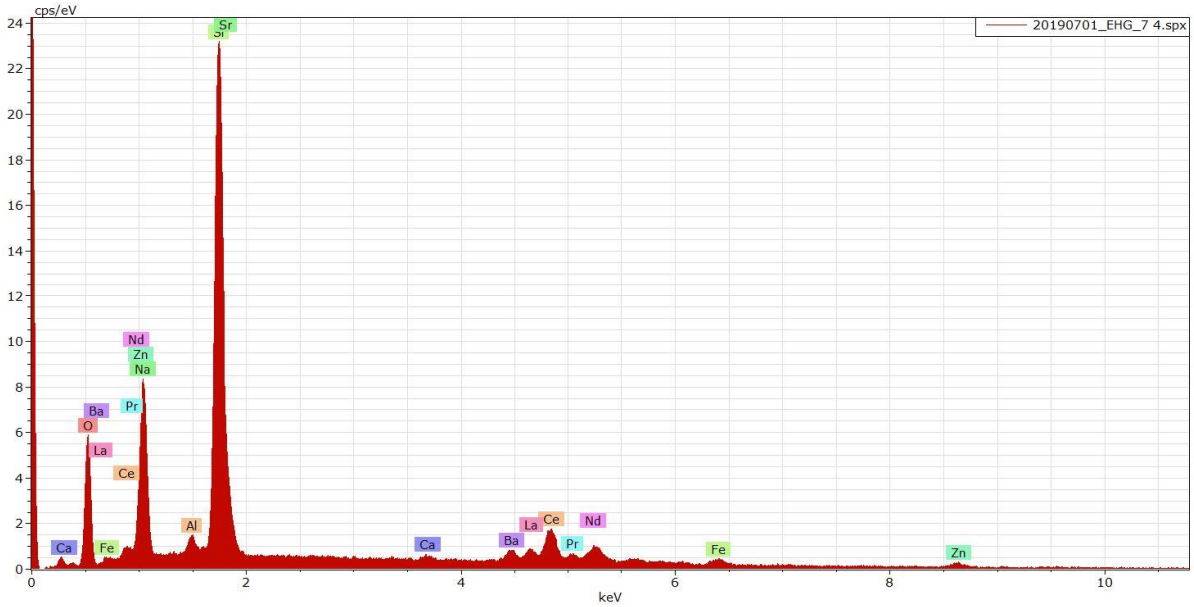

FIGURE 4.13: EDS spectrum of the green point in Fig. 4.15.

Furthermore, there seem to be an elevated Ce content opposed to the other REE when compared to the Igdlutalik sample (Fig. 4.8), but this may also be a consequence of the elemental overlap from Ba. Lastly, the Sr/Si content seems to be higher in EHG7 than in EHG4.

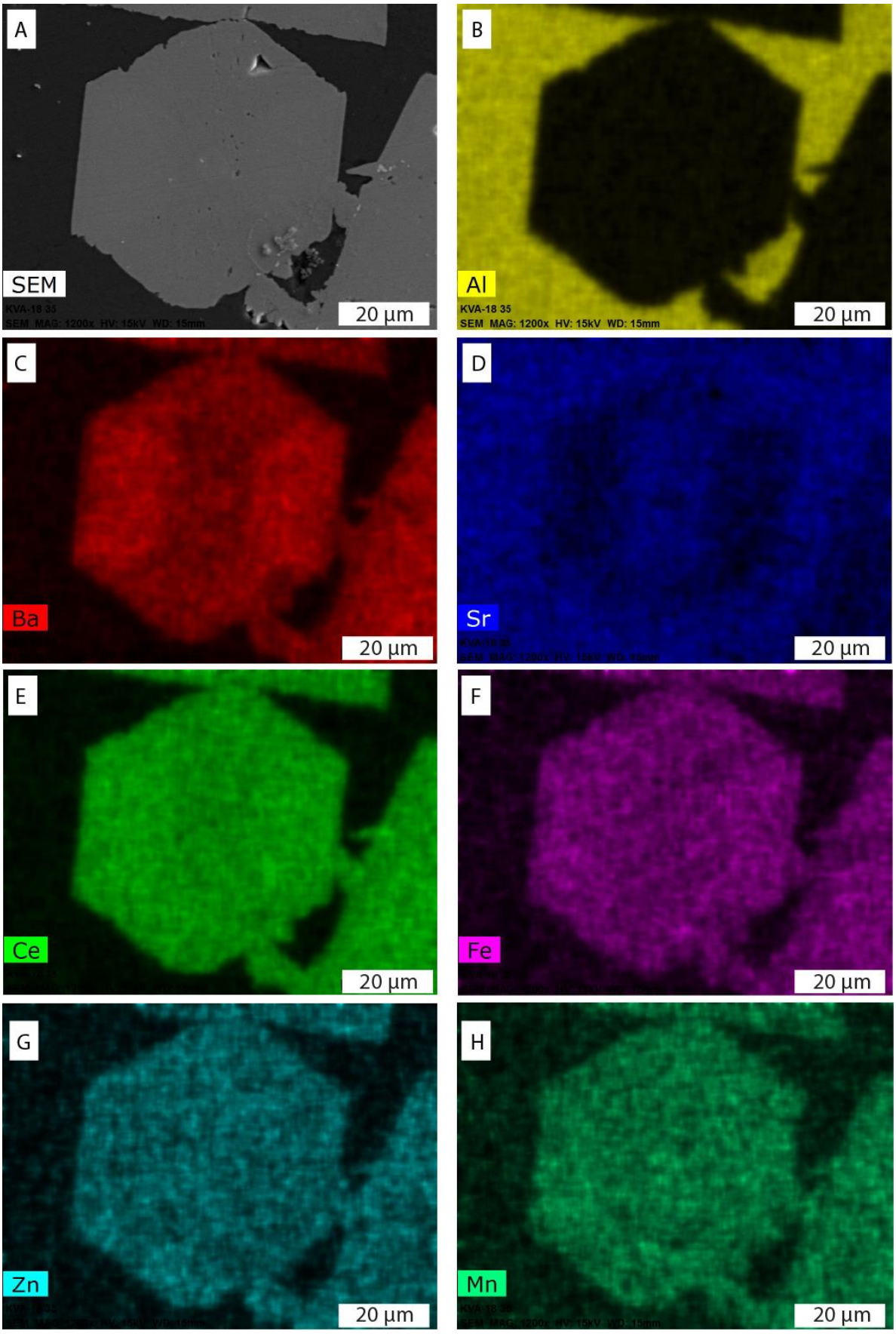

FIGURE 4.14: EDS mapping of elemental distribution in a nordite crystal from Taseq in EHG_EPOXY. A: EDS backscatter image. B: Al map. C: Ba map. D: Sr map. E: Ce map. F: Fe map. G: Zn map. H: Mn map.

Figure 4.14 shows the elemental mapping of the selected elements Al, Ba, Sr, Ce, Fe, Zn and Mn. The backscatter image of the nordite-crystal in Fig. 4.14 A is taken looking down an assumed *c*-axis of the mineral. Figure 4.14 B shows a clear lack of Al in the nordite, while the matrix mineral ussingite shows a higher concentration. By looking at Fig. 4.14 C and 4.14 D there is something that resembles a correlation between Ba and Sr concentrations within the mineral. The eastern and western side of the mineral in Fig. 4.14 C seems to be elevated in Ba, while the central part seems to have less Ba. To add to this, Fig. 4.14 D shows a higher concentration of Sr in the central part, but a decrease towards the eastern and western part of the crystal. However, in the core of the mineral, there is a clear increase in Ba again. If looked carefully the Ba zonation can be seen in the backscatter image.

One must note that the Sr-mapping could have been influenced by Si content, because the two elements have a considerable overlap in the EDS spectrum. This is why Fig. 4.14 D shows a relatively high Sr concentration in the matrix mineral ussingite, even though ussingite does not normally contain Sr.

From the mapping of Ce, Fe, Zn, and Mn, the distribution of the elements seems more or less homogeneous throughout the crystal as apparent in Fig. 4.14 E-H. Cerium represents the REE elements, due to the large overlap of the elements in the EDS spectrum, it is not possible to use the other REEs for mapping (Fig. 4.13). In Fig. 4.14 E there appears to be a small increase in Ce when Ba is also increased (Fig. 4.14 C).

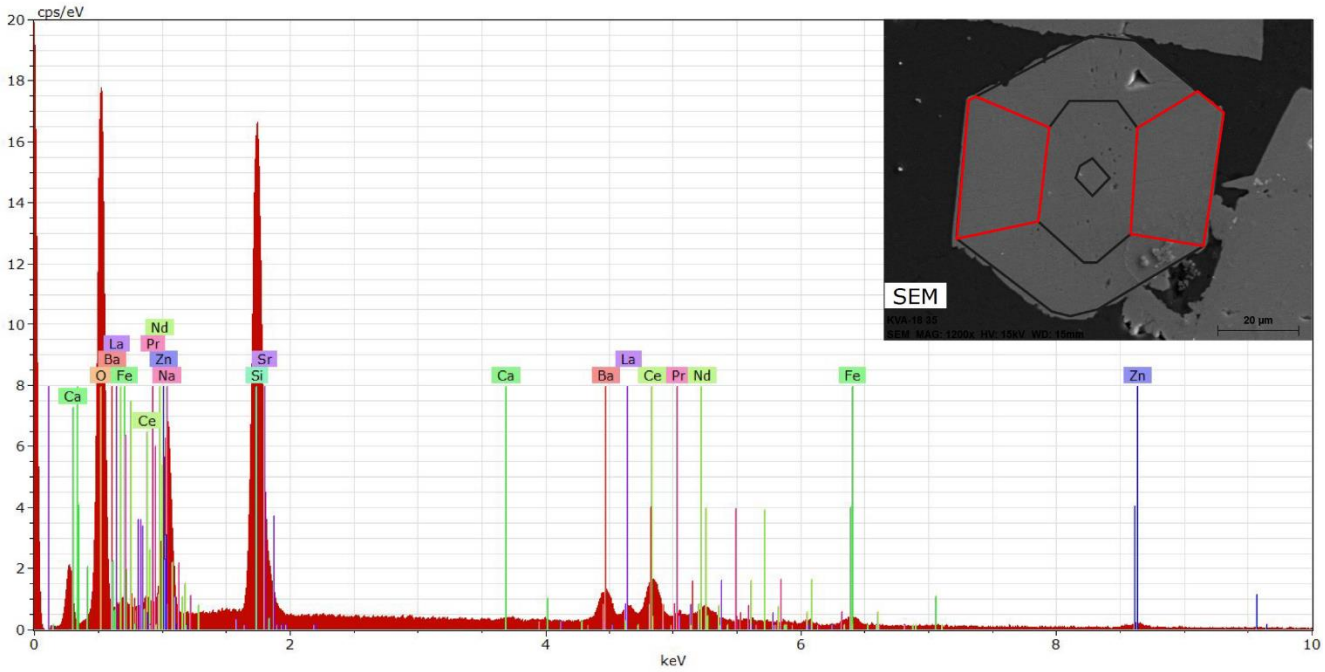

FIGURE 4.15: EDS spectrum representing the eastern and western sides (red) of the nordite crystal.

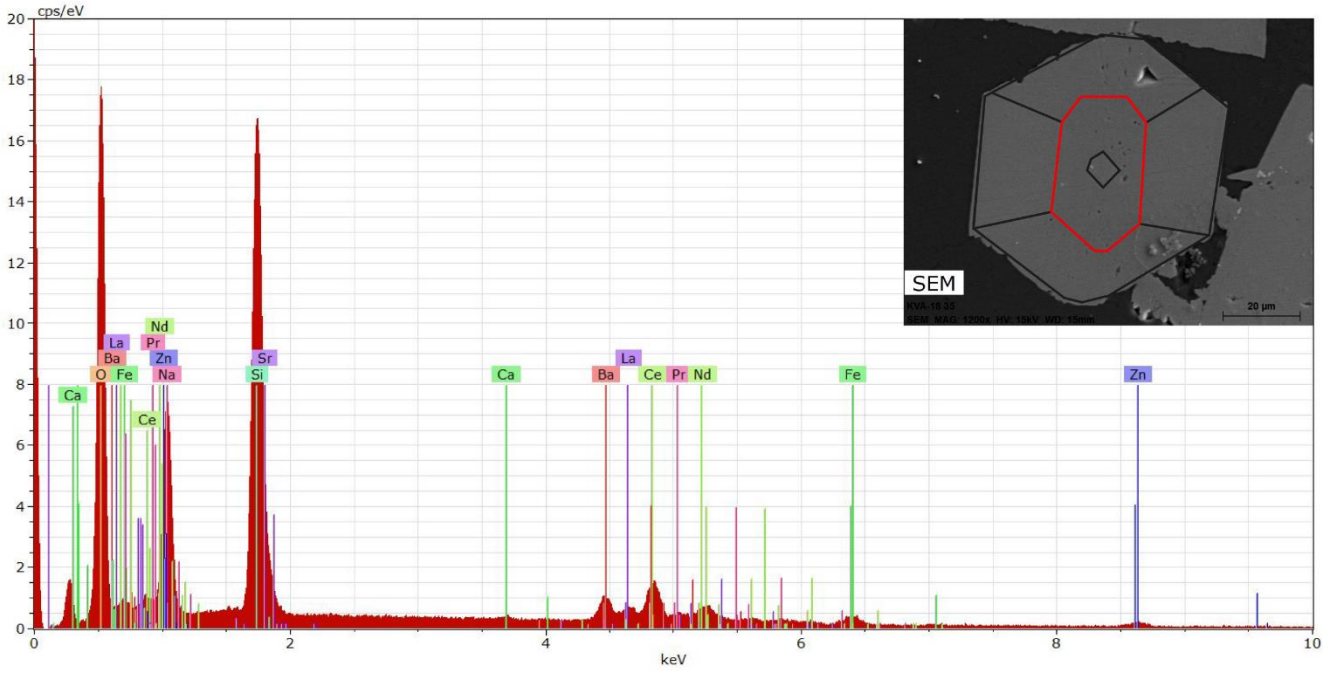

FIGURE 4.16: EDS spectrum representing the central part (red) of the nordite crystal.

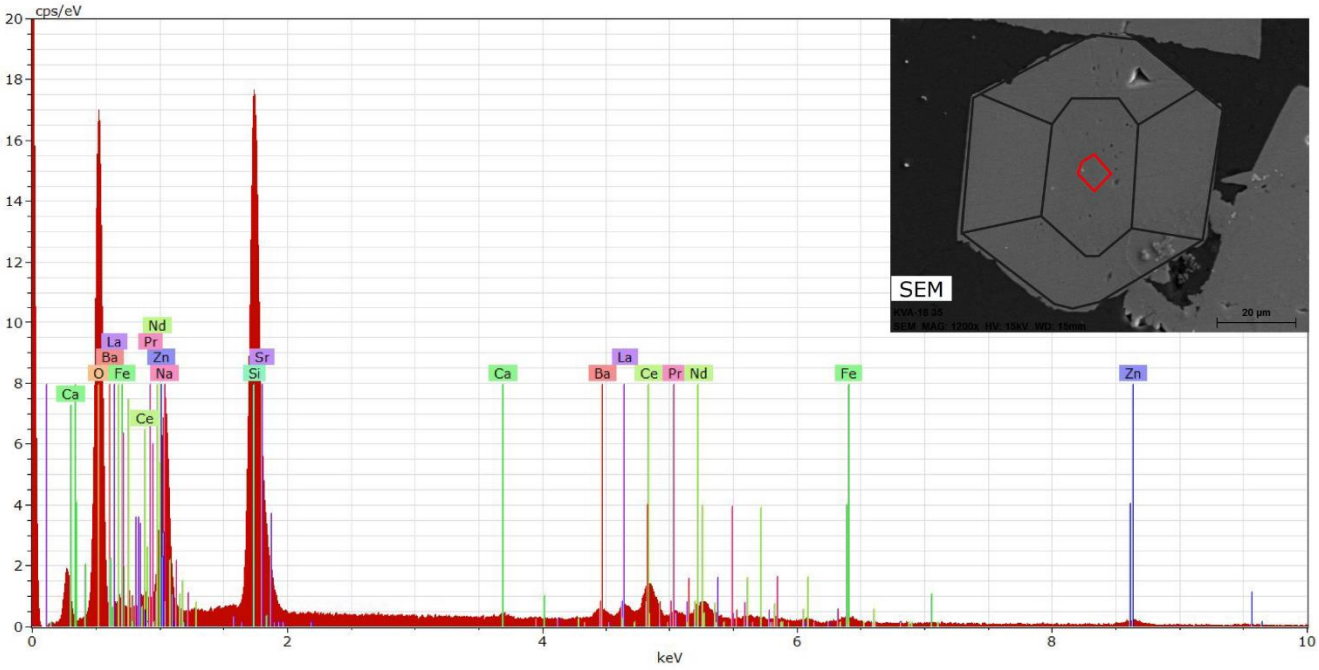

FIGURE 4.17: EDS spectrum representing the core (red) of the nordite crystal.

Figures 4.15, 4.16 and 4.17 shows the spectrums of different parts of the nordite crystal. These specific areas are based upon the results of the EDS elemental mapping shown in Fig. 4.14. Although Fig. 4.14 C and D clearly shows different zonations of Ba and Sr respectively, these are not that apparent in in Figs. 4.15 and 4.16. Despite this, a slight increase in Ba can be observed. If we include Fig. 4.17 which represents the core of the crystal there is a clear decrease in the Ba content, while the Sr peak seems to be elevated. This is contradictory to the Sr mapping in Fig. 4.14 D. In addition, it is once again important to note that the results of the EDS are only semi-qualitative and is only of supporting aid to the qualitative work of the EPMA results.

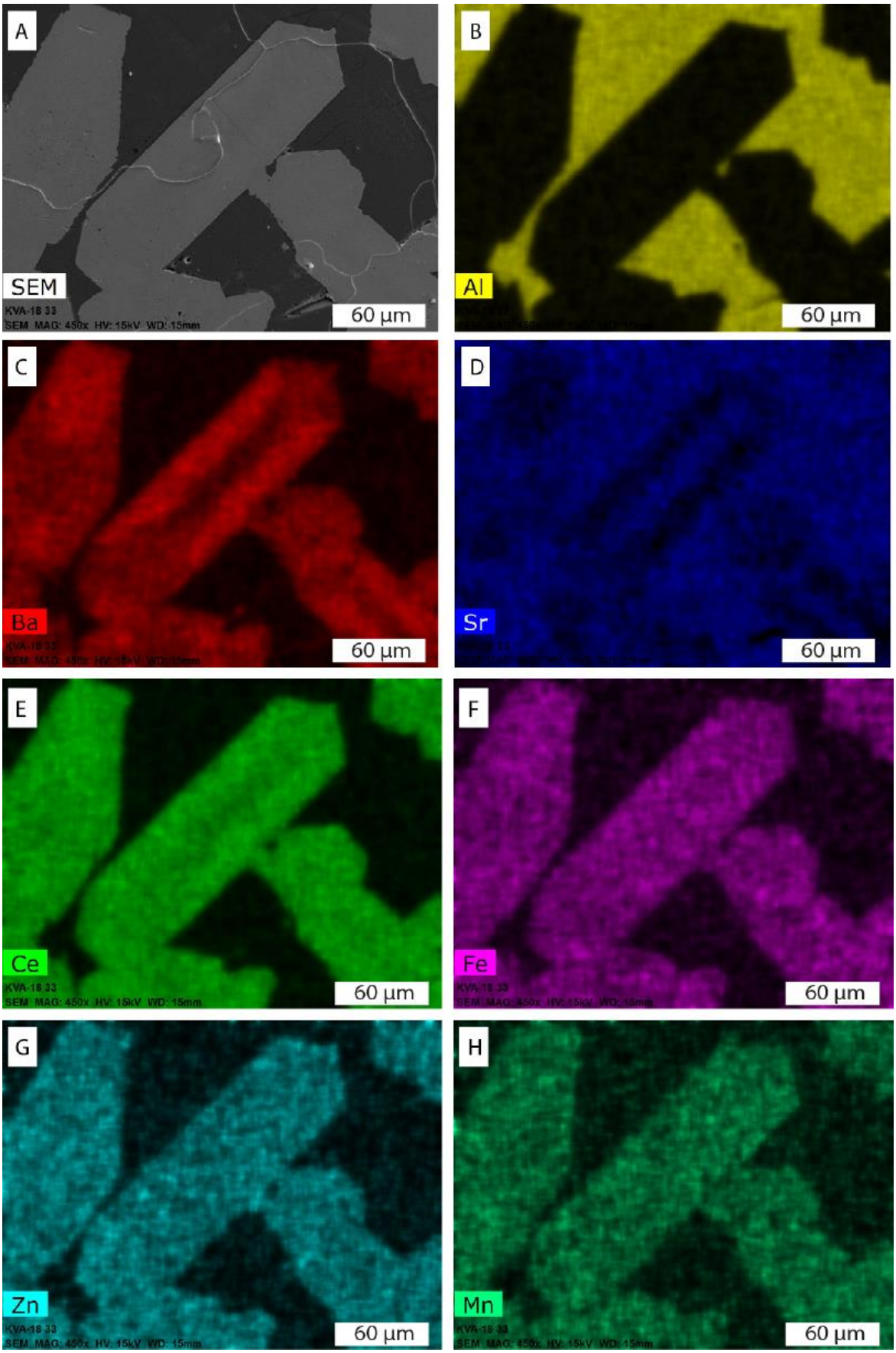

FIGURE 4.18: EDS mapping of elemental distribution in a nordite crystal from EHG_EPOXY. A: SEM image. B: Al map. C: Ba map. D: Sr map. E: Ce map. F: Fe map. G: Zn map. H: Mn map.

Figure 4.18 shows the same elemental mapping of elements as Fig. 4.14. Figure 4.18 is however of another orientation of the nordite crystal. The “cracks” in Fig. 4.18 A are cracks in the carbon coating of the epoxy, but resulted in no charging issues while doing the elemental mapping. Once again, Fig. 4.18 B shows a lack of Al in the nordite, while the ussingite shows a relative high concentration. In Fig. 4.18 C and D, the same trend as in Fig. 4.14 C and D is apparent. Parts of the long sides of the crystal shows a Ba elevation, while the central part shows a decrease from the sides. In the Sr map (Fig. 4.18 D), the central part of the crystal shows an elevated Sr value, while the elongated sides shows a lower Sr content.

In Fig. 4.18 E the elongated sides which were saturated Ba is also concentrated in Ce. The other elements (Fig 4.18 F-H) Fe, Zn and Mn shows an equal distribution. EDS spectrums given in earlier figures (Figs. 4.15-4.17) is also representative of the different parts of the crystals seen in Fig. 4.18.

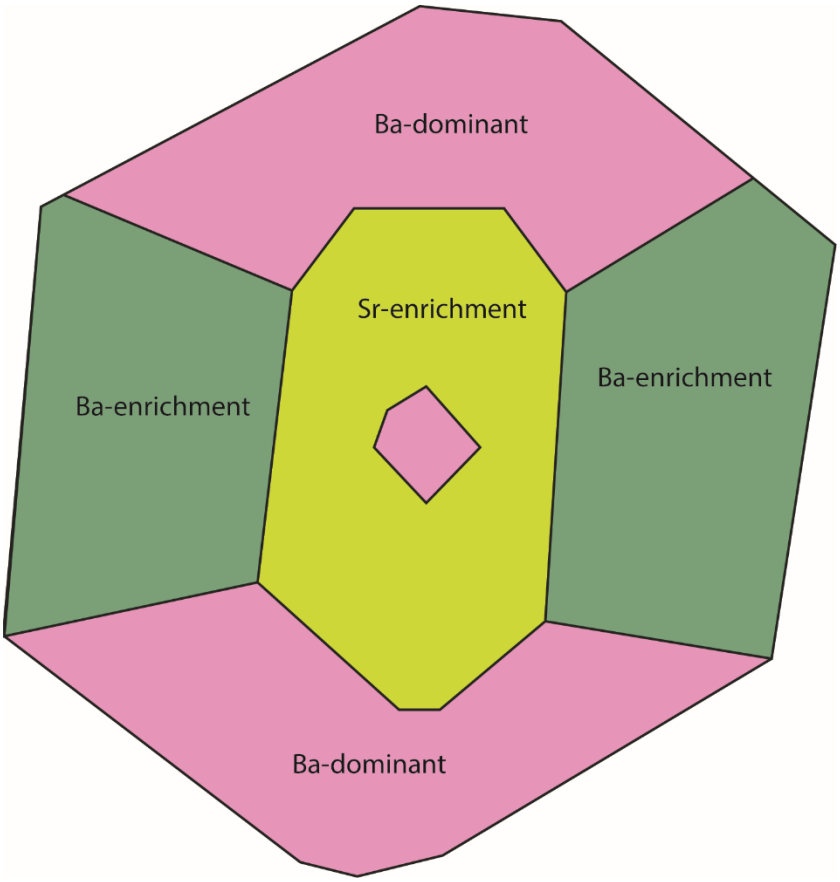

FIGURE 4.19: Theoretical elemental distribution in the Taseq nordite. Looking down an assumed *c*-axis.

From the EDS mapping, theoretical distribution figures (Figs. 4.19 and 4.20) are constructed based on the observations in Figs. 4.14-4.18. The two figures divide the nordite crystal into different zones, classified by whether the zones are Ba or Sr dominated. In addition, the green sides represent zones where the crystal is "enriched" in Ba. This sort of zonation is called sector zoning, and has only been observed in nordites from Taseq.

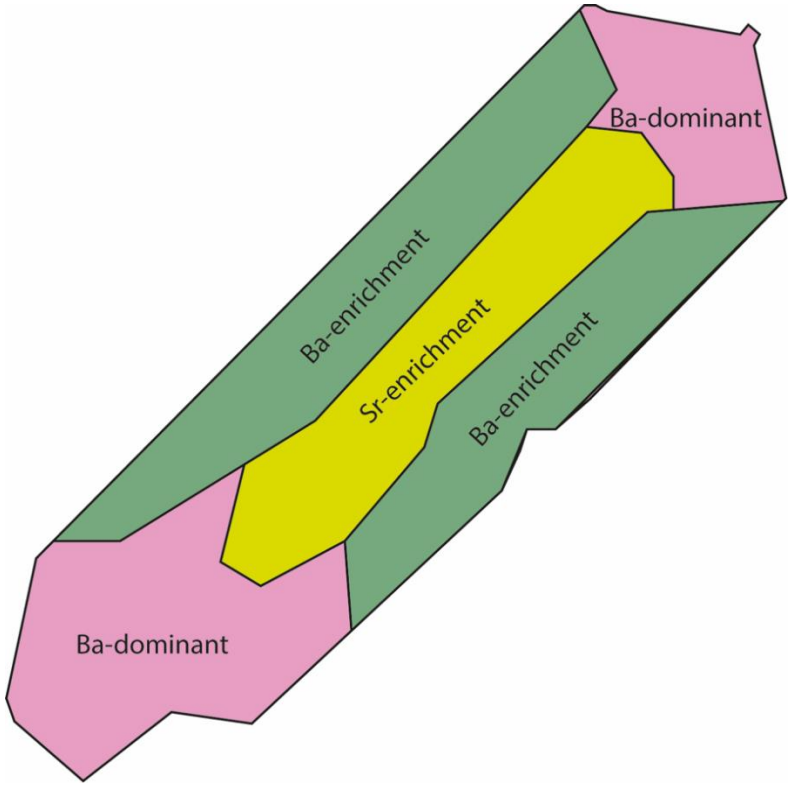

FIGURE 4.20: Theoretical elemental distribution in the Taseq nordite. Perpendicular to the assumed *c*-axis.

4.3 Composition of nordite from Ilímaussaq

When comparing the chemical data from both the EPMA and the ICPMS, there are a fairly good correspondence between the two methods. The Si content measured during the EPMA are used for an internal standard for the ICPMS data. The other elements measured are normalized to the Si content. By comparing the resulting Si content of the two methods of analysis, the EPMA/ICPMS ratio between them varies from 0.994 in EHG EPOXY to 1.023 in EHG 7.

However, there are especially one element that stick out. Zinc seems to differentiate between the two methods of analysis. The Zn value is underestimated in the microprobe data (Appendix 8.13) compared to the ICPMS data (Appendix. 8.13). This is somehow explained due to the problems with the EPMA spectra during analysis combined with the complex overlapping peaks discussed in Section 3.5. Due to this, the average Zn content from ICPMS data, was combined with the normal microprobe data to get full chemical data and is presented in Table 4.1. In addition, Li was discovered as a potential substituting element, but due to the late discovery of this it was only analyzed during the last ICPMS session of EHG 10 and EHG 15. The average from the Li analyzed in these samples are used for all Taseq samples.

Table 4.1 contains the microprobe data gathered from six of the thin section samples from both the Igdlutalik Island (EHG4) and the Taseq Slope (EHG7, 10, 13, 15 and EPOXY). The table also includes the atoms per formula unit (*apfu*) calculated based on 17 anions.

The five samples from the Taseq Slope are quite different from the Igdlutalik Island sample. As previously mentioned, the ICPMS data on Zn are used in the formula calculations, despite this there are some slight variations of up to 0.04 *apfu* between EHG EPOXY and EHG7. The Igdlutalik sample (EHG4) is clearly the sample with the highest concentration of Zn with an 46.45% increase from the Taseq nordites. Conversly, EHG4 has a low Fe^{2+} value of 0.02 *apfu* while the Taseq samples varies between 0.27-0.32 *apfu*. The Mn content is low from both localities, 0.07-0.09 *apfu* for the Taseq samples, but only 0.01 for EHG4, which is also the only sample with any Mg (0.02 *apfu*).

The differences between the samples continues when looking at the large monovalent cations Sr and Ba. EHG4 has the highest value of 0.75 *apfu* Sr, while there is also significant difference within the nordites from Taseq. For example, EHG10 has the highest Sr value of the Taseq nordites with 0.50 *apfu*, while the others ranges from 0.37-0.43 *apfu*. It must also be noted that the standard deviation of the Sr values is large with values ranging as high as 3 wt%. Opposite to the high Sr content in EHG4, we find that the Igdlutalik nordite has the lowest Ba content with 0.05 *apfu*. On the other hand, the nordites from Taseq has a high Ba content that ranges from 0.32-0.52 *apfu*. For the Ba content the uncertainty is fairly extreme with values ranging up to 7 wt%. For discussion on high uncertainties see section 5.1.

The REE content shows considerable variations between samples aswell. EHG4 is the sample with the highest La content of 0.44 *apfu*. In the other samples from the Taseq nordites the La content varies from 0.26-0.33 *apfu*. As a general trend both the Ce^{3+} and Nd content in EHG7, 10, 13, 15 and EPOXY are significantly higher than in EHG4. In the Taseq nordites the Ce^{3+} ranges from 0.68-0.72 *apfu* and the Nd ranges from 0.09-0.15 *apfu*. The Ce^{3+} and Nd content in EHG4 is 0.53 *apfu* and 0.05 *apfu* respectively.

Finally, the Ca content is considerably higher in EHG4 with a value of 0.21 *apfu*, while in EHG7, 10, 13, 15 and EPOXY it ranges from 0.04-0.06 *apfu* Ca.

TABLE 4.1: Chemical composition of nordite.

Sample	EHG4	EHG7	EHG10	EHG13	EHG15	EHG EPOXY
n	*8*	*23*	*12*	*33*	*10*	*13*
Weight percent oxides (wt%)						
SiO_2	45.2(5)	43(1)	44.2(6)	43(1)	43.2(9)	44(1)
ZnO*	9.6(6)	5.0(4)	4.8(4)	5.0(2)	5.1(4)	4.7(9)
FeO	0.2(1)	2.7(8)	2.4(2)	2.7(7)	2.5(7)	2.8(9)
MnO	0.09(4)	0.8(3)	0.62(6)	0.8(4)	0.7(2)	0.7(3)
MgO	0.10(4)	-	-	-	-	-
La_2O_3	9(1)	5(3)	5(3)	5(3)	6.4(6)	6.1(6)
Ce_2O_3	11.0(9)	13(2)	14(2)	13(2)	14(1)	13(1)
Nd_2O_3	1.1(5)	3(4)	3(2)	3(3)	2.0(9)	1.9(9)
Pr_2O_3	0.6(3)	1.1(8)	1.1(4)	1.0(6)	0.9(3)	0.9(3)
SrO	9.8(6)	5(3)	6(1)	5(3)	5(3)	5(3)
BaO	1.0(6)	9(6)	6(2)	9(6)	7(6)	9(7)
CaO	1.5(1)	0.3(2)	0.4(1)	0.3(2)	0.4(2)	0.3(2)
Na_2O	12.0(2)	11.4(4)	11(3)	11.1(3)	11(1)	11.3(7)
Li_2O**	-	0.25(1)	0.25(1)	0.25(1)	0.25(1)	0.25(1)
Total	101.12	99.55	99.07	99.15	98.45	99.95
Atoms per formula unit (*apfu*)						
Si	5.95	5.92	5.97	5.93	5.92	5.95
Zn	0.93	0.51	0.49	0.51	0.51	0.47
Fe^{2+}	0.02	0.32	0.27	0.31	0.29	0.32
Mn	0.01	0.09	0.07	0.09	0.08	0.09
Mg	0.02	-	-	-	-	-
La	0.43	0.26	0.26	0.28	0.32	0.31
Ce^{3+}	0.53	0.67	0.69	0.67	0.71	0.68
Nd	0.05	0.14	0.15	0.14	0.10	0.09
Pr	0.04	0.05	0.06	0.05	0.05	0.04
Sr	0.75	0.36	0.50	0.39	0.42	0.36
Ba	0.05	0.51	0.32	0.47	0.40	0.49
Ca	0.21	0.04	0.06	0.05	0.06	0.04
Na	3.06	3.02	2.99	2.96	2.99	3.00
Li	-	0.07	0.07	0.07	0.07	0.07

*Zn data from ICPMS, an average from samples EHG7, EHG10, EHG13, EHG15, EHG EPOXY. Zn problems with EPMA data as stated, values applied to all zonations even though they are not differentiated on the ICPMS. **Li data from ICPMS, Li discovered as a potential substituting element, and were not included in the early analysis of nordite. The Li value is therefore an average from samples EHG10 and EHG15 and applied to all nordites of the Taseq Slope.

TABLE 4.2: Empirical formulas of Igdlutalik and Taseq nordites.

Samples	Empirical formula
EHG4	$Na_{3.06}(Sr_{0.75}Ca_{0.21}Ba_{0.05})_{\Sigma 1.01}(Ce_{0.53}La_{0.43}Nd_{0.05}Pr_{0.05})_{\Sigma 1.06}(Zn_{0.93}Fe_{0.02}Mg_{0.02}Mn_{0.01})_{\Sigma 0.98}Si_{5.95}O_{17}$
EHG7	$Na_{3.02}(Ba_{0.51}Sr_{0.36}Ca_{0.04})_{\Sigma 0.91}(Ce_{0.67}La_{0.26}Nd_{0.14}Pr_{0.06})_{\Sigma 1.13}(Zn_{0.51}Fe_{0.32}Mn_{0.09}Li_{0.07})_{\Sigma 0.99}Si_{5.92}O_{17}$
EHG10	$Na_{2.99}(Sr_{0.50}Ba_{0.32}Ca_{0.06})_{\Sigma 0.88}(Ce_{0.69}La_{0.26}Nd_{0.15}Pr_{0.06})_{\Sigma 1.16}(Zn_{0.49}Fe_{0.27}Mn_{0.07}Li_{0.07})_{\Sigma 0.90}Si_{5.97}O_{17}$
EHG13	$Na_{2.99}(Ba_{0.47}Sr_{0.39}Ca_{0.05})_{\Sigma 0.91}(Ce_{0.67}La_{0.28}Nd_{0.14}Pr_{0.05})_{\Sigma 1.14}(Zn_{0.51}Fe_{0.31}Mn_{0.09}Li_{0.07})_{\Sigma 0.98}Si_{5.93}O_{17}$
EHG15	$Na_{2.99}(Sr_{0.42}Ba_{0.40}Ca_{0.06})_{\Sigma 0.88}(Ce_{0.71}La_{0.32}Nd_{0.10}Pr_{0.05})_{\Sigma 1.18}(Zn_{0.51}Fe_{0.29}Mn_{0.08}Li_{0.07})_{\Sigma 0.95}Si_{5.92}O_{17}$
EPOXY	$Na_{3.00}(Ba_{0.49}Sr_{0.36}Ca_{0.04})_{\Sigma 0.89}(Ce_{0.68}La_{0.31}Nd_{0.09}Pr_{0.04})_{\Sigma 1.12}(Zn_{0.47}Fe_{0.32}Mn_{0.09}Li_{0.07})_{\Sigma 0.95}Si_{5.95}O_{17}$

The empirical formulas in Table 4.2 are based on the previous nordite publications (Table 1.5) and uses chemistry of the nordites in Table 4.1. Based on the suggested general formula $A_2BXYZT_6O_{17}$ Na is occupying the *A*- and *B*-sites, Sr, Ba and Ca in the *X*-site, REEs in the *Y*-site, Zn, Fe, Mn and Mg in the *Z*-site and Si in the *T*-site. Further investigation of the formula of nordite is discussed in section 5.2.

Three of the five Taseq samples (EHG7, 13, and EPOXY) have Ba as the dominant element in the *X*-site, while the two others (EHG10 and 15) have Sr as the dominant element in the same site. When you sum up the *X*-site position there is a clear deficiency varying from 0.12 *apfu* to 0.09 *apfu*. However, there is an abundance of total REE ranging from 1.12 *apfu* to 1.18 *apfu*. At the *Z*-site there is a slight lack of total divalent cations, with values ranging from 0.91 *apfu* to 0.99 *apfu*. A deficiency is also apparent in the Si with saturations ranging from 5.92 *apfu* to 5.96 *apfu*.

TABLE 4.3: Trace elements (PPM) in nordites of the Igdlutalik Island and the Taseq slope.

Sample	EHG4	EHG7	EHG10	EHG13	EHG15	EHG EPOXY
n	24	19	16	26	59	38
Trace elements (PPM)						
Li	-	-	998	-	1195	-
Zn	77404	39303	38794	39479	41163	37836
Cs	1	1	1	1	1	-
Hf	<1	1	<1	1	<1	1
Nb	11	15	24	24	18	-
Rb	<1	<1	1	1	1	-
Ta	<1	<1	<1	<1	<1	-
Th	80	112	128	99	83	65
U	1	<1	<1	<1	<1	1
Zr	7	2	1	1	2	-
Y	1	3	2	3	2	-
La	71352	50274	49194	47609	54154	49152
Ce	89264	108759	110365	102500	118499	102849
Pr	6361	9728	9863	9172	9716	8796
Nd	11194	21386	22214	20507	19743	17173
Sm	239	767	869	688	526	381
Eu	6.96	16	18	13	10	7
Gd	166	250	200	225	177	227
Tb	3	6	5	5	4	5
Dy	1	1	1	<1	<1	<1
Ho	<1	<1	<1	<1	<1	<1
Er	4	8	7	8	6	7
Tm	<1	<1	<1	<1	<1	<1
Yb	<1	<1	<1	<1	<1	<1
Lu	<1	<1	<1	<1	<1	<1
ΣLREE	178584	191181	192724	180717	202826	178588
ΣHREE	9	14	13	14	11	12
ΣREE	178593	191196	192737	180730	202837	178600

Note that when dealing with minerals from alkaline complexes such as Ilímaussaq, REE's are so abundant that they are main constituents of the mineral. This results in some uncertainties in the LA-ICP-MS data due to their high concentration. Values are reported on minimum detection limit (MDL) at 99% confidence level determined by Poisson counting statistics: MDL = 2.3*√(2B) (B = the total counts in the background interval) (Van Achterbergh *et al.*, 1999).

There is a high abundance of La in both the Taseq Slope and Igdlutalik nordites, with values ranging from 47609 ppm to 54154 ppm in samples EHG7, EHG10, EHG13, EHG15 and EHG_EPOXY. This is considerably less than that of EHG4, which has a La of 71352 ppm based on the mean of 24 analysis points. In comparison, the Ce concentration is far superior in the Taseq nordites with values ranging from 102849 ppm to 118499 ppm. This is much higher proportion than that of EHG4, which has 89264 ppm Ce.

An interesting observation is that there is a fairly high overall content of Nd. Compare to the Pr content, there is a ratio between them ranging from 1.7-2.2 Nd/Pr.

When looking at the U content in the samples, they are hovering around the MDL in the Taseq samples, while EHG4 has a content of 1 ppm. The Th content on the other hand are significantly higher with values ranging from 65-128 ppm.

It must be mentioned that there have not been done analysis for elements Li, Cs, Nb, Rb, Ta, Zr and Y for EHG_EPOXY, since it was the first sample to be analyzed in LA-ICP-MS. Furthermore, Li was only analyzed for EHG10 and EHG15 because it was at a late stage in the research process discovered that Li might substitute in the nordite structure formula. Due to this, Li was only included for the last samples that were analyzed by the LA-ICP-MS.

There is an overall abundance of the LREE opposed to the HREE (Fig. 4.21). Despite this, there is a clear elevation in the Er in the nordite minerals. The high overall concentration of the LREE leads back to what previously stated that the LREE elements are major constituents of the nordite mineral. When examining Fig. 4.21 EHG4 seems to differentiate from the other samples. It has a higher La content, but lower on the other LREEs (Total of 178584 ppm). The EHG4 also has a lower total HREE content of 9 ppm compared to the Taseq nordite samples that ranges from 11-14 ppm HREE (Table 4.3).

The common negative Eu-anomaly is apparent in the nordites from both localities. There is however both a positive Gd- and Er-anomaly present in the nordites.

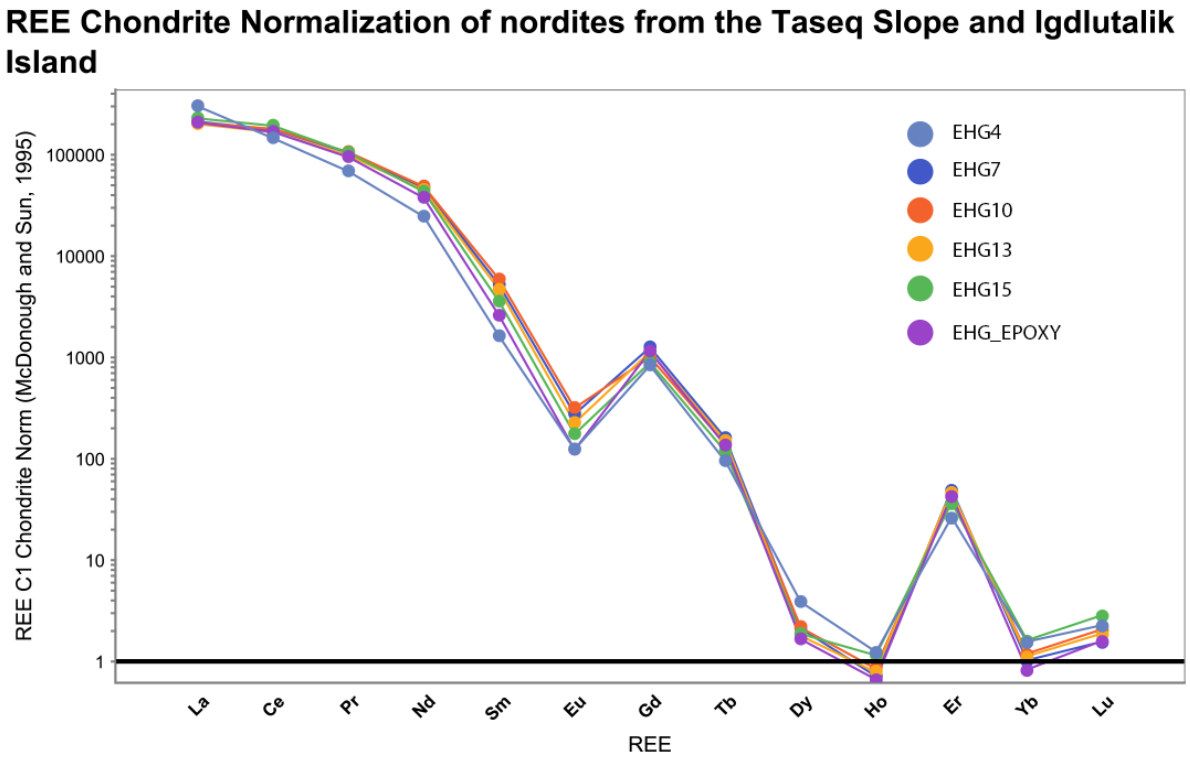

FIGURE 4.21: REE chondrite normalization of nordites based on McDonough & Sun (1995).

4.4 Accessory minerals

To get a deeper understanding of the paragenesis of nordites selected accessory minerals was chemical analyzed by EPMA and LA-ICP-MS.

TABLE 4.4: Chemical composition of accessory minerals of nordite.

Sample	EHG4	EHG7	EHG10	EHG10	EHG4 and 3	EHG7
Mineral	Pyroxene	Pyroxene	Pyroxene	Pyroxene	Narsarsukite	Amphibole
Color	Green	Brown	Green	Brown	-	-
n	6	28	16	10	51	12
Weight percent oxides						
SiO_2	52.3(4)	52.4(6)	52.6(5)	52.4(4)	61.8(9)	51.5(7)
Al_2O_3	1.1(6)	1.3(4)	1.4(5)	1.5(9)	0.43(4)	0.8(2)
Fe_2O_3	29(2)	32.1(8)	32(1)	31(2)	3.5(4)	-
FeO	-	-	-	-	-	28(1)
Cr_2O_3	-	-	-	-	-	-
MnO	0.09(4)	0.5(4)	0.6(3)	0.9(6)	0.11(4)	3(2)
MgO	0.7(4)	-	-	-	0.17(6)	0.02(4)
CaO	1(1)	-	-	-	-	0.03(5)
K_2O	-	-	-	-	0.04(2)	4.1(1)
Na_2O	12.9(9)	13.5(2)	13.6(2)	13.6(1)	16.1(3)	7.4(2)
ZrO_2	0.3(4)	-	-	-	-	0.01(3)
TiO_2	2(1)	0.2(1)	0.3(3)	0.3(2)	15.6(4)	0.3(2)
Nb_2O_5	-	-	-	-	1.6(7)	-
F^-	-	-	-	-	1.2(1)	-
-O=F					0.51	
Total	100.25	100.09	100.28	100.23	100.15	95.7
Atoms per formula unit						
Si	2.00	2.00	2.00	2.00	3.96	-
Al	0.05	0.06	0.06	0.07	0.03	-
Fe^{3+}	0.84	0.92	0.91	0.90	0.17	-
Fe^{2+}	-	-	-	-	-	-
Cr	-	-	-	-	-	-
Mn	0.00	0.02	0.02	0.03	0.01	-
Mg	0.04	-	-	-	0.02	-
Ca	0.04	-	-	-	-	-
K	-	-	-	-	-	-
Na	0.96	1.00	1.00	1.01	2.00	-
Zr	0.01	-	-	-	-	-
Ti	0.14	0.01	0.01	0.01	0.75	-
Nb	-	-	-	-	0.05	-
F	-	-	-	-	0.24	-

Pyroxene *apfu* calculations based on 6 O. Narsarsukite *apfu* calculations based on 11 O.

In all the accessory minerals (both in Igdlutalik and Taseq) there is occurrence of Ti, but in Taseq it is a very minor constituent (up to 0.3 wt%). The narsarsukite is enriched in the high field strength elements (HFSE) Ti (15.6 wt%) and Nb (1.6 wt%). The Igdlutalik pyroxenes also has a higher Ti content than the pyroxenes from Taseq with an average of 0.14 *apfu*.

The classification of the pyroxene can be seen in Fig. 4.22. The pyroxenes are classified as aegirines. The aegirine in EHG4 separates from the ones of the Taseq slope with a higher Ca+Mg content of 0.08 *apfu*.

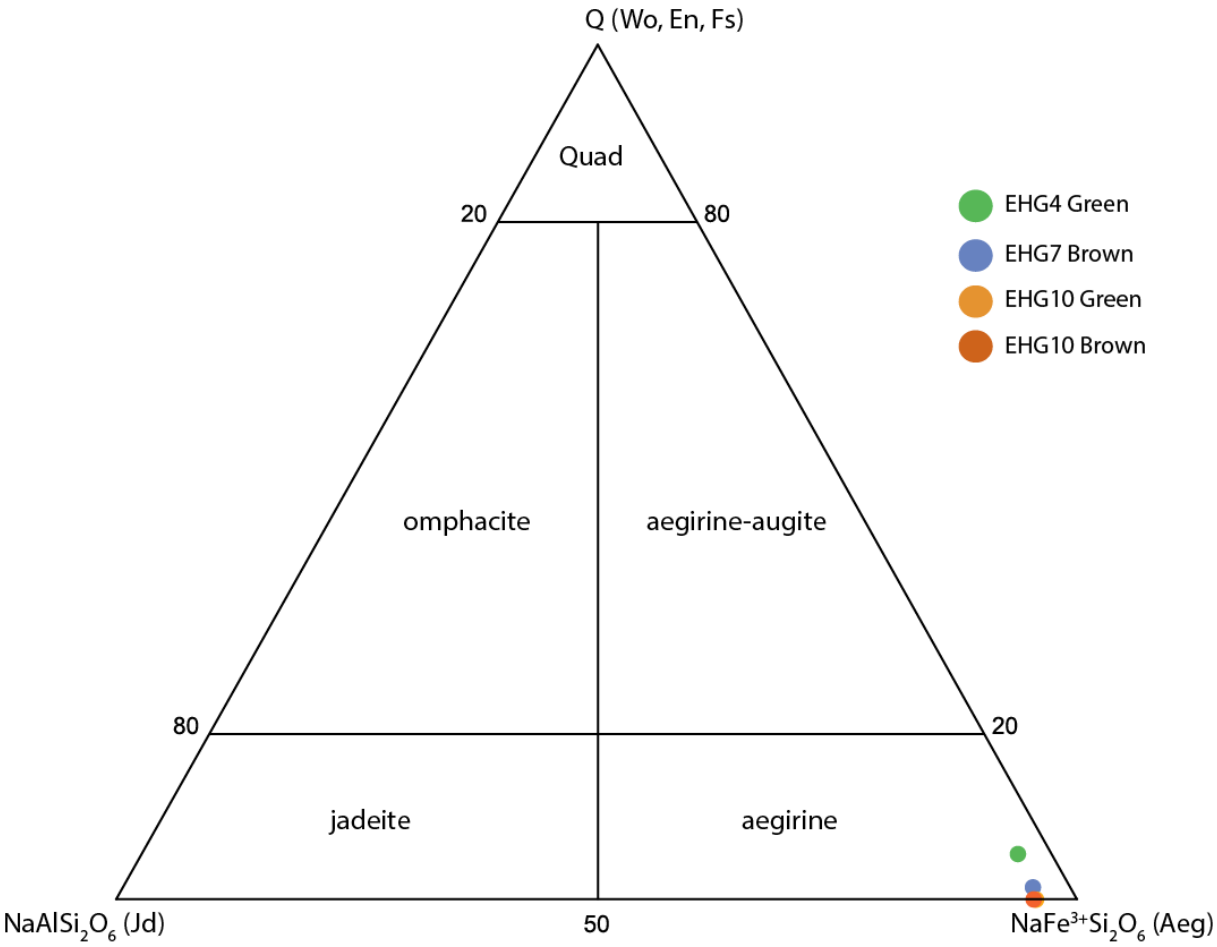

FIGURE 4.22: Classification of pyroxene after Morimoto (1988).

Table 4.5 contains the empirical formulas of the accessory minerals based on the chemical data in Table 4.4. The aegirine formulas were determined based on the nomenclature of aegirines (Morimoto, 1988). Upton *et al.* (1976) was used for determination of the narsarsukite formula.

TABLE 4.5: Empirical formulas for selected accessory minerals of nordite.

Samples	Empirical formula
EHG4: Aegirine Green	$(Na_{0.96}Ca_{0.04})_{\Sigma 1.00}(Fe^{3+}_{0.84}Ti_{0.14}Al_{0.05}Mg_{0.04})_{\Sigma 1.07}Si_2O_6$
EHG7: Aegirine Brown	$Na_{1.00}(Fe^{3+}_{0.92}Al_{0.06}Mn_{0.02}Ti_{0.01})_{\Sigma 1.01}Si_2O_6$
EHG10: Aegirine Green	$Na_{1.00}(Fe^{3+}_{0.91}Al_{0.06}Mn_{0.02}Ti_{0.01})_{\Sigma 1.00}Si_2O_6$
EHG10: Aegirine Brown	$Na_{1.01}(Fe^{3+}_{0.90}Al_{0.07}Mn_{0.03}Ti_{0.01})_{\Sigma 1.01}Si_2O_6$
EHG4: Narsarsukite	$Na_{2.00}(Ti_{0.75}Fe^{3+}_{0.17}Nb_{0.05}Mg_{0.02}Mn_{0.01})_{\Sigma 0.99}(Si_{3.96}Al_{0.03})_{\Sigma 3.99}O_{10}(O_{0.76}F_{0.24})_{\Sigma 1.00}$

The amphibole stoichiometry was not solved and is further discussed in Section 5.3.3. The amphibole is however assumed to be arfvedsonite based on the high wt% Fe (28 wt%) (Hawthorne *et al.*, 2012) and that arfvedsonite is a common amphibole from the Taseq slope (Mindat[2]).

Table 4.6 contain the trace elements in the accessory minerals to nordite from both the Taseq slope and Igdlutalik Island.

TABLE: 4.6: Trace elements (PPM) in accessory minerals of nordite.

Sample	EHG4		EHG10	EHG13	EHG4
Mineral	Aegirine		Arfvedsonite	Aegirine	Narsarsukite
Color	Green	Brown		Green	
n	17	6	5	6	23
Trace elements (PPM)					
Sr	8	8	15	189	-
Ba	13	14	12	28	-
Cs	1	1	11	1	1
Hf	8	8	2	2	4
Nb	306	347	1099	2497	6770
Rb	18	19	48	117	1
Ta	1	1	2	1	4
Th	1	1	1	<1	<1
U	4	7	1	<1	2
Zr	236	220	38	64	185
Y	5	5	<1	5	9
La	6	7	5	1	1
Ce	11	15	12	7	1
Pr	2	3	1	2	<1
Nd	9	12	4	20	2
Sm	2	2	<1	2	<1
Eu	0	<1	<1	<1	<1
Gd	2	2	1	1	1
Tb	<1	<1	<1	<1	<1
Dy	1	1	<1	1	1
Ho	<1	<1	<1	<1	<1
Er	1	<1	<1	<1	1
Tm	<1	<1	<1	<1	<1
Yb	1	<1	<1	1	3
Lu	<1	<1	<1	<1	1
ΣLREE	31	40	23	21	4
ΣHREE	4	4	1	3	7
ΣREE	35	44	24	24	11

Europium was used as the cutoff element between LREE and HREE.

Figure 4.23 shows the REE chondrite normalization pattern of the aegirines analyzed from both the Taseq slope (EHG 10) and Igdlutalik Island (EHG 4). The normalization was done with the help of the software IoGAS and based on McDonough and Sun (1995). There is a clear correspondence between the brown and green aegirines in EHG4. The brown aegirine has a higher LREE content ranging from 7 ppm in La to 12 ppm in Nd. On the other hand, the green aegirine from the same locality seems to be slightly elevated in the HREE (Dy-Lu) with a peak difference of 60% increase in Lu.

The green aegirine from the Taseq slope (EHG10) shows a different pattern than the ones from Igdlutalik Island. Nd is the REE with the highest concentration (10 ppm), with steep downwards trends towards both lighter and heavier elements. An interesting observation is that the main REEs (i.e. La, Ce) in the nordite from the same locality, have low concentrations in the aegirine.

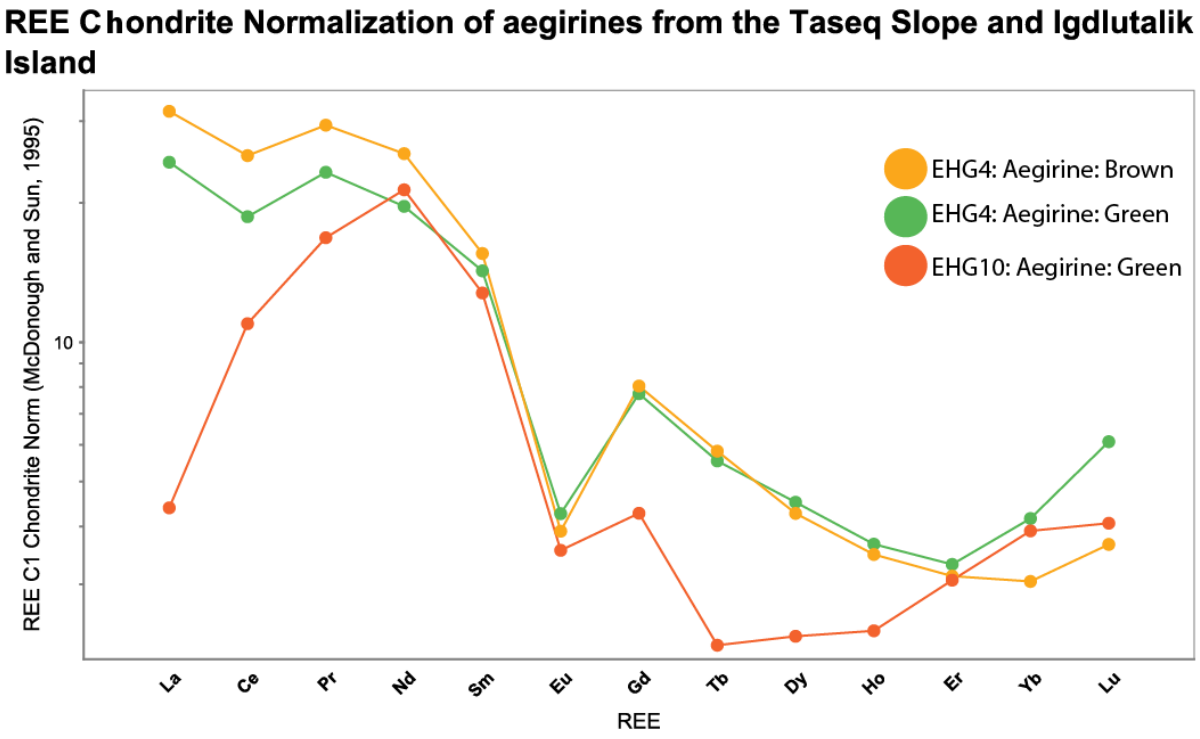

FIGURE 4.23: REE Chondrite normalization of accessory aegirines to nordite. Data from Table 4.6 is used with McDonough and Sun (1995) normalization.

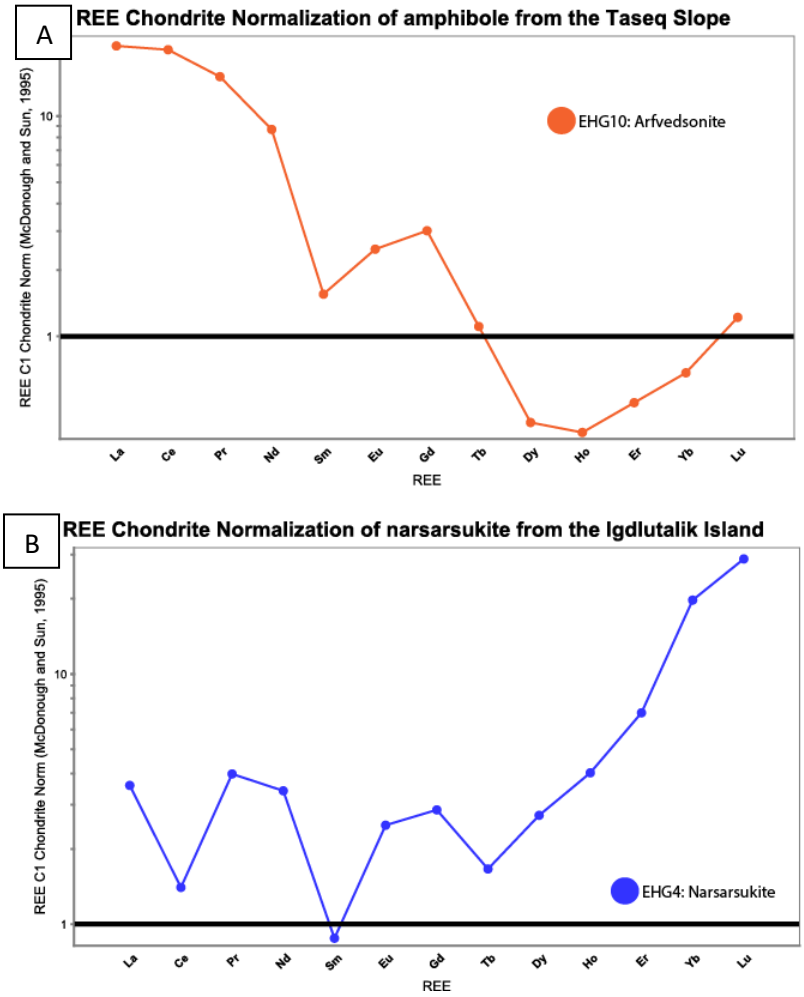

FIGURE 4.24: REE Chondrite normalization of accessory (A) arfvedsonite and (B) narsarsukite.

Figure 4.24 contains the REE chondrite normalization for an arfvedsonite from EHG 10 (a) and a narsarsukite (b) from EHG 4. LREE (Σ23 ppm) is heavily favored in the arfvedsonite, while the HREE (Σ7 ppm) is favored in the narsarsukite. Comparing the aegirines from the Igdlutalik Island to the narsarsukite, the aegirines are LREE (Σ up to 40 ppm) favored while the narsarukite is HREE (Σ7 ppm) favored. An important note is that all of accessory minerals have a very low REE content (Table 4.6) compare to the nordite (Table 4.3). This includes the fact that several elements in the accessory minerals (e.g. HREE in arfvedsonite) are hovering around the minimum detection limit.

4.5 Crystal structure of nordite

A crucial part of the thesis is acquiring quality data for structure refinement of the nordite. Several attempts of attaining a crystal of nordite was made prior to the first successful experiment labelled Exp_420_Mo. The material used for this experiment was from the EHG_4 hand samples. All the different parameters affect the time of the experiment, for example Exp_431_Mo and Exp_478_A_Mo have exposure times of 46s and 105s respectively. This yielded an experiment that ran over several days.

TABLE 4.7: Structural parameters for already known nordites, nordites from the Taseq slope and Igdlutalik Island and meieranite.

Mineral	Nordite-(Ce)	Nordite-(La)	Ferronordite-(Ce)	Ferronordite-(La)	Manganonordite-(Ce)	Meieranite
Ideal chemical formula	$Na_3SrCeZnSi_6O_{17}$	$Na_3SrLaZnSi_6O_{17}$	$Na_3SrCeFe^{2+}Si_6O_{17}$	$Na_3SrLaFe^{2+}Si_6O_{17}$	$Na_3SrCeMn^{2+}Si_6O_{17}$	$Na_2Sr_3MgSi_6O_{17}$
Crystal symmetry	Orthorhombic	Orthorhombic	Orthorhombic	Orthorhombic	Orthorhombic	Orthorhombic
Space group	*Pcca*	*Pcca*	*Pcca*	*Pcca*	*Pcca*	*P21nb*
a (Å)	14.432(2)	14.27(3)	14.46(1)	14.440(5)	14.44(2)	7.9380(2)
b (Å)	5.1955(8)	5.16(1)	5.194(3)	5.191(2)	5.187(5)	10.4923(3)
c (Å)	19.816(3)	19.45(15)	19.874(9)	19.86(1)	19.82(1)	18.2560(6)
V(Å^3)	1485.8(3)	1432.2	1492.39	1489(2)	1485.10	1520.50(8)
Z	4	4	4	4	4	4
(g/cm^3)				3.62		3.44
2θ range for data collection			≤100.26		≤102.84	≤64.86
No. Of reflections collected			4016		5265	12218
No. Of independent reflections		1335	3803		3534	5296
No. Reflections with $I>2\sigma$			3623*		3433*	4738
No. Of parameters refined						265
R(int)						0.023
Final R1, wR2 factors		0.122			0.044	0.027, 0.063
Goodness-of-fit						1.034
Reference	(1)u	(2)	(3)	(4)	(3)	(5)

TABLE 4.7 (continued): Structural data of nordites from the Igdlutalik Island and Taseq slope.

Mineral (Experiment)	Igdlutalik (420)	Igdlutalik (422)	Taseq (430)	Taseq (431)	Taseq (478)
Ideal chemical formula	$Na_3SrCeZnSi_6O_{17}$	$Na_3SrCeZnSi_6O_{17}$	$NaBa_{0.5}Sr_{0.5}CeZnSi_6O_{17}$	$NaBa_{0.5}Sr_{0.5}CeZnSi_6O_{17}$	$NaBa_{0.5}Sr_{0.5}ZnSi_6O_{17}$
Crystal symmetry	Orthorhombic	Orthorhombic	Orthorhombic	Orthorhombic	Orthorhombic
Space group	*Pcca*	*Pcca*	*Pcca*	*Pcca*	*Pcca*
a (Å)	14.3846(3)	14.3891(2)	14.5335(5)	14.5596 (4)	14.4925 (7)
b (Å)	5.1779(1)	5.1799(1)	5.2147(2)	5.2213 (1)	5.2091 (2)
c (Å)	19.7526(3)	19.7554(2)	19.8265(6)	19.8270 (4)	19.8095 (7)
V(Å^3)	1471.23(5)	1472.44(3)	1502.6(1)	1507.25 (6)	1495.5 (1)
Z	4	4	4	4	4
(g/cm^3)	3.624	3.822	3.637	3.626	4.423
2θ range for data collection	≤33.264	≤34.385	≤33.096	≤31.455	≤33.366
No. Of reflections collected	22610	67858	20398	29642	8564
No. Of independent reflections	2663	2998	2677	2362	2569
No. Reflections with $I>2\sigma$	2250	2641	2102	1902	1762
No. Of parameters refined	140	140	140	140	140
R(int)	0.0230	0.0267	0.0428	0.0396	0.0363
Final R1, wR2 factors	0.0158, 0.0404	0.0128, 0.0354	0.0363, 0.0973	0.0246, 0.0665	0.0331, 0.0745
Goodness-of-fit	1.059	1.062	1.143	1.072	1.015
Reference	(6)	(6)	(6)	(6)	(6)

*3σ

(1)u RRUFF data, unpublished

(2) Bakakin *et al*. (1970)

(3) Pushcharovskii *et al.* (1999)

(4) Pekov *et al.* (2001)

(5) Yang *et al.* (2019)

(6) This study

The structures solved during this study (Table 4.7) gives the full structural parameters of the nordite minerals analyzed. This is something that has not been done before for nordites (Table 4.7). Especially the Goodness-of-fit value has never been reported in previous published structural data (Bakakin *et al.*, 1970; Pushcharovskii *et al.*, 1999; Pekov *et al.*, 2001). In addition, the R(int) value is also documented in this study. Although, R(int) and GoF are not considered as important for descriptions of crystal structures, they provide information about the quality of the data and refinement.

There is a clear difference between the Igdlutalik experiments and the Taseq ones. Firstly, the unit cell with the parameters *a, b* and *c* are all longer in the Taseq experiments than in the Igdlutalik. The *a*-axis is on average 0.142 Å longer in the Taseq samples, while the *b* axis is on average 0.037 Å longer and the *c*-axis 0.067 Å longer. The longer unit cell parameters in turn results in an overall larger volume of the unit cell, where the Taseq nordites are on average 29.94 $Å^3$ (2%) larger in volume.

The results of the two refinement of nordite from Igdlutalik (420 and 422) are similar with an average unit cell of *a*: 14.387, *b*: 5.177 and *c*: 19.754 Å (Table 4.7). The average unit cell volume for Igdlutalik nordite is 1471.83 $Å^3$.

On the other hand, the Taseq experiments (430, 431 and 478) shows significant differences in their cell parameters. Experiment 478 has a volume that is 7.1 $Å^3$ smaller than experiment 430, while experiment 431 has a volume of 4.65 $Å^3$ more than experiment 430. What seems to be the deciding factor is the *a*-axis in the unit cell. This parameter varies from the lowest 14.492 Å in experiment 478, to 14.560 Å in experiment 431. This is the same trend seen when comparing the experiments from the different localities in the previous segment.

When comparing the results from this study to what has previously been published (Table 4.7), the Igdlutalik experiments are the most similar. From Table 4.1, EHG4 is clearly Ce dominant; this means the samples analyses for this study should be best comparable to that. Experiments 420 and 422 is on average 13.97 $Å^3$ smaller in volume than the nordite-(Ce) structural data (Table 4.7). This is a result of all the unit cell axis being shorter with the *a*-axis being on average 0.04 Å shorter, *b* axis shorter by 0.02 Å and the *c*-axis by 0.06 Å.

Furthermore, there are no current known structural datasets (Table 4.7) that compares to the structural datasets of the Taseq nordites. The Taseq nordites boasts a larger unit cell than any other previously published data (Bakakin *et al.*, 1970; Pushcharovskii *et al.*, 1999; Pekov *et al.*, 2001).

Figure 4.25 shows all known nordites along with the nordites analyzed for this thesis when plotting the *a*-axis parameter against unit cell volume. As described in the previous section, the Taseq nordites are clearly the ones with the largest unit cell volume and longest *a*-axis (black circle). An interesting observation is that the Igdlutalik nordites (blue circle) have both a shorter *a*-axis and a smaller unit cell than nordite-(Ce), ferronordite-(Ce), ferronordite-(La) and manganonordite-(Ce) (yellow circle). However, the nordite-(La) has a considerably smaller unit cell volume and shorter *a*-axis than the rest of the nordites plotted in Figure 4.25.

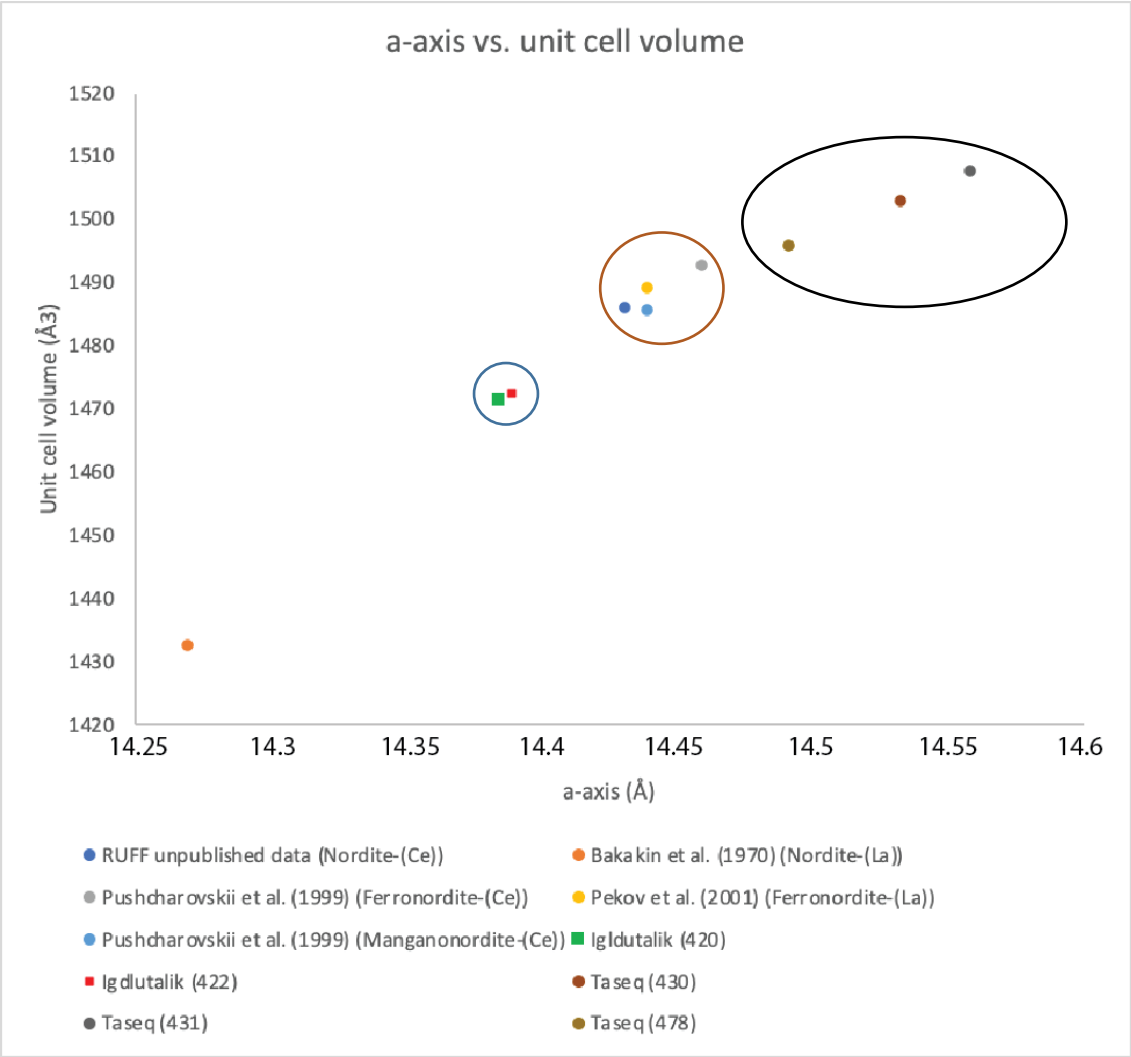

FIGURE: 4.25 a-axis vs. unit cell volume of known nordites and nordite structures analyzed in this thesis.

TABLE 4.8: Refined site-scattering (RSS) from SXRD experiments on nordite from the Igdlutalik Island and Taseq slope.

Exp	Locality	*A*-Site (*e*)	*B*-Site (*e*)	*X*-Site (*e*)	*Y*-Site (*e*)	*Z*-Site (*e*)
420	Igdlutalik	10.64	11.14	36.94	55.92	28.79
422	Igdlutalik	10.69	10.99	35.93	56.27	28.85
430	Taseq	10.39	11.52	48.21	58.00	26.80
431	Taseq	10.69	11.58	50.19	57.19	26.68
478	Taseq	10.54	11.19	47.49	57.36	26.86

Based on the calculations from Table 4.8, Fig. 4.28 shows the RSS for the *X*-site and *Z*-site plotted against the volume of the unit cell. The *Z*-site and *X*-site refinements were chosen for comparison due to difference in chemical composition of the sites between the two experiments (431 and 422).

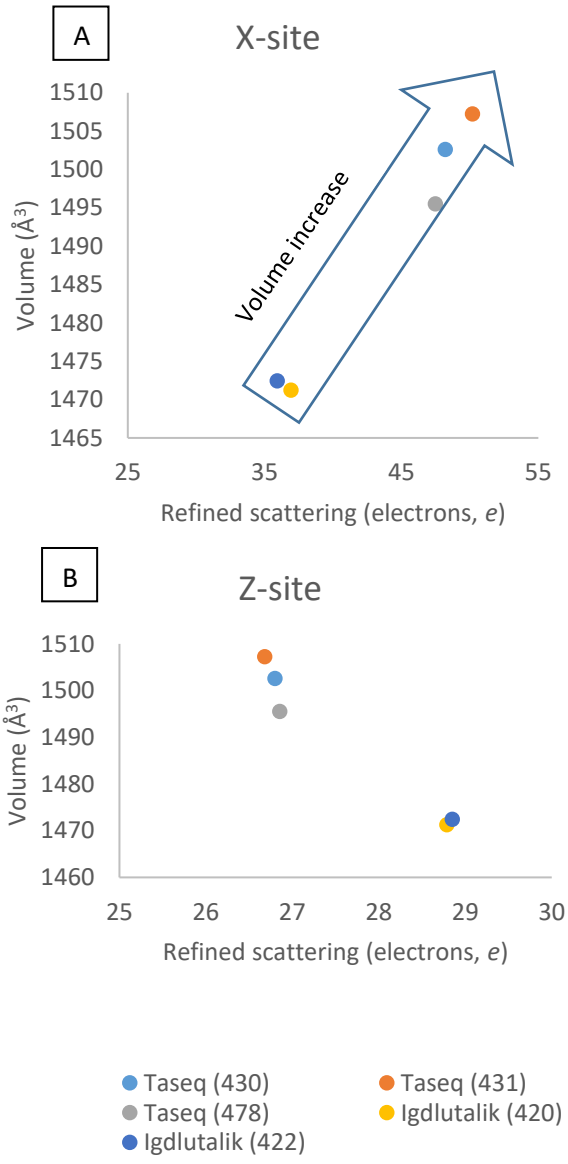

The general trend as seen from the arrow in Fig. 4.26a is that with an increase to the refined scattering electrons in the *X*-site, the volume of the unit cell increases. Experiment 431 has 2.70 *e* more in the *X*-site than exp. 478, and 11.75 Å^3 larger volume. This is however not the case for the Igdlutalik experiments. With an increase of 0.99 *e* from exp. 422 to exp. 420 in the *X*-site, the volume decreases by 1.21 Å^3. The opposite is observed in Fig. 4.26b, where exp. 422 has 0.06 *e* more in the *Z*-site and a larger volume as stated. For the Taseq nordites, there is a decline in *Z*-site *e* with an increase in unit cell volume. One must however note that value of the difference (i.e. 0.06 *e*) is extremely almost inconsequential, so should be considered with caution.

FIGURE: 4.26: *X*-site (A) and *Z*-site (B) refined scattering vs. unit cell volume.

TABLE 4.9: Selected bond distances in Taseq slope nordite (Exp. 431) and Igdlutalik Island nordite (Exp. 422).

Exp. 431	Distance (Å)		Distance (Å)	Exp. 422	Distance (Å)		Distance (Å)
***A*-site**		***Z*-site**		***A*-site**		***Z*-site**	
A-O(1)	2.397(2)x2	*Z*-O(2)	1.961(2)x2	*A*-O(1)	2.394(1)x2	*Z*-O(2)	1.937(1)x2
A-O(3)	2.587(2)x2	*Z*-O(6)	1.985(2)x2	*A*-O(3)	2.53(1)x2	*Z*-O(6)	1.961(1)x2
A-O(4)	2.307(2)x2			*A*-O(4)	2.327(1)x2		
Ave	2.430	Ave	1.973	Ave	2.417	Ave	1.949
***B*-site**		***T(1)*-site**		***B*-site**		***T(1)*-site**	
B-O(1)	2.687(2)	*T(1)*-O(1)	1.663(2)	*B*-O(1)	2.688(1)	*T(1)*-O(1)	1.661(1)
B-O(2)	2.472(2)	*T(1)*-O(2)	1.602(2)	*B*-O(2)	2.432(1)	*T(1)*-O(2)	1.601(1)
B-O(4)	2.434(2)	*T(1)*-O(3)	1.585(2)	*B*-O(4)	2.443(1)	*T(1)*-O(3)	1.683(1)
B-O(5)	2.653(2)	*T(1)*-O(4)	1.578(2)	*B*-O(5)	2.639(1)	*T(1)*-O(4)	1.577(1)
B-O(6)	2.53(2)			*B*-O(6)	2.492(1)		
B-O7	3.316(3)			*B*-O(7)	3.326(1)		
B-O(8)	2.412(2)			*B*-O(8)	2.407(1)		
B-O(8')	3.119(3)			*B*-O(8')	3.101(1)		
Ave	2.703	Ave	1.607	Ave	2.691	Ave	1.631
***X*-site**		***T*(2)-site**		***X*-site**		***T(2)*-site**	
X-O(2)	2.649(2)x2	*T(2)*-O(5)	1.643(1)	*X*-O(2)	2.577(1)x2	*T(2)*-O(5)	1.637(1)
X-O(3)	2.824(2)x2	*T(2)*-O(6)	1.619(2)	*X*-O(3)	2.743(1)x2	*T(2)*-O(6)	1.614(1)
X-O(4)	2.687(2)x2	*T(2)*-O(7)	1.677(2)	*X*-O(4)	2.591(1)x2	*T(2)*-O(7)	1.677(1)
X-O(9)	2.642(2)x2	*T(2)*-O(8)	1.583(2)	*X*-O(9)	2.56(1)x2	*T(2)*-O(8)	1.581(1)
Ave	2.701	Ave	1.631	Ave	2.618	Ave	1.627
***Y*-site**		***T(3)*-site**		***Y*-site**		***T(3)*-site**	
Y-O(6)	2.492(2)x2	*T(3)*-O(1)	1.648(2)	*Y*-O(6)	2.509(1)x2	*T(3)*-O(1)	1.647(1)
Y-O(7)	2.754(2)x2	*T(3)*-O(3)	1.649(2)	*Y*-O(7)	2.697(1)x2	*T(3)*-O(3)	1.648(1)
Y-O(8)	2.507(2)x2	*T(3)*-O(7)	1.649(2)	*Y*-O(8)	2.481(1)x2	*T(3)*-O(7)	1.648(1)
Y-O(9)	2.462(2)x2	*T(3)*-O(9)	1.586(2)	*Y*-O(9)	2.457(1)x2	*T(3)*-O(9)	1.583(1)
Ave	2.554	Ave	1.633	Ave	2.536	Ave	1.632

Table 4.9 shows selected bond distances in one analyzed nordite from the Taseq slope and one nordite from the Igdlutalik Island. The bond distances for the remaining experiments are in appendix 8.10 and 8.11 alongside the atomic coordinates (Appendix 8.5-8.9).

Figure 4.27 shows the outline for the different sites in the structure along with the bond-lengths to their respective oxygen-atom. Bond-lengths are taken from SXRD experiment 430.

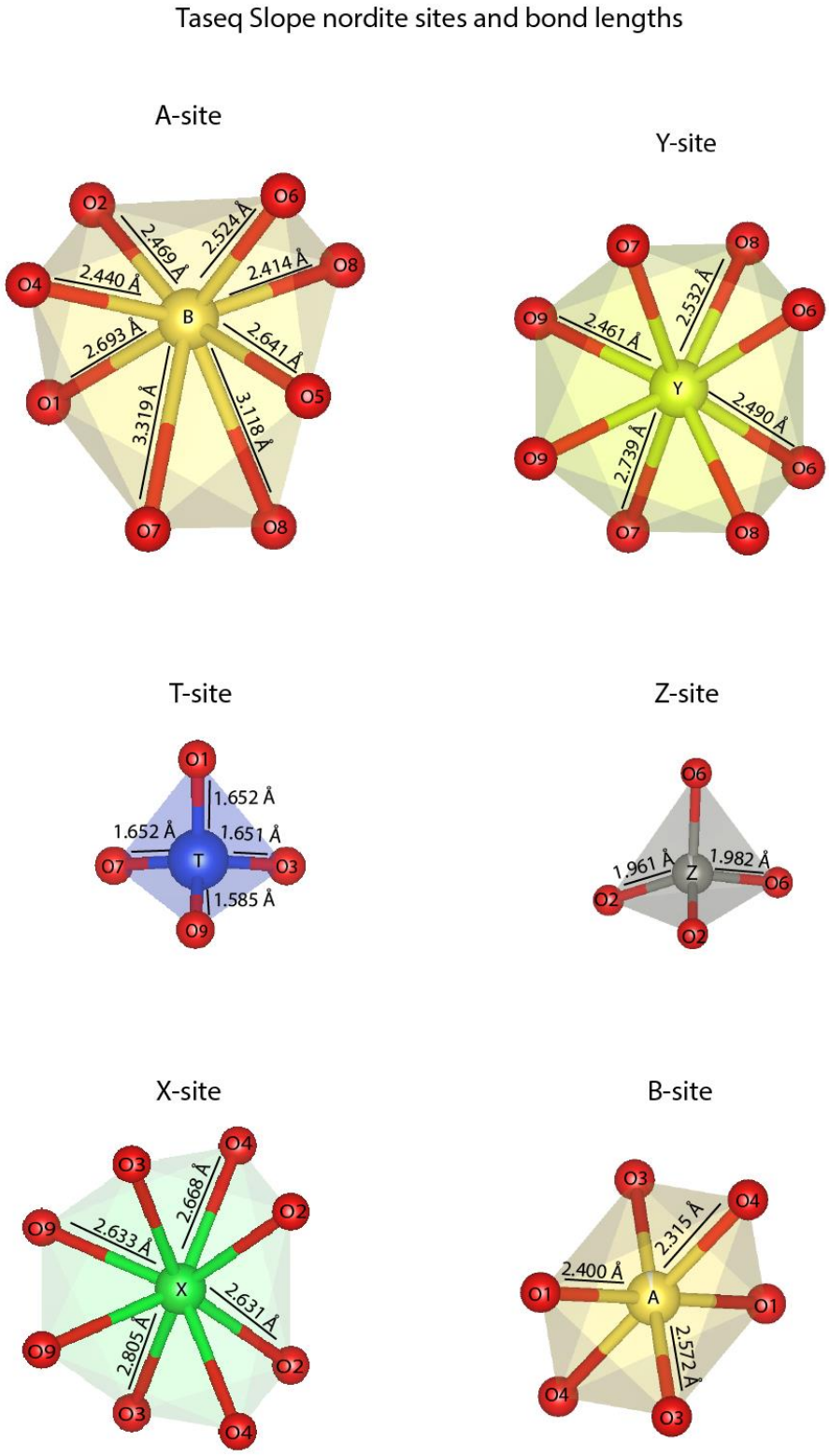

FIGURE 4.27: Overview of Taseq Slope nordite sites and bond lengths.

Tables 4.10 and 4.11 consists of the bond-valence sums of two nordites, one from Taseq (431) and one from Igdlutalik (422). Experiment 431 (Table 4.10) yielded the highest Ba occupancy (0.68 sof Ba) of the Taseq nordites analyzed and was therefore chosen for comparison.

The two tables generally show the same trend when it comes to the bond-valence summations. The *X*-site sums up to 2.071 charge in exp.431 (Table 4.10) and 2.049 in exp. 422 (Table 4.11). This is almost equal to the ideal charge of 2 in the *X*-site. On the other side, the REE-site, represented by *Y* in the tables, has a lower total sum of the bond-valence than the ideal 3 positive charge. In exp. 422 there is a lack of 0.121 charge while in exp. 431 the deficiency is 0.463 charge.

The *Z*-site also has less than ideal charge (2) with exp 431 and exp. 422 lacking 0.269 and 0.101 charge respectively.In both of the experiments, the *A*-site has more or less an ideal charge. However, the *B*-site has low charge sum of 0.752 in exp. 422 and 0.842 in 431.

Finally, the *T*-sites are close to the valence of 4 which is the ideal for a Si-filled site.

When it comes to the bond-valence summation of the anions, in this case only oxygen, the result varies. The summation of O1, O3 and O5 individually has the highest valence, and differs from the ideal valence of 2 with 0.101, 0.094 and 0.112 surplus charge in exp. 422 and 0.098, 0.084 and 0.091 in exp. 431, both respectively.

On the other side, O4, O8 and O9 has the lowest bond-valence sum of 1.778, 1.727 and 1.834 in exp. 422 and 1.774, 1.663 and 1.789 in exp. 431.

TABLE 4.10: Bond-valence sums for Taseq nordite (experiment 431).

	X	*Y*	*Z*	*A*	*B*	*T(1)*	*T(2)*	*T(3)*	SUM	
O1				0.173 2x↓	0.088	0.900		0.937	2.098	
O2	0.288 2x↓		0.445 2x↓		0.148	1.061			1.942	
O3	0.192 2x↓			0.110 2x↓		0.848		0.935	2.084	
O4	0.264 2x↓			0.214 2x↓	0.151	1.135			1.774	
O5					0.096 2x→		0.950 2x→		2.091	
O6		0.358 2x↓	0.420 2x↓		0.128		1.014		1.921	
O7		0.178 2x↓			0.020		0.867	0.935	1.999	SUM O8
O8'		0.344 2x↓			0.170		1.117		1.632	1.663
O8"					0.032				0.032	
O9	0.293 2x↓	0.388 2x↓						1.108	1.789	
SUM	2.071	2.537	1.731	0.992	0.843	3.945	3.947	3.915		

Note: (1) Parameters for calculations of bond-valence sums were taken from Gagné & Hawthorne (2015). (2) The bond valence sum for *X* was calculated based on (0.51Ba+0.36Sr+0.13Ce). (3) The bond valence sum for *Y* was calculated based on (0.54Ce+0.26La+0.14Nd+0.05Pr). (4) The bond valence sum for *Z* was calculated based on (0.51Zn+0.32Fe+0.09Mn+0.07Li). These were all recalculations made after site-assignment discussion in 5.2.1.

TABLE 4.11: Bond-valence sums for Igdlutalik nordite (experiment 422).

	X	*Y*	*Z*	*A*	*B*	*T(1)*	*T(2)*	*T(3)*	SUM	
O1				0.173 2x↓	0.086	0.905		0.937	2.101	
O2	0.278 2x↓		0.490 2x↓		0.152	1.056			1.976	
O3	0.192 2x↓			0.115 2x↓		0.850		0.937	2.094	
O4	0.269 2x↓			0.212 2x↓	0.159	1.139			1.778	
O5					0.093 2x→		0.963 2x→		2.112	
O6		0.383 2x↓	0.459 2x↓		0.131		1.025		1.988	
O7		0.226 2x↓			0.019		0.867	0.935	2.046	SUM O8
O8'		0.403 2x↓			0.168		1.126		1.697	1.727
O8"					0.031				0.031	
O9	0.286 2x↓	0.428 2x↓						1.120	1.834	
SUM	2.049	2.879	1.899	0.999	0.752	3.949	3.980	3.929		

Note: (1) Parameters for calculations of bond-valence sums were taken from Gagné and Hawthorne (2015). (2) The bond valence sum for *X* was calculated based on (0.75Sr + 0.21Ca + 0.05Ba). (3) The bond valence sum for *Y* was calculated based on (0.49Ce + 0.43La + 0.05Nd + 0.03Pr). (4) The bond valence sum for *Z* was calculated based on (0.94Zn + 0.02Fe + 0.02Mg + 0.01Mn). These were all recalculations made after site-assignment discussion in 5.2.1.

5. Discussion

5.1 Sector zoning in nordite

The Taseq Slope nordite has a pronouced sector zoning (Figs. 4.19 and 4.20). where Ba and Sr are they main elements that vary between the sectors. The Taseq nordite may be divided into four chemically distinct zonations based on the suggested thresholds in Table 5.1. Strontium was chosen as the separating element due to the large variation in concentration from zone to zone. Barium could also be used as a separating element, but the uncertainties are higher in the Ba chemical data, which was also a deciding factor to why Sr was chosen.

TABLE 5.1: Zonations based on Sr-thresholds in nordites from the Taseq slope.

Zonation	**Threshold (*apfu*)**
Very low Sr	0.2
Low Sr	0.3
High Sr	0.4
Very high Sr	0.5+

The following table (Table 5.2) displays the chemical data from the different zones based on the thresholds in Table 5.1. The thresholds were applied to all EPMA datasets (EHG7, EHG10, EHG13, EHG15 and EHG_EPOXY). EHG4 (Igdlutalik dataset) is there for comparison, while the “Core” column is analysis that was taken in the cores of the nordites and are separate from the core zonations. The names of the zonation are just too easily separate between them, and is only internally relative between the data produced for this thesis.

TABLE 5.2: Chemical data (EPMA) of the different zonations in Taseq nordites. Based on Sr-thresholds in Table 5.1.

Zonation/Sample	V.H. Sr	H. Sr	L. Sr	V.L. Sr	Core	EHG4
n	*20*	*17*	*25*	*25*	*9*	*8*
Weight percent oxides						
SiO_2	44(1)	43.6(8)	43(1)	42.7(6)	43(1)	45.2(5)
ZnO*	5.0(3)	5.0(3)	5.0(3)	5.0(3)	5(3)	9.6(6)
FeO	2.3(1)	2.5(3)	2.6(5)	3.2(2)	2.4(6)	0.2(1)
MnO	0.7(1)	0.7(2)	0.7(3)	0.8(1)	0.9(6)	0.09(4)
MgO	-	-	-	-	-	0.10(4)
La_2O_3	5(2)	6(2)	6(2)	6.1(4)	2.1(4)	9(1)
Ce_2O_3	14(2)	14(2)	14(2)	13.2(5)	12(2)	11.0(9)
Nd_2O_3	3(2)	2(2)	2(2)	1.5(3)	6.5(9)	1.1(5)
Pr_2O_3	1.2(3)	1.0(3)	0.9(4)	0.7(2)	1.7(3)	0.6(3)
SrO	6.9(7)	5.9(5)	5(1)	2.9(6)	5(4)	9.8(6)
BaO	5(2)	7(2)	8(3)	13(1)	8(7)	1.0(6)
CaO	0.4(1)	0.4(2)	0.4(2)	0.2(5)	0.3(1)	1.5(1)
Na_2O	11.5(6)	11.3(3)	11.3(7)	10.9(3)	11.3(4)	12.0(2)
Li_2O**	0.25(1)	0.25(1)	0.25(1)	0.25(1)	0.25(1)	n.a.
Total	99.62	99.62	99.79	100.52	99.03	101.12
Atoms per formula unit						
Si	5.94	5.95	5.94	5.91	5.95	5.95
Zn	0.50	0.50	0.50	0.51	0.51	0.94
Fe^{2+}	0.26	0.28	0.30	0.37	0.27	0.02
Mn	0.08	0.08	0.08	0.10	0.11	0.01
Mg	-	-	-	-	-	0.02
La	0.27	0.29	0.32	0.31	0.11	0.43
Ce^{3+}	0.70	0.69	0.69	0.67	0.59	0.53
Nd	0.15	0.12	0.10	0.07	0.32	0.05
Pr	0.06	0.05	0.05	0.04	0.08	0.03
Sr	0.55	0.47	0.36	0.23	0.43	0.75
Ba	0.27	0.37	0.45	0.70	0.45	0.05
Ca	0.05	0.05	0.05	0.03	0.04	0.21
Na	3.01	2.99	3.01	2.93	3.01	3.05
Li	0.07	0.07	0.07	0.07	0.07	-

*Zn data from ICPMS, an average from samples EHG7, EHG10, EHG13, EHG15, EHG EPOXY. Zn problems with EPMA data as stated, values applied to all zonations even though they are not differentiated on the ICPMS.

**Li data from ICPMS, Li discovered as a potential substituting element with Na, and were not included in the early analysis of nordite. The Li value is therefore an average from samples EHG10 and EHG15 and applied to all nordites of the Taseq Slope.

Figure 5.1 illustrates the different zones in the Taseq nordite and the respective *X*- and *Y*-site composition for each sector. The composition of nordite is further discussed in Section 5.2.

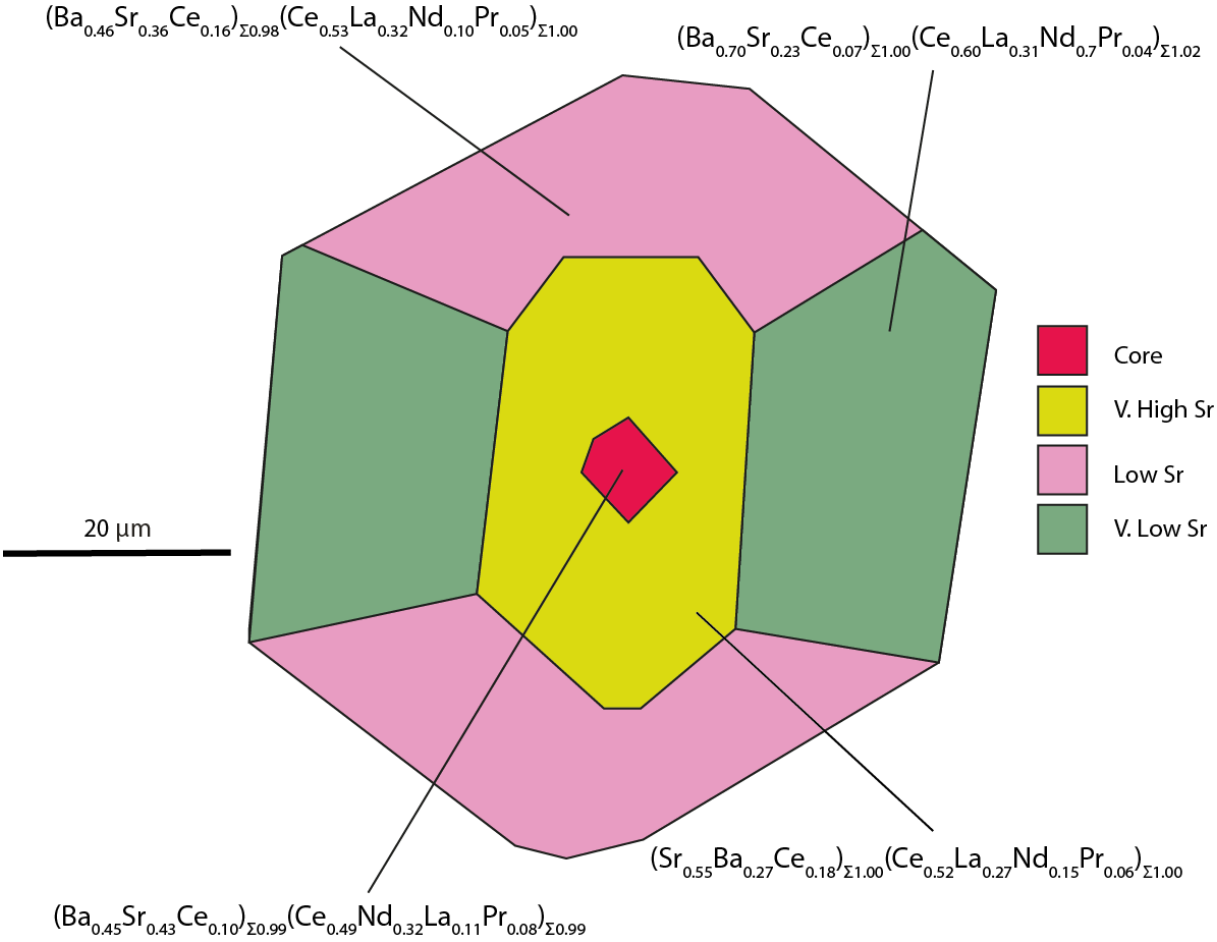

FIGURE 5.1: Illustrative view of the sector zoning of the Taseq nordite. Looking down an assumed c-axis.

Apart from the obvious variations between Ba and Sr in the different zonations, there is a variation in the REE-content in particularly. The general trend is that with a decreasing Sr content the REE-content also decreases. This is the case for Ce (0.70 → 0.67 *apfu*), Nd (0.15 → 0.07 *apfu*) and Pr (0.06 → 0.04 *apfu*). On the contrary, the La content increases (0.27 → 0.31 *apfu*). However, the most interesting observation is how the core differs compared to the other zones. The core contains a high amount of Nd (0.32 *apfu*) while the La content is the lowest of all the zones (0.11 *apfu*). This difference makes the Nd the second most dominant REE in the *Y*-site, which is something that is not the case for the other zones. The high concentration of Ba and Nd in the core may indicate that the core preferentially incorporates the most incompatible elements. Unfortunately, due to the ICPMS beam size being 40 µm it is not possible to get an accurate measurement on the trace elements in the core.

The differentiated uptake of REE and Ba/Sr in a nordite is a sector zoning, which is defined as having different chemical compositions in different growth sectors (Dowty, 1976). Sector zoning has been described in several minerals, i.e. dolomite (Fouke & Reeder, 1992), titanite (Paterson *et al.*, 1992) monazite (Cressey *et al.*, 1999), fluorite (Bosze & Rakovan, 2002) and uraninite (Alexandre *et al.*, 2015). It is commonly believe that chemical differences in sector-zoned crystals are related to differences in atomic structure on different growth surfaces e.g. (Reeder & Paquette, 1989; Fouke & Reeder, 1992; Rakovan *et al.*, 1997). Cressey *et al.*, (1999) concluded that the sector zoning of the monazite was governed by differences in the REE ionic size. In Cressey *et al.* (1999) monazites the sectors were defined by variations in uptake of La and Nd, while Ce remained close to constant throughout the sectors. The same type of trend can be seen in the nordites (Fig. 5.2) where the uptake of La and Nd in the different Sr zonations are opposite (Fig. 5.2 A and C). In addition, there is a more or less even partitioning of Ce in all the zones except the core (Fig. 5.2 B). The lower amount of La and Ce in the core (Fig. 5.2 A and B) could be explained by their higher uptake of Pr and Nd (Fig. 5.2 C and D).

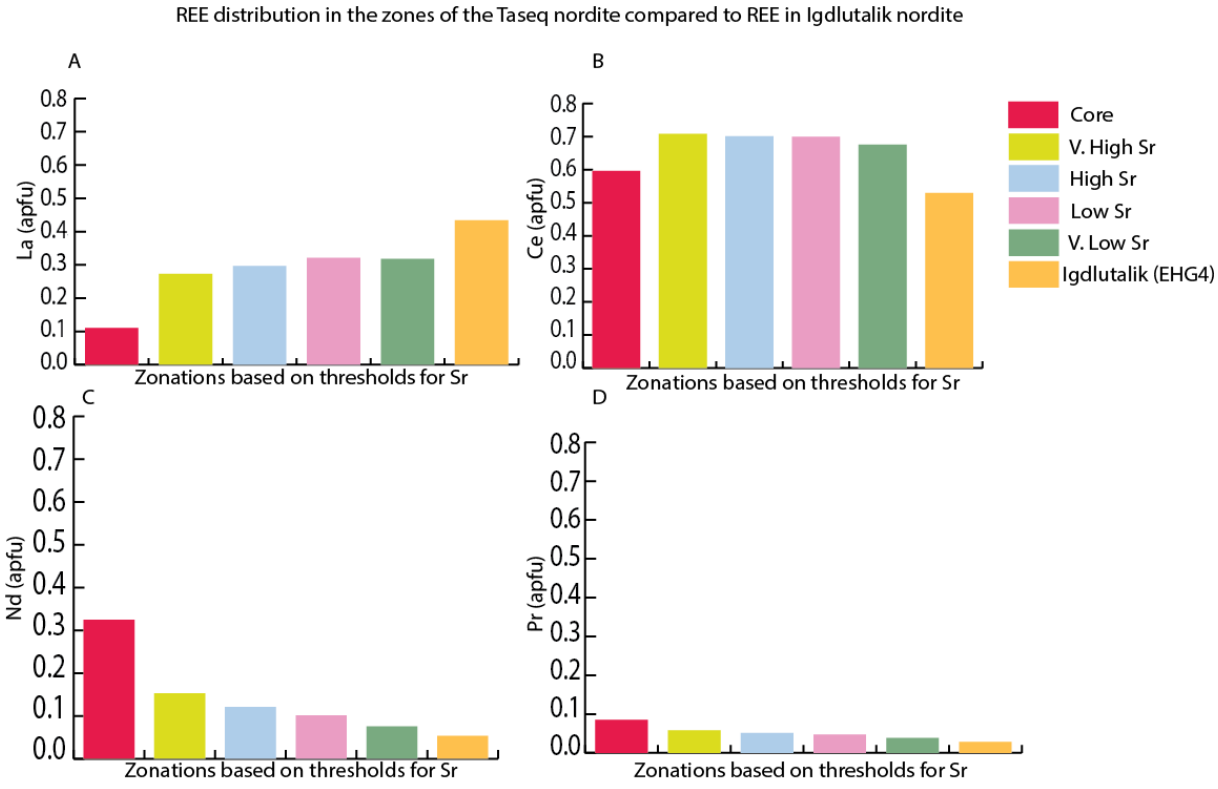

FIGURE 5.2: REE distribution in the *Y*-site based on Sr-thresholds in Table 5.4.

The Igdlutalik nordite (EHG4) does not exhibit the same zonation as with the Taseq nordite, with the *X*-site being dominated by Sr throughout the crystal (Fig. 5.3).

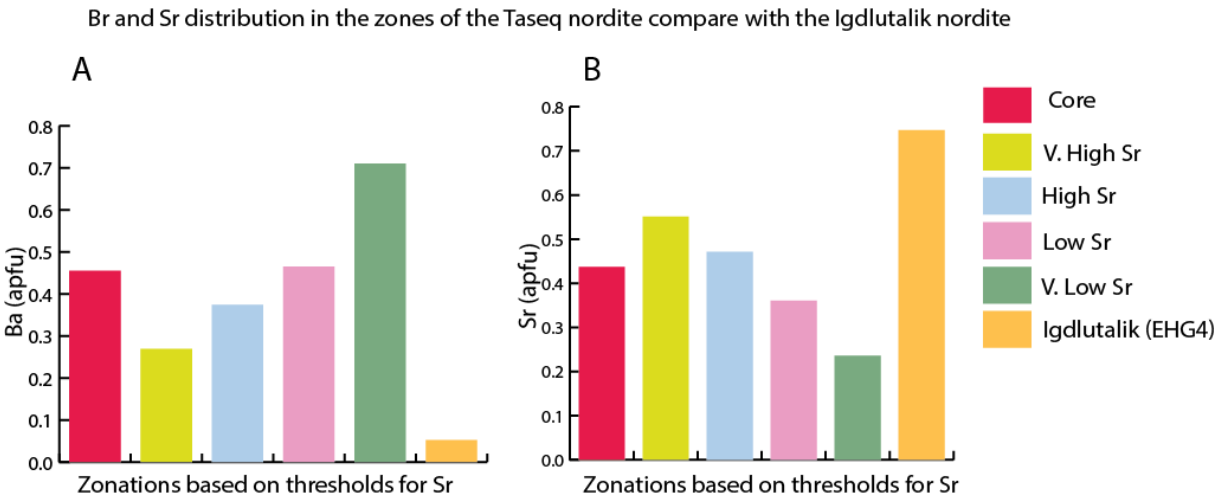

FIGURE 5.3: *X*-site distribution based on Sr-thresholds in Table 5.4.

In the monazites, Cressey *et al.* (1999) came to the suggestion that by having a combination of partially-constructed sites, or "protosites" (Nakamura, 1973), and a constant REE ion-exchange, the different REE site occupancies could be preserved within each sector.

The same type of hypothesis could be a possible explanation for the differentiated Ba/Sr uptake of the zones in nordite. By having the *X*-sites in nordite as protosites, combined with a free ion-exchange between Sr and Ba, the elements could potentially partition into separate *X*-sites during crystal growth. Sr and Ba zonation has been described in plagioclase phenocrysts (Zellmer *et al.*, 2003). However, Zellmer *et al.* (2003) results are incomplete and only propose that the Ba/Sr zonation in the plagioclase is a result of complex crystal growth history, rapid crystal growth and variable crystal residence time.

For the Igdlutalik nordite, the absence of Ba at the locality, might be the reason why we do not see zonations in the "common" nordite aswell. Because even though the Igdlutalik nordite is rich in Ca the zonation does not occur between Sr and Ca. Interestingly, Pekov (2000) have mentioned that it is possible to find zonal nordite crystals with different parts representing by nordite-(Ce), manganonordite-(Ce) and ferronordite-(Ce). He does not further elaborate on what type of zonation it is or present data on it. The zonation mentioned by Pekov (2000) would be related by the *Z*-site in the nordite with zones varying from Mn-dominant, Fe-dominant and Zn-dominant. This is not something that is observed from Igdlutalik, and differs from the sector zoning in the Taseq nordites which is determined by the *X*-site.

As discussed in the previous segments, the "sector-zoning" is the main reason we see the high variations in the elements (i.e. Sr, Ba, REE), which again leads to high uncertainties as seen in

Table 4.1. Due to high internal variances of the Taseq nordites, uncertainties are also related to the amount of analysis points done. In an ideal scenario there would be an equal amount of analysis points from the different zonations of the nordite. To the best of ability, this was done in this study. The sector-zoning also have further consequences for the structural discussion done in Section 5.2.1. The chemical zonation of the Taseq nordites, makes it so the SXRD analyses is an average of all the zones, due to the impossible task to extract a specific zonation for analysis.

5.2 Composition of nordites from Ilímaussaq

When analyzing simple minerals like members of the olivine group it is often straightforward to use chemical data to understand the crystal chemistry of the mineral and assign the elements to the sites in the structure. However, in minerals with complex chemistry and crystal structure, EPMA data is rarely enough to understand the mineral. This is particularly true for the nordites of this study, which contain elements with large overlaps during EPMA analysis (see Sections 3.4 and 3.5). Therefore, it is necessary to combine several analytical techniques to get the full picture, which in this study includes EPMA, LA-ICPMS and SXRD. The chemical analysis provide information on which element is occurring and their concentration in minerals, but not where in the structure they are placed. On the contrary, the SXRD gives information on the number of electrons present at each site in the structure, but not what specific elements they are. Below I combine the information from chemistry and crystal structure analysis to provide the formula of the nordites from Ilímaussaq.

From the preceding section it is clear that the nordites form Taseq are chemically heterogeneous, which makes it difficult to perfectly combine chemical and structural data. Ideally, the same single crystal sample should be used for both SXRD and microprobe analysis. The structure experiments are taken from one single crystal, without knowing if the crystal possesses characteristics such as different zonations. The EPMA data is on the other hand an average of several analysis points. The dataset used for the Taseq experiment was EHG 7 that contain an average from several different zonations throughout the crystal. These different zonations, as illustrated in Section 4.2 (Paragenesis and petrography), contain different elemental concentrations which is something we do not know about the crystal used for SXRD. The EHG7 EPMA dataset was used for chemical data input in the Taseq calculations (Table 5.3), due to it having the highest average concentration of Ba (Table 4.1). SXRD experiment 431 was used as it yielded the highest initial refined occupancy of Ba/Sr (0.677/0.323) in the

X-site. For the Igdlutalik site-scattering calculations (Table 5.2), EPMA dataset EHG4 and SXRD experiment 422 was used.

Moreover, this is another uncertainty when it comes to the calculations of the site-scattering. The different datasets are not equal, even though they are gathered from the same material of the Taseq slope. This can be exemplified by microprobe dataset EHG10 and EHG15 (Table 4.1) which has Sr as the dominant element in the *X*-site.

5.2.1 Site assignment

To determine which elements are hosted in the different structural sites, a site scattering table is common to use (Tables 5.3 and 5.4). The table consists of several different parameters that helps determine the site-compositions of the structure. Firstly, the refined site scattering (RSS, *epfu*) is based on the site occupancy factor (sof) from the SXRD refinement and estimates how many electrons the site contains. By multiplying the sof with the respective atom number you get the RSS and the chemical data. The site-population is initially a trial and error process, where the goal is to get a calculated site scattering (CSS, *apfu*) that correlates with the RSS. By using the proportions of each element (from the site-population) and multiply them with their respective atom number before adding them up, you get the CSS. It is important to have a RSS and a CSS that correlates well, because it shows that there is a correlation between chemistry and structural data and therefore shows that the site-assignment is realistic.

The coordination number (CN) the number of anions bonding to the central cation and used to calculate the average observed bond-distance (ABL, Å). This is calculated based on the data presented in Table 4.10. Similar to what is done with the RSS and the CSS, calculated bond-distances (CBL, Å) are used to compare structure and chemistry. By using the proportion of each element (from the site-population) and multiplying it with the ionic radii of said element you get the CBL.

Calculated bond-valence sum (BVS) is calculated by the bond-lengths from the structural dataset and the site-population, and is used to express how much charge each site yields. Bond valence (s) is calculated by using formula $s = \exp[(R_0 - R)/B]$, where R is the observed bond-length in the structural dataset and R_0 and B are empirical parameters determined for most commonly encountered bonds (Urusov, 1995; Brown, 1996). The BVS is highly dependent on which source you use for the empirical parameters such as Brown & Altermatt (1985) and Brese & O'keeffe (1991). For the calculations in this study the latest values by Gagné and Hawthorne (2015) was used. There are a lot of uncertainties when calculating the BVS, and is only used to

check that the site-assignment is ok. For example, if a site is believed to be full of Zn and the BVS is 3, there is a problem, but smaller variations like 2.1 and 1.9 are normal for a site that ideally should be 2. The same is true for the other parameters discussed below. The correlation between observed and calculated values will never be exactly equal in natural samples.

5.2.1.1 Site-assignment - Igdlutalik nordite

TABLE 5.2: Site-assignment for Igdlutalik nordite. SXRD experiment 422 was used in combination with EPMA dataset for EHG4.

Site	RSS (*e*)	Site-population	CSS (*e*)	CN	ABL (Å)	CBL (Å)*	BVS (S)**
X	35.93	$Sr_{0.75}Ca_{0.20}Ba_{0.05}$	35.30	8	2.618	2.660	1.94
Z	28.85	$Zn_{0.94}Fe_{0.02}Mg_{0.02}Mn_{0.01}$	29.21	4	1.949	1.975	1.90
Y	56.27	$Ce_{0.49}La_{0.43}Nd_{0.05}Pr_{0.03}$	57.70	8	2.554	2.568	2.88
A	10.69	$Na_{1.00}$	11.00	6	2.430	2.580	1.00
B	10.99	$Na_{1.00}$	11.00	8	2.531	2.600	0.75

*Ideal bond-distances are calculated using the ionic radius of Shannon (1976).

**Bond-valence parameters from Gagné and Hawthorne (2015) corrected according to site-population.

The refined site scatter (RSS) for the Igdlutalik nordite *X*-site is 35.93 *e*, which is lower than the 38 *e* the site would have had if fully occupied by Sr (Table 5.2). The lower RSS showes that some elements lighter than Sr occupies the site. This is in good agreement with the chemical data where a significant Ca substitutes for Sr on the site. The suggested site-population of the *X*-site yields a similar CSS of 35.50 *e* and there is a good agreement with both the CBL, ABL and BVS. The *Z*-site has an RSS of 28.85 which indicates that something lighter than Zn (30 *e*) is substituting for Zn. As Fe, Mn and Mg all have small concentrations in the nordite (Table 4.1), substituting these lighter (26, 25, 12 *e* respectively) elements for Zn would lower the total *e* of the site. In addition, ABL, CBL and BVS correlates well with having Fe, Mn and Mg in the site-population yielding a CSS of 29.21 *e*. Because the *Y*-site is a pure REE site, there is not much to discuss on the site-population, with all the parameters showing an agreement with each other. The RSS of the *A*-site is 10.69 *e*, which would suggest that some lighter element is substituting for Na. However, from the EPMA data (Table 4.1) there is not analyzed any potential substitute. Although the Na content is slightly elevated (mentioned in Section 3.5), there should not be room for any other element to substitute for Na (3.06 *apfu*). A potential element that could substitute would be Li, this is discussed further in Section 5.2.3 (Crystal chemistry).

After satisfying the sites with the correct *apfu* there is still an excess of 0.01 *apfu* Ca, 0.04 *apfu* Ce and 0.06 *apfu* Na (Table 4.1), while the Z-site is lacking 0.01 *apfu* to be filled. In addition, the total sum of the EHG4 analysis is high with a total oxide content of 101.12 wt% (Table 4.1). This will also have small consequences for the stoichiometry of the *apfu* calculation.

5.2.1.2 Site-assignment - Taseq nordite

TABLE 5.3: Site-assignment for Taseq nordite. SXRD experiment 431 was used in combination with EPMA dataset for EHG7.

Site	RSS (*e*)	Site-population	CSS (*e*)	CN	ABL (Å)	CBL (Å)*	BVS (S)**
X	50.19	$Ba_{0.51}Sr_{0.36}Ce_{0.13}$	49.78	8	2.701	2.746	2.07
Z	26.68	$Zn_{0.51}Fe_{0.32}Mn_{0.09}Li_{0.07}$	26.08	4	1.973	1.988	1.73
Y	57.12	$Ce_{0.54}La_{0.26}Nd_{0.14}Pr_{0.05}$	57.49	8	2.554	2.550	2.54
A	10.69	$Na_{1.00}$	11.00	6	2.430	2.592	0.99
B	11.58	$Na_{0.96}Ca_{0.04}$	11.36	8	2.531	2.644	0.84

*Ideal bond-distances are calculated using the ionic radii of Shannon (1976)

**Bond-valence parameters from Gagné and Hawthorne (2015) corrected according to the site population.

In all published data on nordite, the *X*-site has been a site dominated by Sr followed by smaller amounts of Ca and Ba (Table 1.4 and 1.5).This is also the case for the Igdlutalik nordite, discussed in the previous paragraph. However, the Taseq nordite exhibits a RSS of 50.19 *e* for the *X*-site, which is significantly higher than it was for the Igdlutalik nordite (Table 5.2). This indicates that there is an element heavier than Sr and Ca occupying the site. The CSS value of 49.78 *e* shows that the site-population suggested gives a result that correlates well with the RSS calculated from the structure. The *Z*-site RSS and CSS has a difference of 0.60 *e*, which indicates that the site-population of $Zn_{0.51}Fe_{0.32}Mn_{0.09}Li_{0.07}$ is most likely. The *Y*-site containing the REEs has RSS and CSS values that closely compare to each other with a difference of 0.37 *e*.

Based on the discussion above, the site-population of the *X*-site is most likely $Ba_{0.51}Sr_{0.36}Ce_{0.13}$. This can be argued further with that unlike previously described nordites, there is more Ce (20-25% more) and far less Ca (71-80%) in the Taseq nordite. Previously, as evident in Table 5.2, Ca have been allocated to the *X*-site, but due to the small amount of Ca in the Taseq nordite, the *X*-site could not be properly accommodated with only Ba and Sr. What is suggested here is that the excess Ce from the *Y*-site, goes into the *X*-site. This would fill up the *X*-site while

simultaneously satisfy the *Y*-site with a total of 1 *apfu*. In addition, having heavy elements such as REE in the *X*-site, would explain the high RSS of the site and the BVS of 2.07 (Table 5.3).

5.2.1.3 Formula

The site assignment enables the distribution of the elements derived from chemical analysis to be distributed between the various sites in the structure. The resulting formula are presented in Table 5.4.

TABLE 5.4: Suggested formula for Igdlutalik and Taseq nordite.

Suggested formula
Igdlutalik Island
$Na_{2.06}Na_{1.00}(Sr_{0.75}Ca_{0.21}Ba_{0.05})_{\Sigma 1.01}(Ce_{0.53}La_{0.43}Nd_{0.05}Pr_{0.05})_{\Sigma 1.06}(Zn_{0.93}Fe_{0.02}Mg_{0.02}Mn_{0.01})_{\Sigma 0.98}Si_{5.95}O_{17}$
Taseq Slope
$Na_{2.05}(Na_{0.96}Ca_{0.04})_{\Sigma 1.00}(Ba_{0.51}Sr_{0.36}Ce_{0.13})_{\Sigma 1.00}(Ce_{0.54}La_{0.26}Nd_{0.14}Pr_{0.05})_{\Sigma 0.99}(Zn_{0.51}Fe_{0.32}Mn_{0.09}Li_{0.07})_{\Sigma 0.99}Si_{5.92}O_{17}$

The Igdlutalik Island nordite analyzed in this thesis is a nordite-(Ce), which matches what is described in Upton *et al.* (1976). If we compare the chemical composition from the two studies, the datasets are very similar. Table 5.5 shows the comparison of the two datasets.

TABLE 5.5: Comparison of chemical data (wt%) on nordite from Upton (1976) and this study.

Oxide	Upton *et al.* (1976)	This study
n	8	8
SiO_2	46.48	45.2(5)
ZnO	9.74	9.6(6)
FeO	0.22	0.2(1)
MnO	-	0.09(4)
La_2O_3	8.48	9(1)
Ce_2O_3	11.37	11.0(9)
Nd_2O_3	1.35	1.1(5)
Pr_2O_3	-	0.6(3)
SrO	9.73	9.8(6)
BaO	0.99	1.0(6)
CaO	1.48	1.5(1)
Na_2O	11.15	12.0(2)
Total	101.12	101.12

*As previously mentioned in the footnote of Table 2.4 Upton *et al*. (1976) wrongly reported a BaO content of 8.99 wt%. The correct value is 0.99 wt%.

With these almost identical datasets, one can assume that the nordite analyzed in this study is the same species of the nordite-group as the one reported in Upton *et al.* (1976). However, as mentioned in the footnote of Table 2.4, Upton *et al.* (1976) reported the BaO content to be 8.99 wt%. This lead to the initial thought that the data were erroneous, but a recalculation of the formula using the data from Upton *et al.* (1976) showed that it is a typo in the paper and that the real number should be 0.99, as listed in Table 5.5. The Taseq nordite on the other hand has a composition that has never been described before.

5.2.2 Naming of the new nordite-group species

Since it is now evident that the Taseq nordite studied in this thesis is a new mineral to the world, it has to be given a name. The nordite-group already have both a prefix and a suffix determined by the *Z*-site and *Y*-site composition, respectively. Therefor it would be complicated to give it a second prefix or suffix. Ba-ferronordite-(Ce), is not something that flows of the tongue. We suggest the name illoqite as the root name for the new nordite species. Illoq is the Greenlandic word for cousin, and would describe the Ba-bearing nordites chemical relation to the other group members. Analogous to nordite nomenclature, the *Z*-site should determine the prefix, but when the *Z*-site is dominated by Zn no prefix is required. In accordance with Bayliss & Levinson (1988) the suffix is determined by the dominant REE, which in nordites is the composition of the *Y*-site. Therefore, the correct name for the Taseq nordite would be illoqite-(Ce). Although, the name has not yet been proposed to the International Mineralogical Association, I will use it throughout this discussion. The suggested naming with illoqite as the root name for the Zn dominated species will make it possible to name other members in accordance with the known nordite minerals (Table 5.6).

TABLE 5.6: Proposed nomenclature for the nordite-group.

Name	Ideal formula	Status
Nordite-(La)	$Na_3SrLaZnSi_6O_{17}$	Exists
Nordite-(Ce)	$Na_3SrCeZnSi_6O_{17}$	Exists
Ferronordite-(La)	$Na_3SrLaFeSi_6O_{17}$	Exists
Ferronordite-(Ce)	$Na_3SrCeFeSi_6O_{17}$	Exists
Manganonordite-(La)	$Na_3SrLaMnSi_6O_{17}$	Theoretic
Manganonordite-(Ce)	$Na_3SrCeMnSi_6O_{17}$	Exists
Illoqite-(La)	$Na_3BaLaZnSi_6O_{17}$	Theoretic
Illoqite-(Ce)	$Na_3BaCeZnSi_6O_{17}$	Exists - this thesis
Ferroilloqite-(La)	$Na_3BaLaFeSi_6O_{17}$	Theoretic
Ferroilloqite-(Ce)	$Na_3BaCeFeSi_6O_{17}$	Theoretic
Manganoilloqite-(La)	$Na_3BaLaMnSi_6O_{17}$	Theoretic
Manganoilloqite-(Ce)	$Na_3BaCeMnSi_6O_{17}$	Theoretic

5.2.3 Crystal chemistry

Crystal chemistry is an important tool in the process of determining if a site assignment is valid. By comparing atoms size and charge, aswell as coordination number, one can determine if an element can enter and substitute with other elements in the different sites in the crystal structure. For example, in a tetrahedral coordinated site, $^{IV}Zn^{2+}$ with ionic radius of 0.60 Å can easily substitute for $^{IV}Fe^{2+}$ with ionic radius 0.63 Å, due to their similar size and same charge. On the other hand, even though for example Ba has the same charge of +2 it cannot enter the tetrahedral coordinated site. This is because of the atomic size difference between Ba and Fe/Zn, and due to this Ba only occurs in VI or higher coordinated sites, with its lowest atomic radius being ^{VI}Ba with 1.35 Å (Shannon, 1976). The atomic radius of ^{VI}Ba is over twice the size of $^{IV}Fe/^{IV}Zn$ and shows the importance of crystal chemistry and furthermore how it affects the site assignment in the crystal structure.

5.2.3.1 Validation of sign assignment for illoqite-(Ce)

The addition of Ce^{3+} in the *X*-site would leave the site with a 0.13 extra positive charge, which would need to be compensated by another site, seeing as the *X*-site now is containing a total of 1 *apfu* from Ba, Sr and Ce. This correction can be achived by having a vacancy in a site or that an element of a lower valence substitute an element with higher valence. In this dataset it seems to be the later, where 0.07 *apfu* Li that accommodates into the *Z*-site. The addition of this monovalent cation into a site already occupied by divalent cations (Zn, Fe and Mn) totals

the *Z*-site up to 0.99 *apfu*. The valence of the *Z*-site then adds up to 1.91, leaving it with a 0.09 charge deficiency. This deficiency would help balance out the excess from the *X*-site and reduce the surplus charge to 0.04. With the relative high internal variations of elements combined with challenges of the chemical analyses, a variation of just 0.04 electron, but be considered within the overall uncertainty of the chemical analyses.

When it comes to the size differences of the elements, $^{VIII}Ce^{3+}$ has an ionic radius of 1.143 Å, while ^{VIII}Ba and ^{VIII}Sr have 1.42 and 1.26 Å, respectively. Therefore, Ce^{3+} easily fits the *X*-site purely from a size perspective. Lithium has a comparable ionic radius (0.59 Å) to those of Fe^{2+} and Zn (0.63 and 0.60 Å, respectively) in tetrahedral coordination (Shannon, 1976). Consequently, Li would be able to substitute in to the *Z*-site.

Another hypothesis is related to the common observation in most nordites, that there is a general deficiency of Si. This deficiency might be a vacancy, which would help balance out the charge difference if needed. This might be the case in this analysis as the total of Si only adds up to 5.92 *apfu*. However, this sort of Si vacancy is not common, and should be considered with caution.

A third hypothesis is that the Li may enter into the *A*-site instead of the *Z*-site. Lithium cannot enter the *B*-site for the following reasons:

i) the site-scatter of *B* is already above 11 electrons and

ii) the site is truly eight coordinated, which is too big for Li.

If Li enters the A-site rather than the *Z*-site, the latter would only have 0.92 *apfu*. The occupancy of *A*-site (in exp. 431) is 0.972(8), which would indicate that something lighter than Na is also present in the site. Table 5.2 shows a total site-scatter of *A*-site to be 10.69 *e*, which can be achieved by a sire composition of $Na_{0.96}Li_{0.04}$ resulting in 10.68 *e*. In addition, adding Li to the Na sites means that 0.04 *apfu* Na (from EPMA) would need to substitute into the *Z*-site. However, this is unlikely as tetrahedrally coordinated Na is not common. Furthermore, according to Wenger & Armbruster (1991) the average tetrahedral Li-O bond is 1.960 Å, while in an octahedral coordination Li-O equals 2.150 Å. The average bond-length of the *A*- and *Z*-site in experiment 431 are 2.430 and 1.973 Å respectively (Table 4.10). If we compare the Li in the different sites, ^{VI}Li has a 0.280 Å longer bond, while ^{IV}Li has 0.017 Å longer bond. Therefore, from a crystal-chemical point of view it seems most reasonable to assign Li to the

Z-site. As with the Igdlutalik sample, there is an excess of Na (0.05 *apfu*) after the *A*- and *B*-sites are satisfied.

Figure 5.4 shows the full structure of nordite (exp.422 used for illustration) alongside a comparison of the site population between Igdlutalik nordite and Taseq nordite.

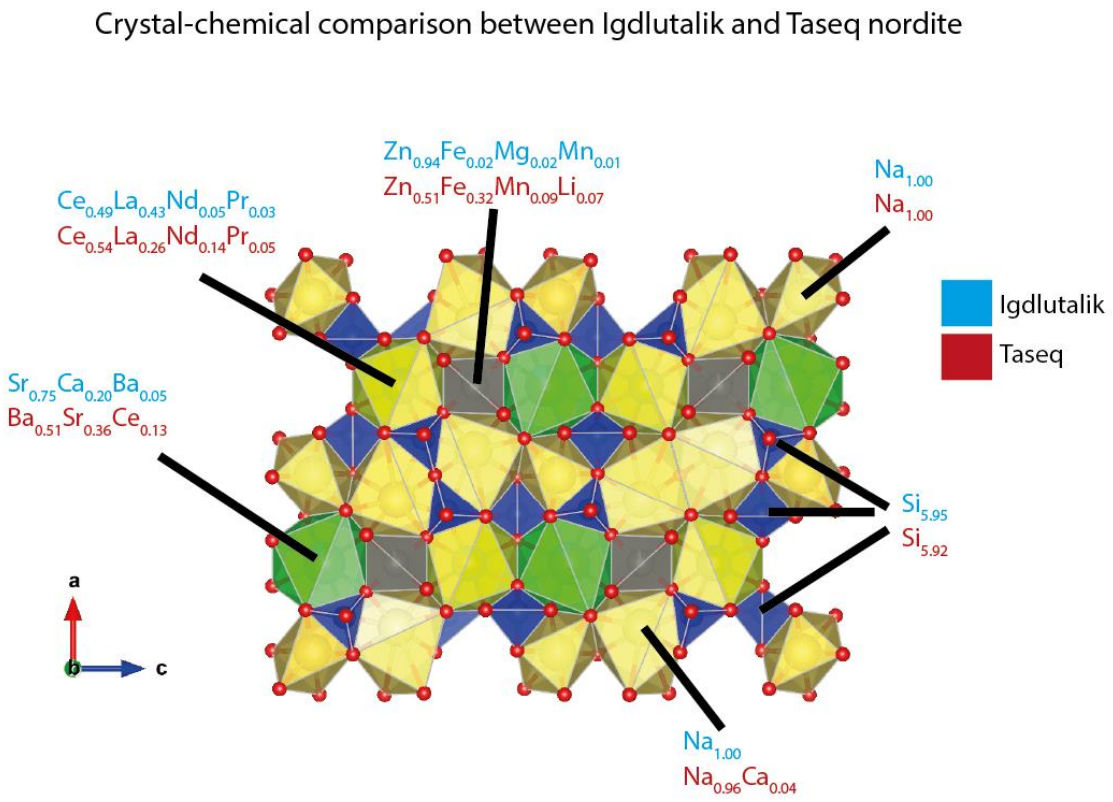

FIGURE 5.4: The structure of nordite seen along the *b*-axis with site-assignments.

5.2.3.2 Effects on the unit cell

After determination and validation of the site-assignment (Section 5.2.3.1) in illoqite-(Ce), it is clear that the occupancy of Ba into the *X*-site is the reason we see the increase in unit cell size compared to other nordite-group members (Fig. 4.26). From Fig. 4.25 all the illoqite-(Ce) experiments have a longer *a*-axis compared to the nordite-group members. The same can be seen in both the *b*- and *c*-axis as they are on average 0.067 Å longer than the nordite-group members. This in turn increases the unit cell volume by 29.94 $Å^3$ on average.

An interesting observation is that alongside the illoqite-(Ce), "normal" nordite-(Ce) also occurs. This is shown in the chemical datasets of EHG 10 and 13 (Table 4.1), where the Sr is more concentrated than Ba. There is also internal difference between EHG 10 and 13 with EHG 10

having a Sr/Ba ration of 0.50/0.32 *apfu*, while EHG 13 has a ratio of 0.42/0.40 *apfu*. Unfortunately, neither SXRD experiment (478 and 430) showed an initial Sr dominant occupancy of the *X*-site, so there are no comparable single-crystal experiments to datasets EHG 10 and EHG 13. This in turn makes it hard to compare how it structurally is related to both previous described nordites (Table 4.7) and the nordite-(Ce) and illoqite-(Ce) described in this study. However, one could assume that both datasets (EHG 10 and 13) would have a smaller unit cell than the illoqite-(Ce), but bigger than the nordite-(Ce) due to its significant Ba content. The data from Taseq indicates that there may very well be a full solid-solution between the nordite-(Ce) and illoqite-(Ce).

5.3 Nordite paragenesis

Table 5.6 shows the nordites paragenesis from the two different localities. Minerals marked with a star (*) was not observed in studied material, but has been previously described to occur with the Igdlutalik nordite (Upton *et al.*, 1976). Aegirines, arfvedsonite and narsarsukite are further discussed below Table 5.7 as they were the accessory minerals analyzed for this study.

TABLE 5.7: Paragenesis of Igdlutalik and Taseq nordite.

Paragenesis of nordite	
Nordite-bearing pegmatite from Taseq Slope	Nordite-bearing trachyte dyke from Igdlutalik Island
Major components:	Major components:
- Ussingite	- Aegirine
- Aegirine	- Albite
	- Narsarsukite
Minor components:	Minor components:
- Arfvedsonite	- Apatite*
- Ancylite-(Ce)	- Biotite*
- Britholite-(Ce)	- Calcite*
- Ba-bearing nordite-(Ce)	- Emeleusite*
- Epistolite	- Hematite*
- Chkalovite	- Lalondeite
	- Nordite-(Ce)
	- Pectolite
	- Riebeckite
	- Vitusite-(Ce)
	- Zircon*

The differences in paragenesis of nordite between the Igdlutalik Island locality and the Taseq slope are large, and shows that nordite can occur in different evolutions of alkalinity. As seen in Fig. 4.4 the nordites in the trachyte dyke of Igdlutalik Island are sparsely distributed in the aegirine and ablite matrix. While the nordites of the Taseq slope occurs as up to 5 mm clusters in the ussingite matrix (Fig. 4.5). The crystal growth of the two different species are also different with the Igdlutalik forming 20 µm -100 µm euhedral crystals, while the Taseq slope nordite exhibits a more radiating growth. From Fig 4.6 the diverging growth of the nordites seem to be growing out from a core resulting in concentric circles.

In both the localities the nordite is most likely early stage crystallizing mineral. This mainly due to the nordites large concentration of incompatible elements such as REE (Table 4.3). In normal crystallizing condition, this would indicate late stage crystallization, seeing as incompatible elements preferably remains in the melt. However, in alkaline complexes such as Ilímaussaq this is not the case. Minerals such as steenstrupine-(Ce), vitusite-(Ce) and eudialyte are early crystallizing primary minerals in alkaline complexes (Sørensen, 2001). In addition, both optical (Figs. 4.4-4.6) and BSE observations (Figs. 4.7, 4.11-4.12, 4.14 and 4.18) shows that the nordites crystal shape is close to euhedral, which would also suggest early formation.

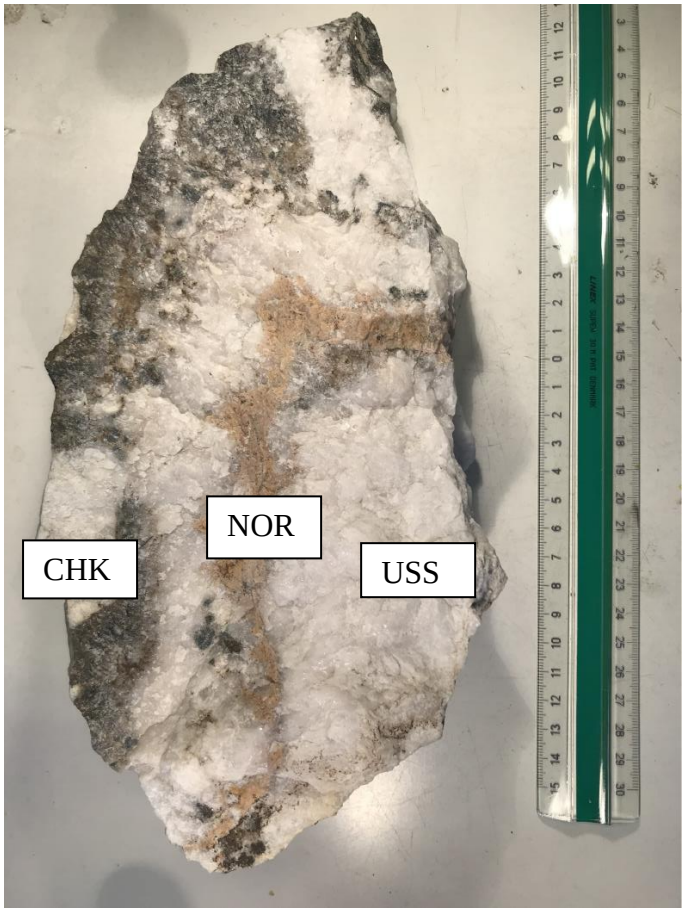

There is not observed any alteration of nordite in matrix from either locality. However, as seen from Fig. 5.5 samples from Taseq often has a brownish powdery coating on weathered surfaces. Investigation using powder XRD and SEM, confirmed the alteration product to be ancylite-(Ce).

FIGURE 5.5: Sample from the nordite-boulder in the Taseq slope. The brown "band" running through the sample is weathered nordite. Ussingite (USS) and chalkovite (CHK) is marked respectivly.

5.3.1 Igdlutalik Island nordite occurrence

An interesting question about nordite and its occurrence is why it is occurring at the locality at the Igdlutalik Island. From previous published literature about nordite, (Table 1.3) the mineral occurs in alkaline complexes paragenesis. Contrary to this, the nordite-bearing trachyte dyke at the Igdlutalik Island is far less evolved than alkaline complexes such as the Lovozero and Khibiny Massif and Mt. Saint-Hilaire.

In the material brought back from the fieldtrip to the locality, it was discovered that the locality contains vitusite-(Ce) (Friis, unpublished data, 2020). Vitusite-(Ce) usually only occur in hyper-agpaitic rocks, where it is one of the main REE-bearing minerals (Pekov & Ekimenkova, 2001). Structurally, vitusite-(Ce) can form through cation exchange between a sodium- and REE-rich late-stage hydrothermal fluid and apatite (Finch & Fletcher, 1992). However, as mentioned in the previous section, minerals such as vitusite-(Ce) occurs as early primary minerals in alkaline complexes. In addition, together with the vitusite-(Ce) discovery, lalondeite have also been identified (Friis, unpublished data, 2020). Lalondeite is believed to form during late-stage hydrothermal activity, however complete knowledge regarding its mode of occurrence is lacking (McDonald & Chao, 2009).

Both vitusite-(Ce) and nordite-(Ce) normally occur in highly evolved alkaline rocks (Pekov & Ekimenkova, 2001, Table 1.3), whilst the locality at the Igdlutalik Island is less evolved. The presence of narsarsukite is indicative of relatively low alkalinity as it typically does not occur in the highly evolved parts of alkaline complexes. Besides Igdlutalik, narsarsukite is known from veins situated approximately 100 m outside the complex in the Julianehåb granite (Petersen *et al.*, 1999). At this locality, which we visited during the fieldtrip, narsarsukite occurs with quartz, which is typical for narsarsukites from for example Mt. Flora in Lovozero (Pekov, 2000) and from the type locality of narsarsukite in the Narssâssuk pegmatite, South Greenland.

Upton *et al.* (1976) theory of origin of suggests that the nordite-bearing trachyte dyke was developed through a reaction between alkaline solutions from the subjacent comendite (Fig. 1.2) and the quartz diorite basement. Another possibility is that during crystallization of the trachyte, a small volume of more evolved melt or fluid was exsolved from the trachyte melt. Such an exsolved melt could have a higher alkalinity than the main melt and therefore enable the formation of more alkaline minerals such as nordite-(Ce) and vitusite-(Ce). Because the vitusite-(Ce) sample was not found *in-situ* at the locality it is not possible to link it to the rest of the dyke and therefore, its geochemical origin cannot be accurately determined. However, it is clear that the process forming the nordite-(Ce) at Igdlutalik are complicated.

5.3.2 Nordite-Ba occurrence

From the previous literature of nordite, there have never been reported more than 1.00 wt% BaO in nordite (Table 1.5). This is also the case for the Igdlutalik nordite analyzed for this thesis, while the Taseq slope nordite differs drastically. By having up to 13 wt% BaO in the Ba-dominated zones (Table 5.2 and Fig. 5.1), there must clearly have been a considerable amount of Ba during formation of the mineral. Illoqite-(Ce) is only the sixth Ba-mineral to be described from Ilímaussaq after barylite, ilímaussite-(Ce), joaquinite-(Ce), kuannersuite-(Ce) and ortho-joaquinite-(La) (Petersen, 2001). All of these minerals are rare in Ilímaussaq, but interestingly the Taseq slope is the type locality of ilímaussite-(Ce) and the ussingite vein of this study is where most ilímaussite-(Ce) has been found. This mineral has Ba concentrations up to 26.20 wt%, equivalent to 6.87 *apfu* and is the dominant element in three 12-coordinated sites of the ilímaussite-(Ce) structure (Ferraris *et al.*, 2004). There are no studies that have investigated this local enrichment in Ba, but it must be related to the large size of the ussingite vein (Fig. 2,10), which is the large known in Ilímaussaq. Many of the ussingite veins in Ilímaussaq have a simple mineralogy without many minerals that can incorporate incompatible elements. It might be that the size of this ussingite vein means that these unique Ba-minerals can form.

Historically, the nordite-group has not been host to Li (Table 1.5). However, there is nothing that compares to the nordite from the Taseq slope. The fact that Li is in the Taseq nordite, is not that surprising considering that the slope hosts minerals such as neptunite and polylithionite (Mindat[2]). These minerals have Li as a main constituent in their formula and indicates that there is a significant amount of Li in the Taseq slope. This would explain why Li is a substitute mineral for the Z-site position in the Taseq nordite structure.

The Taseq slope is the only known occurrence of ilimaussite-(Ce), however a "Ti-dominant ilímaussite-(Ce)" called diversilite-(Ce) has its type locality from Mt. Yukspor (Khibiny massif, Kola Peninsula, Russia) (Khomyakov *et al.*, 2003). This is the only known locality. Diversillite-(Ce) hosts a comparable Ba content to the ilímaussite-(Ce) with up to 24.85 wt% (7.20 *apfu*) (Khomyakov *et al.*, 2003). With having these distinct but similar minerals from two different alkaline complexes, there is reason to believe that the new nordite described in this study might yet to be discovered in the Khibiny Massif.

5.3.2.1 Gd + Er anomaly

The Gd and Er anomaly in Fig. 4.21 is something that is extremely rare. There could be several explanations to this:

i) Inflation: Due to the adjacent elements (Ho and Yb) of Er having values close to the detection limit (MDL, Table 4.3 subscript) the anomaly might be inflated. However, with Er values up to 7.88 ppm, the presence of the element is significant.

ii) Overlap: There could be elemental overlap when analyzing that overestimates the elements in question. Because of large concentrations of Ba in nordite, a potential overlap on ^{130}Ba + ^{36}Ar with 166Er is plausible, but should be almost negligible due to 130Ba being 0.11% (WebElements[1]) of natural occurrence of Ba and ^{36}Ar being 0.34% (WebElements[2]) of natural occurrences of Ar. For ^{157}Gd there are possible overlaps with BaF, LaF and CeF. However, there is no F in nordites in general. Lastly, there is a general XeAr overlap from the plasma of the LA-ICP-MS, but this is corrected by the background measurement.

iii) Instrument error: Elevated Er and Gd concentrations does not appear in the other minerals analyzed, and excludes an error with the instrument.

There is little if any publications on positive Er anomalies in minerals, and the only publications on positive Gd anomalies revolves around REE content in seawater and rivers e.g. (De Baar *et al.*, 1985; Bau & Dulski, 1996; Knappe *et al.*, 2005). Plausinaitis *et al.* (2018) presents REE data from water that has positive Gd and Er anomalies, but they conclude that the anomalies are derived from Chernobyl nuclear powerplant where these elements are used in the control rods and after the explosion, these elements are now elevated in the water passing the plant.

However, in Schønwandt *et al.* (2016) description of the Tanbreez REE deposit at Kringlerne (Fig. 1.3, white area) it is reported small amounts of Er and Gd. Unfortunately, the raw data is not published in the publication, so exact numbers are not known. In conversation between Greg Barnes and Henrik Friis, Barnes (co-author on Schønwandt *et al.*, 2016) mentioned a mineral (possibly fluorite) in the underlying unit (Black Madonna) of the kakortokite that had a positive Er-anomaly. This is however neither confirmed or explained, but could potentially be linked to the Er-anomaly in the nordites.

5.3.3 Aegirine and arfvedsonite

When looking at the accessory minerals in the Taseq slope, there are two generations of aegirine (Appendix 8.2 D). From the chemical compositions (Table 4.4) there is little that separates them, which makes it hard to distinguish which is primary and secondary. However,

if looked closely through the petrographic microscope, the browner colored aegirine seems to be sitting on top of the greener aegirine. This could indicate that the brown aegirine is secondary, while the yellow/green aegirine is primary.

There are clear differences in the aegirines between the two localities, with it being a main matrix mineral in the Igdlutalik sample, while only occurring as an accessory mineral in Taseq. Their crystal habit is also different with the aegirines in Igdlutalik forming short euhedral crystals up to 10 µm, while the Taseq aegirines forms clusters of larger crystals up to 1 mm.

The aegirines from Taseq show very low LREE in the chondritic normalized plot (Fig. 4.23) whereas the Igdlutalik aegirines have a more normal shaped pattern. The difference in the patterns can be explained by that REE (e.g. Ce, La) is a main constituent of nordite (Y-site) these elements preferentially incorporates into the nordite whereas the HREE do not. This further supports the hypothesis that nordite is an early formed mineral and that the trace elements suggest it formed before the aegirines. However, the same lack of LREE is not observed for the Igdlutalik nordite. This can be explained by the fact that the abundance of nordite-(Ce) and other REE-minerals at Igdlutalik is low compared to aegirine, which is the main matrix mineral. Therefore, the fractionation of LREE into nordite-(Ce) does not influence the bulk REE composition at this locality. The same cannot be said for the Taseq locality, as there is a much larger overall abundance of illoqite-(Ce) compared to the occurrence of nordite-(Ce) in Igdlutalik. At Taseq, the illoqite-(Ce) clearly affects the bulk REE composition of the locality, evident by the low LREE pattern in aegirine from the locality.

However, this same type of decline is not seen in the chondrite normalization pattern (Fig. 4.24 A) for arfvedsonite in the same sample (EHG 10). This could be because the arfvedsonite is formed earlier than the aegirine, and as a result of this incorporates more LREE than the aegirine.

Several attempts were made to calculate the amphibole formula based on the chemical composition in Table 4.4. These attempts involved trying to calculate the formula in the classical way based on 24 anions (Hawthorne *et al.*, 2012), and with the help of several modern spreadsheets e.g. (Locock, 2014; Ridolfi *et al.*, 2018) as well as a spreadsheet supplied by Muriel Erambert. However, none of these yielded a satisfactory result. The problem seemed to revolve around a low Fe_{tot}. Initially, Fe was analyzed as Fe^{3+} due to that aegirines were also analyzed the same day. This should not be an issue as Fe^{3+} can easily be converted to Fe^{2+} by dividing with a factor of 1.1113. However, since the original data has a

low Fe_{tot} this does not solve the issue. As a last attempt to solve the stoichiometry Muriel Erambert reprocessed the original data in the Cameca software to provide FeO instead of Fe_2O_3. Despite this, the same low concentration of Fe_{tot} persisted.

Pfaff *et al.* (2008) analyzed amphiboles from the Ilímaussaq which yielded a better Fe_{tot} (up to 34.88 wt%) and a better total (up to 99.80 wt%) than the amphibole of this study (Table 4.4). Despite better analysis, a proper stoichiometry was not calculated as the total of cations exceeded the maximum of 16. A further investigation of the subject of arfvedsonite is something that could be looked at in further research, and unfortunately did not yield any result in this study.

5.3.4 Narsarsukite

The high concentration of HFSE (especially Ti) in narsarsukite (Table 4.4) makes it easy for other incompatible elements such as the REE (Fig. 4.24 B) to partition into its structure. Due to HREE being more incompatible than the LREE, the high Ti concentration could be the reason why narsarsukite has a higher concentration of HREE than LREE (Table 4.4). The reason being that ^{VI}Ti has an ionic radius of 0.60 Å and that HREE have a smaller ionic radius than the LREE. (Shannon, 1976) This means that HREE partitions easier into the site with ^{VI}Ti. This could also be the reason why there is an elevated HREE trend in the REE chondrite normalization figure (Fig. 4.24 B). Alongside the large green narsarsukites (Fig. 4.4 & appendix 8.1 C and D) there is also observed relatively small pink crystals in the brighter trachyte material pictured in Fig. 4.1B. This might be a pink variety of narsarsukite and which has previously been described from Mayor Island, New Zealand (Read, 1991). This type of narsarsukite was not described by Upton *et al.* (1976) and might be the first occurrence of a pink narsarsukite variety from the Ilímaussaq area. However, this material was not further investigated for this study.

6. Conclusion

To conclude the subjects discussed in this thesis it is important to emphasize that there is a lot of minerals that are yet to be discovered. Even though rare minerals such as the nordite-group do not occur in quantities big enough to be an ore, they hold important information when it comes to REE distribution and other elemental concentrations.

This study propose a nomenclature for the nordite group with general formula of $A_2BXYZT_6O_{17}$, where *A* is Na, *B* is Na or Ca, *X* is Sr, Ca or Ba, *Y* is prominently occupied by Ce or La, *Z* is Zn, Fe, Mn or Mg and *T* is Si.

Furthermore, the study confirms the finding of nordite-(Ce) previously described by Upton *et al.* (1976) from the Igdlutalik Island. With the purposed nomenclature, the nordite-(Ce) from Igdlutalik has the empirical formula of

$Na_{2.06}Na_{1.00}(Sr_{0.75}Ca_{0.21}Ba_{0.05})_{\Sigma 1.01}(Ce_{0.53}La_{0.43}Nd_{0.05}Pr_{0.05})_{\Sigma 1.06}(Zn_{0.93}Fe_{0.02}Mg_{0.02}Mn_{0.01})_{\Sigma 0.98}Si_{5.95}O_{17}$. The nordite occurs in a trachyte dyke which is narsarsukite bearing, indicating a relatively low alkalinity as narsarsukite does not often occur in more evolved parts of alkaline complexes. In earlier publications from the Kola peninsula, nordite only occurs in high alkaline parts of the complex. This leads to the theory of origin that the Igdlutalik nordite is likely an early crystalizing mineral that formed from a more evolved fluid or melt, that exsolved from the main trachyte melt.

Moreover, the discovery of the new nordite-species "illoqite-(Ce)" with the empirical formula $Na_{2.05}(Na_{0.96}Ca_{0.04})_{\Sigma 1.00}(Ba_{0.51}Sr_{0.36}Ce_{0.13})_{\Sigma 1.00}(Ce_{0.54}La_{0.26}Nd_{0.14}Pr_{0.05})_{\Sigma 0.99}(Zn_{0.51}Fe_{0.32}Mn_{0.09}Li_{0.07})_{\Sigma 0.99}Si_{5.92}O_{17}$, occurs in a far more evolved part of the Ilímaussaq Alkaline Complex. There are only five previously described Ba-minerals from the Ilímaussaq Alkaline Complex. The Taseq slope is the type locality of ilímaussite-(Ce) and now illoqite-(Ce), and indicate that there must be significant concentrations of Ba at the locality. A possible theory regarding the origin could be that due to the size of the "large ussingite vein", incompatible minerals such as Ba can incorporate into complex minerals such as illoqite-(Ce).

Before this thesis, all known nordite-members have Sr dominating in the *X*-site. However, with Ba dominating the *X*-site in illoqite-(Ce) it has consequences for the unit cell. Since ^{VIII}Ba has a 0.16 Å larger ionic radius than ^{VIII}Sr, it means that the illoqite-(Ce) is on average 29.94 Å^3 (2%) larger unit cell volume than nordite-(Ce). Illoqite-(Ce) also displays sector zoning, which is unique to this member of the nordite-group. The zones are either Ba-dominated Sr-

dominated, with a chemically distinct core in regards to its high Nd content of 6.5 wt% (0.32 *apfu*). In addition, nordite-(Ce) is occurring alongside illoqite-(Ce), which leads to the notion that there very well be a solid-solution between nordite-(Ce) and illoqite-(Ce). At both localities in Ilímaussaq, nordite minerals are inferred to have formed as early stage minerals, this is evident from their euhedral shape and slo the trace-element data of co-existing aegirines. Although, illoqite-(Ce) is a rare mineral only found in one ussingite vein, it is abundant at this locality to such degree that the LREE content of co-existing aegirines was almost absent. That is, the illoqite-(Ce) formed prior to the aegirine and consequently depleted the source of LREE. No evidence of such an effect was observed in the Igdlutalik aegirines, but here aegirines is also much more abundant and nordite rare.

7. Future research

There are several subjects that could be research further, which was not carried out in this study. Firstly, re-analyzes of nordite on the electron microprobe to get a better measurement of the Zn and Na content is of high priority. This could possibly be done by analyzing Zn on the ZnKα x-ray line instead of the ZnLα x-ray line. To further ensure good quality of the analysis, the nordite samples could be analyzed on a different electron microprobe instrument.

Secondly, another related subject would be to re-analyze the amphibole in the samples, in regards to both chemical trace and major elements. This would help to compare the differences in chemical composition, as this study did for the aegirines in the two localities. In addition, a further look at the published amphibole formula spreadsheets is recommended, as it appears that most of them fail to handle Na-Fe-rich members like arfvedsonite.

Thirdly, a more thorough investigation of the nordite paragenesis is required. This is recommended for both the localities. At the Igdlutalik Island, the origin of nordite-(Ce) and vitusite-(Ce) is not fully understood, and needs to be investigated further. In addition, it would be interesting to take a closer look at the pink narsarsukites occurrence, and figure out if it has any relation to the nordite-(Ce). For the Taseq slope, finding the illoqite-(Ce)-bearing hydrothermalite *in-situ* would be a groundbreaking discovery. This could help explain why Ba-minerals such as illoqite-(Ce) and ilímaussite-(Ce) are occurring, and if it is in fact in relation with the large ussingite vein. Furthermore, the Gd-Er anomaly recorded in the nordite-(Ce) and illoqite-(Ce) needs to explored. A re-analysis of the trace elements with a second instrument could decide if there was a problem during initial analysis or if it is infact an enrichment of Gd and Er in nordite-(Ce) and illoqite-(Ce).

Fourthly, to get a better understanding of the internal relation in the nordite-group minerals, searching for a Sr-dominated crystal in the Taseq material to analyze with the SXRD would be crucial. This would give further information of the crystal-chemistry of the illoqite-(Ce) and nordite-(Ce), and give a deeper understanding on how structure and chemistry combine.

Lastly, the preparation for a proposal for illoqite-(Ce) to be submitted to the Comission on New Minerals, Nomenclature and Classification to get it approved as a new and valid species.

References

Agakhanov, A. A., Pautov, L. A., Sokolova, E., Hawthorne, F. C., Karpenko, V. Y., Siidra, O. I., & Muftakhov, V. A. (2017). Odigitriaite, CsNa5Ca5 [Si14B2O38] F2, a new caesium borosilicate mineral from the Darai-Pioz alkaline massif, Tajikistan: Description and crystal structure. *Mineralogical Magazine, 81*(1), 113-122.

Alexandre, P., Peterson, R., & Joy, B. (2015). Sector zoning in uraninite. *Canadian Mineralogist, 53*(4), 693-703.

Andersen, S., Bailey, J. C., & Bohse, H. (1981). Zr-YU stratigraphy of the kakortokite-lujavrite sequence, southern Ilímaussaq intrusion. *Groenlands Geologiske Undersoegelse Rapport*, 69-76.

Andersen, T., Elburg, M., & Erambert, M. (2017). The miaskitic-to-agpaitic transition in peralkaline nepheline syenite (white foyaite) from the Pilanesberg Complex, South Africa. *Chemical Geology, 455*, 166-181.

Andersen, T., Emeleus, C. H., Secher, K., Sørensen, H., Upton, B., & Weidick, A. (2006). Geological guide, South Greenland. The Narsarsuaq - Narsaq - Qaqortoq region. 131.

Andersen, T., & Friis, H. (2015). The transition from agpaitic to hyperagpaitic magmatic crystallization in the Ilímaussaq alkaline complex, South Greenland. *Journal of Petrology, 56*(7), 1343-1364.

Andersen, T., & Sørensen, H. (2005). Stability of naujakasite in hyperagpaitic melts, and the petrology of naujakasite lujavrite in the Ilímaussaq alkaline complex, South Greenland. *Mineralogical Magazine, 69*(2), 125-136.

Bailey, J. C., Sørensen, H., Andersen, T., Kogarko, L. N., & Rose-Hansen, J. (2006). On the origin of microrhythmic layering in arfvedsonite lujavrite from the Ilímaussaq alkaline complex, South Greenland. *Lithos, 91*(1-4), 301-318.

Bakakin, V., Belov, N., Borisov, S., & Solovyeva, L. (1970). The crystal structure of nordite and its relationship to melilite and datolite-gadolinite. *American Mineralogist: Journal of Earth and Planetary Materials, 55*(7-8), 1167-1181.

Bau, M., & Dulski, P. (1996). Anthropogenic origin of positive gadolinium anomalies in river waters. *Earth and Planetary Science Letters, 143*(1-4), 245-255.

Bayliss, P., & Levinson, A. (1988). A system of nomenclature for rare-earth mineral species: revision and extension. *American Mineralogist, 73*(3-4), 422-423.

Beane, R. J. (2004). Using the scanning electron microscope for discovery based learning in undergraduate courses. *Journal of Geoscience Education, 52*(3), 250-253.

Blake, A. J., Cole, J. M., Evans, J. S., Main, P., Parsons, S., & Watkin, D. J. (2009). Crystal structure analysis: principles and practice. *13*, 387.

Blaxland, A. B., & Upton, B. J. (1978). Rare-earth distribution in the Tugtutôq younger giant dyke complex: evidence bearing on alkaline magma genesis in South Greenland. *Lithos, 11*(4), 291-299.

Bohse, H., Brooks, C. K., & Kunzendorf, H. (1971). Field observations on the kakortokites of the Ilímaussaq intrusion, South Greenland, including mapping and analyses by portable X-ray fluorescence equipment for zirconium and niobium.

Bons, P. D., Baur, A., Elburg, M. A., Lindhuber, M. J., Marks, M. A., Soesoo, A., . . . Walte, N. P. (2015). Layered intrusions and traffic jams. *Geology, 43*(1), 71-74.

Borst, A. M., Friis, H., Nielsen, T. F., & Waight, T. E. (2018). Bulk and mush melt evolution in agpaitic intrusions: Insights from compositional zoning in eudialyte, Ilímaussaq complex, South Greenland. *Journal of Petrology, 59*(4), 589-612.

Bosze, S., & Rakovan, J. (2002). Surface-structure-controlled sectoral zoning of the rare earth elements in fluorite from Long Lake, New York, and Bingham, New Mexico, USA. *Geochimica et Cosmochimica Acta, 66*(6), 997-1009.

Brese, N., & O'keeffe, M. (1991). Bond-valence parameters for solids. *Acta Crystallographica Section B: Structural Science, 47*(2), 192-197.

Brown, I. (1996). VALENCE: a program for calculating bond valences. *Journal of applied crystallography, 29*(4), 479-480.

Brown, I., & Altermatt, D. (1985). Bond-valence parameters obtained from a systematic analysis of the inorganic crystal structure database. *Acta Crystallographica Section B: Structural Science, 41*(4), 244-247.

Cressey, G., Wall, F., & Cressey, B. (1999). Differential REE uptake by sector growth of monazite. *Mineralogical Magazine, 63*(6), 813-828.

Daly, R. A. (1910). Origin of the alkaline rocks. *Bulletin of the Geological Society of America, 21*(1), 87-118.

De Baar, H. J., Brewer, P. G., & Bacon, M. P. (1985). Anomalies in rare earth distributions in seawater: Gd and Tb. *Geochimica et Cosmochimica Acta, 49*(9), 1961-1969.

Dowty, E. (1976). Crystal structure and crystal growth; II, Sector zoning in minerals. *American Mineralogist, 61*(5-6), 460-469.

Engell, J., Hansen, J., Jensen, M., Kunzendorf, H., & Løvborg, L. (1971). Berylium mineralization in the Ilimaussaq intrusion, South Greenland, with description of a field beryllometer and chemical methods. 40.

Farrugia, L. (2013). WinGX, version 2013.3. *Department of Chemistry, University of Glasgow: Glasgow, Scotland*.

Ferraris, G., Gula, A., Zubkova, N. V., Pushcharovsky, D. Y., Gobetchiya, E. R., Pekov, I. V., & Eldjarn, K. (2004). The crystal structure of ilímaussite-(Ce),(Ba, Na) 10K3Na4. 5Ce5 (Nb, Ti) 6 [Si12O36][Si9O18 (O, OH) 24] O6, and the "ilímaussite" problem. *The Canadian Mineralogist, 42*(3), 787-795.

Finch, A. A., & Fletcher, J. G. (1992). Vitusite—An apatite derivative structure. *Mineralogical Magazine, 56*(383), 235-239.

Fitton, J., & Upton, B. (1987). Alkaline igneous rocks. *Geological Society Special Publication*(30), 191-226.

Fouke, B. W., & Reeder, R. J. (1992). Surface structural controls on dolomite composition: Evidence from sectoral zoning. *Geochimica et Cosmochimica Acta, 56*(11), 4015-4024.

Friis, H. (2015). Primary and secondary mineralogy of the Ilímaussaq alkaline complex, South Greenland. *Symposium on critical and strategic materials. British Columbia Geological Survey Paper, 3*, 89.

Friis, H. (2016). First occurrence of moskvinite-(Y) in the Ilímaussaq alkaline complex, South Greenland–implications for rare-earth element mobility. *Mineralogical Magazine, 80*(1), 31-41.

Gagné, O. C., & Hawthorne, F. C. (2015). Comprehensive derivation of bond-valence parameters for ion pairs involving oxygen. *Acta Crystallographica Section B: Structural Science, Crystal Engineering and Materials, 71*(5), 562-578.

Gerasimovsky, V. I. (1941). Nordite, a new mineral of the Lovozero tundras. *Comptes Rendus (Doklady) de l'Académie des Sciences de l'URSS, 32*(7), 498.

Gislev, M., & Grohol, M. (2018). Report on Critical Raw Materials and the Circular Economy. 80.

Hawthorne, F. C., Oberti, R., Harlow, G. E., Maresch, W. V., Martin, R. F., Schumacher, J. C., & Welch, M. D. (2012). Nomenclature of the amphibole supergroup. *American Mineralogist, 97*(11-12), 2031-2048.

Hunt, E. J., Finch, A. A., & Donaldson, C. H. (2017). Layering in peralkaline magmas, Ilímaussaq Complex, S Greenland. *Lithos, 268*, 1-15.

Jackson, E. (1970). The cyclic unit in layered intrusions—a comparison of repetitive stratigraphy in the ultramafic parts of the Stillwater, Muskox, Great Dyke, and Bushveld Complexes. *South Africa (ZAF), Geological Society of South Africa, Johannesburg, South Africa (ZAF)*, 391-424.

Jarosewich, E., & Boatner, L. (1991). Rare-earth element reference samples for electron microprobe analysis. *Geostandards Newsletter, 15*(2), 397-399.

Karup-Møller, S. (1978). *The ore minerals of the Ilímaussaq intrusion: their mode of occurrence and their conditions of formation*: Grønlands geologiske undersøgelse.

Khomyakov, A. P. (1995). *Mineralogy of hyperagpaitic alkaline rocks*: Oxford University Press, USA.

Khomyakov, A. P., Nechelyustov, G., Rastsvetaeva, R., & Zhensheng, M. (2003). Diversilite-(Ce), Na 2 (Ba, K) 6 Ce 2 Fe 2 Ti 3 [Si 3 O 9] 3 [SiO 3 OH] 3 (OH, H 2 O) 9, a new silicate with heterogeneous tetrahedral complexes from the Khibina alkaline massif, Kola Peninsula, Russia. *Zapiski Vserossijskogo Mineralogicheskogo Obshchestva, 132*(5), 34-39.

Kingsnorth, D. (2016). *Rare earths: The China conundrum.* Paper presented at the 12th International Rare Earths Conference. Hong Kong, November.

Knappe, A., Möller, P., Dulski, P., & Pekdeger, A. (2005). Positive gadolinium anomaly in surface water and ground water of the urban area Berlin, Germany. *Geochemistry, 65*(2), 167-189.

Kogarko, L. (1974). Role of volatiles. *The alkaline rocks, 474*, 487.

Krumrei, T. V., Pernicka, E., Kaliwoda, M., & Markl, G. (2007). Volatiles in a peralkaline system: abiogenic hydrocarbons and F–Cl–Br systematics in the naujaite of the Ilímaussaq intrusion, South Greenland. *Lithos, 95*(3-4), 298-314.

Larsen, L. M. (2006). *Mesozoic to Palaeogene dyke swarms in West Greenland and their significance for the formation of the Labrador Sea and the Davis Strait*: GEUS, Geological Survey of Denmark and Greenland.

Larsen, L. M., & Sørensen, H. (1987). The Ilímaussaq intrusion—progressive crystallization and formation of layering in an agpaitic magma. *Geological Society, London, Special Publications, 30*(1), 473-488.

Lindhuber, M. J., Marks, M. A., Bons, P. D., Wenzel, T., & Markl, G. (2015). Crystal mat-formation as an igneous layering-forming process: textural and geochemical evidence from the 'lower layered'nepheline syenite sequence of the Ilímaussaq complex, South Greenland. *Lithos, 224*, 295-309.

Locock, A. J. (2014). An Excel spreadsheet to classify chemical analyses of amphiboles following the IMA 2012 recommendations. *Computers & Geosciences, 62*, 1-11.

Lurie, J. (2004). The Pilanesberg: Geology, Geochemistry and Economic Potential. Thesis submitted to Rhodes University in 1973 for which the PhD degree was awarded, supplemented by more recent work.

Mancheri, N. A., Sprecher, B., Bailey, G., Ge, J., & Tukker, A. (2019). Effect of Chinese policies on rare earth supply chain resilience. *Resources, Conservation and Recycling, 142*, 101-112.

Marks, M. A., Hettmann, K., Schilling, J., Frost, B. R., & Markl, G. (2011). The mineralogical diversity of alkaline igneous rocks: critical factors for the transition from miaskitic to agpaitic phase assemblages. *Journal of Petrology, 52*(3), 439-455.

Marks, M. A., & Markl, G. (2017). A global review on agpaitic rocks. *Earth-Science Reviews, 173*, 229-258.

Maughan, T. (2015). The dystopian lake filled by the world's tech lust. Retrieved from https://www.bbc.com/future/article/20150402-the-worst-place-on-earth

McDonald, A. M., & Chao, G. Y. (2009). Lalondeite, a new hydrated Na–Ca fluorosilicate species from Mont Saint-Hilaire, Quebec: Description and crystal structure. *The Canadian Mineralogist, 47*(1), 181-191.

McDonough, W. F., & Sun, S.-S. (1995). The composition of the Earth. *Chemical Geology, 120*(3-4), 223-253.

Momma, K., & Izumi, F. (2011). VESTA 3 for three-dimensional visualization of crystal, volumetric and morphology data. *Journal of applied crystallography, 44*(6), 1272-1276.

Morimoto, N. (1988). Nomenclature of pyroxenes. *Mineralogy and Petrology, 39*(1), 55-76.

Nakamura, Y. (1973). Origin of sector-zoning of igneous clinopyroxenes. *American Mineralogist: Journal of Earth and Planetary Materials, 58*(11-12), 986-990.

Pakhomovsky, Y. A., Ivanyuk, G. Y., & Yakovenchuk, V. (2014). Loparite-(Ce) in rocks of the Lovozero layered complex at Mt. Karnasurt and Mt. Kedykvyrpakhk. *Geology of Ore Deposits, 56*(8), 685-698.

Paterson, B., Stephens, W., Rogers, G., Williams, I., Hinton, R., & Herd, D. (1992). The nature of zircon inheritance in two granite plutons. *Earth and Environmental Science Transactions of The Royal Society of Edinburgh, 83*(1-2), 459-471.

Pekov, I., Chukanov, N., Kononkova, N., Belakovsky, D., Pushcharovsky, D., & Vinogradova, S. (1998). Ferronordite-(Ce) Na3SrFeSi6O17 and manganonordite-(Ce) Na3SrMnSi6O17–the new minerals from Lovozero massif, Kola Peninsula. *Zapiski Vserossijskogo Mineralogicheskogo Obshchestva, 127*(1), 32-41.

Pekov, I., Chukanov, N., Turchkova, A., & Grishin, V. (2001). Ferronordite-(La), Na3Sr (La, Ce) FeSi6O17, a new mineral of the nordite group from the Lovozero massif, Kola Peninsula. *Zapiski Vserossiyskogo Mineralogicheskogo Obshchestva, 130*, 53-58.

Pekov, I. V. (1998). Minerals first discovered on the territory of the former Soviet Union.

Pekov, I. V. (2000). *Lovozero massif: history, pegmatites, minerals*: Ocean Pictures Ltd.

Pekov, I. V. (2005). The Palitra pegmatite: a newly discovered hyperalkaline pegmatite in the Lovozero massif, Kola Peninsula, Russia. *Mineralogical Record, 36*(5), 397.

Pekov, I. V., & Ekimenkova, I. A. (2001). Two new rare-earth-rich mineral associations in the Ilímaussaq alkaline complex, South Greenland. *Geology of Greenland Survey Bulletin, 190*, 143-144.

Petersen, O. V. (2001). List of all minerals identified in the Ilímaussaq alkaline complex, South Greenland. *GEUS Bulletin*, 25-33.

Petersen, O. V., Johnsen, O., & Micheelsen, H. (1999). Turkestanite from the Ilímaussaq alkaline complex, South Greenland. *Neues Jahrbuch für Mineralogie-Monatshefte*(9), 424-432.

Pfaff, K., Krumrei, T., Marks, M., Wenzel, T., Rudolf, T., & Markl, G. (2008). Chemical and physical evolution of the 'lower layered sequence'from the nepheline syenitic Ilímaussaq intrusion, South Greenland: Implications for the origin of magmatic layering in peralkaline felsic liquids. *Lithos, 106*(3-4), 280-296.

Plausinaitis, D., Prokopchik, A., Karaliunas, A., Bohdan, L., & Balashevska, Y. (2018). Erbium concentration anomaly as an indicator of nuclear activity: Focus on Natural waters in the Chernobyl exclusion zone. *Science of the total environment, 621*, 1626-1632.

Pushcharovsky, D. Y., Pekov, I. V., Pluth, J., Smith, J., Ferraris, G., Vinogradova, S., . . . Semenov, E. (1999). Raite, manganonordite-(Ce), and ferronordite-(Ce) from the Lovozero massif: Crystal structures and mineralogical geochemistry. *Crystallography Reports, 44*(4), 565-574.

Rakovan, J., McDaniel, D. K., & Reeder, R. J. (1997). Use of surface-controlled REE sectoral zoning in apatite from Llallagua, Bolivia, to determine a single-crystal SmNd age. *Earth and Planetary Science Letters, 146*(1-2), 329-336.

Ratschbacher, B. C., Marks, M. A., Bons, P. D., Wenzel, T., & Markl, G. (2015). Emplacement and geochemical evolution of highly evolved syenites investigated by a combined structural and geochemical field study: The lujavrites of the Ilímaussaq complex, SW Greenland. *Lithos, 231*, 62-76.

Read, A. J. (1991). Narsarsukite from Mayor Island, New Zealand. *New Zealand Journal of Geology and Geophysics, 34*(3), 337-340.

Reeder, R. J., & Paquette, J. (1989). Sector zoning in natural and synthetic calcites. *Sedimentary Geology, 65*(3-4), 239-247.

Ridolfi, F., Zanetti, A., Renzulli, A., Perugini, D., Holtz, F., & Oberti, R. (2018). AMFORM, a new mass-based model for the calculation of the unit formula of amphiboles from electron microprobe analyses. *American Mineralogist: Journal of Earth and Planetary Materials, 103*(7), 1112-1125.

Schønwandt, H. K., Barnes, G. B., & Ulrich, T. (2016). A description of the world-class rare earth element deposit, Tanbreez, South Greenland. In *Rare Earths Industry* (pp. 73-85): Elsevier.

Semenov, E. (1961). New data on nordite. *Tr. Mineral. Muz. Akad. Nauk SSSR, 11*, 199-201.

Semenov, E., & Barinskii, R. (1957). The composition characteristics of the rare earths in minerals. *Presented at the Jubilee Session of the Scientific Council of the Institute*, 419.

Semenov, E., & Tichonenkova, R. (1967). The mineralogical-geochemical types of derivatives of nepheline syenites. The activity of alkalis and volatiles. In (pp. 52-71): Nauka, Moskva.

Shannon, R. D. (1976). Revised effective ionic radii and systematic studies of interatomic distances in halides and chalcogenides. *Acta crystallographica section A: crystal physics, diffraction, theoretical and general crystallography, 32*(5), 751-767.

Sheldrick, G. (2013). SHELXS-2013/1, program for the solution of crystal structures. *Institute for Inorganic Chemistry. University of Göttingen, Göttingen, Germany*.

Sheldrick, G. M. (2015). Crystal structure refinement with SHELXL. *Acta Crystallographica Section C: Structural Chemistry, 71*(1), 3-8.

Simpson, R. (2015). Kvanefjeld Feasibility Study Completed. 42.

Sjöqvist, A. S., Cornell, D. H., Andersen, T., Erambert, M., Ek, M., & Leijd, M. (2013). Three compositional varieties of rare-earth element ore: eudialyte-group minerals from the Norra Kärr Alkaline Complex, Southern Sweden. *Minerals, 3*(1), 94-120.

Sørensen, H. (1974). Alkali syenites, feldspathoidal syenites and related lavas. *The alkaline rocks*, 22-52.

Sørensen, H. (1997). The agpaitic rocks-an overview. *Mineralogical Magazine, 61*(407), 485-498.

Sørensen, H. (2001). Brief introduction to the geology of the Ilímaussaq alkaline complex, South Greenland, and its exploration history. *Geology of Greenland Survey Bulletin, 190*, 7-23.

Sørensen, H., Bailey, J. C., Kogarko, L., Rose-Hansen, J., & Karup-Møller, S. (2003). Spheroidal structures in arfvedsonite lujavrite, Ilímaussaq alkaline complex, South Greenland—an example of macro-scale liquid immiscibility. *Lithos, 70*(1-2), 1-20.

Sørensen, H., Bailey, J. C., & Rose-Hansen, J. (2011). The emplacement and crystallization of the U–Th–REE-rich agpaitic and hyperagpaitic lujavrites at Kvanefjeld, Ilímaussaq alkaline complex, South Greenland. *Bulletin of the Geological Society of Denmark, 59*, 69-92.

Sørensen, H., Bohse, H., & Bailey, J. C. (2006). The origin and mode of emplacement of lujavrites in the Ilímaussaq alkaline complex, South Greenland. *Lithos, 91*(1-4), 286-300.

Sørensen, H., & Larsen, L. M. (1987). Layering in the Ilímaussaq alkaline intrusion, South Greenland. In *Origins of igneous layering* (pp. 1-28): Springer.

Upton, B. (2013). Tectono-magmatic evolution of the younger Gardar southern rift, South Greenland. *Geological Survey of Denmark and Greenland Bulletin, 29*(2013), 128.

Upton, B., Hill, P., Johnsen, O., & Petersen, O. (1978). Emeleusite: a new LiNaFe III silicate from South Greenland. *Mineralogical Magazine, 42*(321), 31-34.

Upton, B., Macdonald, R., Hill, P., Jefferies, B., & Ford, C. (1976). Narsarsukite: a new occurrence in peralkaline trachyte, south Greenland. *Mineralogical Magazine, 40*(315), 737-746.

Urusov, V. S. (1995). Semi-empirical groundwork of the bond-valence model. *Acta Crystallographica Section B: Structural Science, 51*(5), 641-649.

Ussing, N. V. (1912). *Geology of the country around Julianehaab, Greenland* (Vol. 38): Bianco Luno.

Van Achterbergh, E., Ryan, C., & Griffin, W. (1999). *GLITTER: On-line interactive data reduction for the laser ablation inductively coupled plasma mass spectrometry microprobe.* Paper presented at the Ninth Annual VM Goldschmidt Conference.

Waight, T., Baker, J., & Willigers, B. (2002). Rb isotope dilution analyses by MC-ICPMS using Zr to correct for mass fractionation: towards improved Rb–Sr geochronology? *Chemical Geology, 186*(1-2), 99-116.

Wenger, M. & Armbruster, T. (1991). Crystal chemistry of lithium: oxygen coordination and bonding. *European Journal of Mineralogy, 3*, 387-399.

Wight, Q., & Chao, G. Y. (1995). Mont Saint-Hilaire: Revisited Part 2. *Rocks & Minerals, 70*(2), 90-138.

Yakovenchuk, V., Ivanyuk, G., Pakhomovsky, Y. A., & Men'shikov, Y. (2005). *Khibiny*: Laplandia Minerals in association with the Mineralogical Society of Great Britain & Ireland.

Yakovenchuk, V. N., Ivanyuk, G. Y., Krivovichev, S. V., Pakhomovsky, Y. A., Selivanova, E. A., Korchak, J. A., . . . Zalkind, O. A. (2011). Eliseevite, Na1. 5Li [Ti2Si4O12. 5 (OH) 1.5]· 2H2O, a new microporous titanosilicate from the Lovozero alkaline massif (Kola Peninsula, Russia). *American Mineralogist, 96*(10), 1624-1629.

Yang, H., Gu, X., Downs, R. T., Evans, S. H., Van Nieuwenhuizen, J. J., Lavinsky, R. M., & Xie, X. (2019). Meieranite, Na2Sr3MgSi6O17, a New Mineral from the Wessels Mine, Kalahari Manganese Fields, South Africa. *The Canadian Mineralogist, 57*(4), 457-466.

Zellmer, G., Sparks, R., Hawkesworth, C., & Wiedenbeck, M. (2003). Magma emplacement and remobilization timescales beneath Montserrat: insights from Sr and Ba zonation in plagioclase phenocrysts. *Journal of Petrology, 44*(8), 1413-1431.

Website references

Mindat[1]: https://www.mindat.org/loc-4302.html

Mindat[2]: https://www.mindat.org/loc-1957.html

WebElements[1]: https://www.webelements.com/barium/

WebElements[2]: https://www.webelements.com/argon/

Grønlandsportalen: https://www.geus.dk/produkter-ydelser-og-faciliteter/data-og-kort/groenlandsportalen/

IMA Database if Mineral Properties: https://rruff.info/ima/

IoGAS™ 7.2. Build: 104772. Build data: 06 Des 2019.

8. Appendix

APPENDIX 8.1: THIN SECTION IMAGES, IGDLUTALIK ISLAND

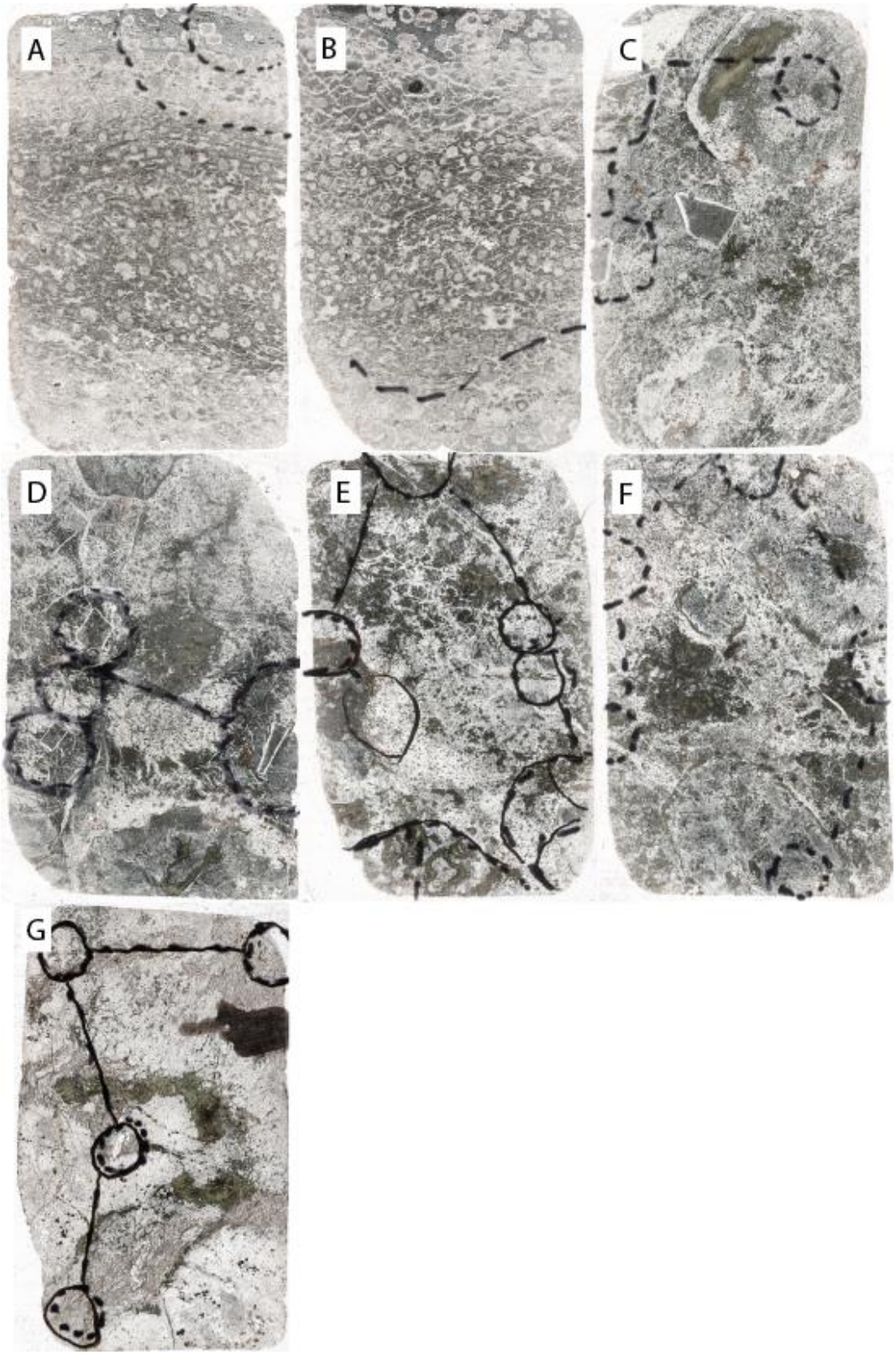

APPENDIX 8.1: A: EHG 1. B: EHG 2. C: EHG 3. D: EHG 4. E: EHG 5. F: EHG 6. G: EHG 8. The black areas shows which areas that were further examined.

APPENDIX 8.2: THIN SECTION IMAGES, TASEQ SLOPE

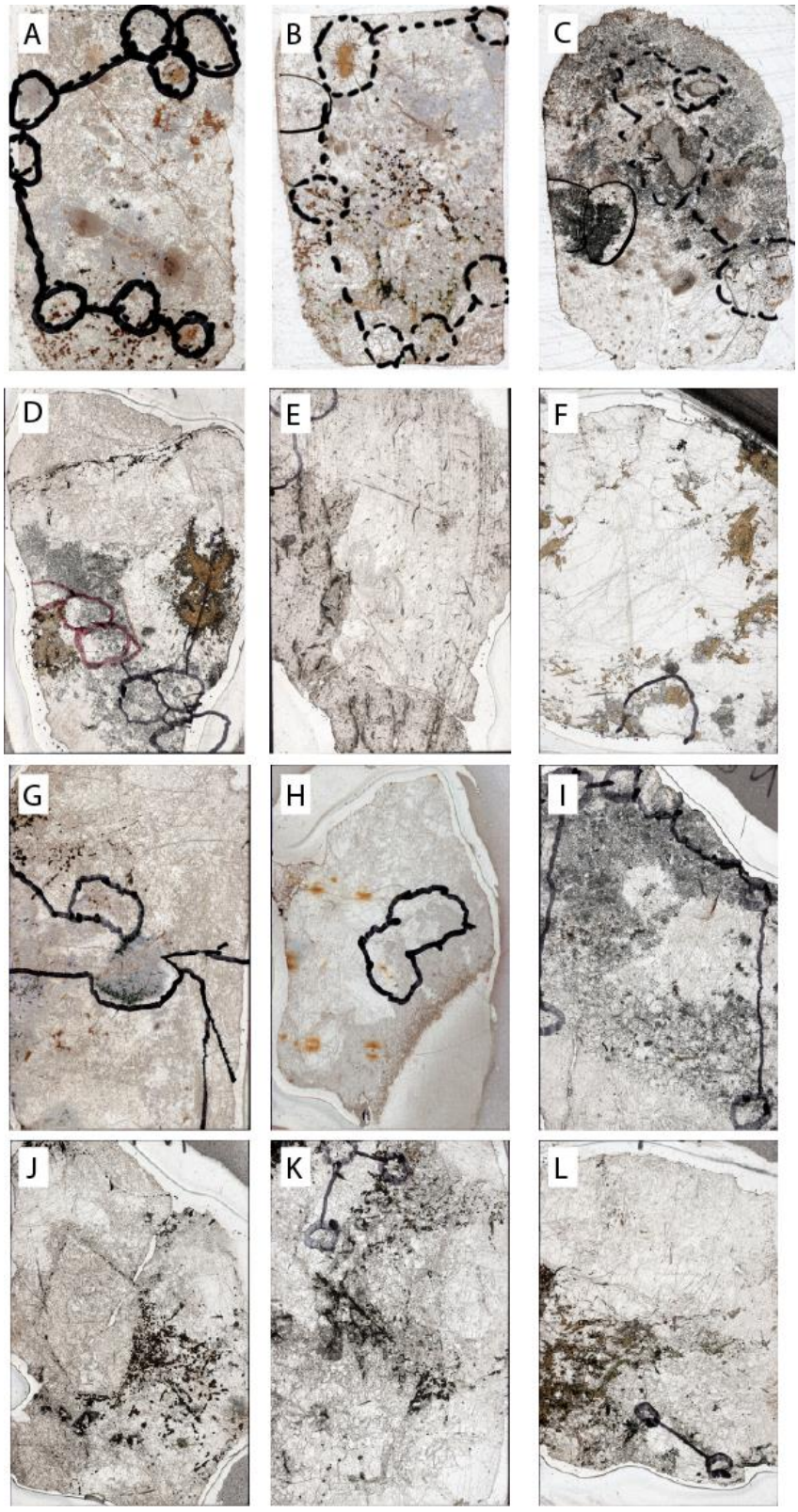

APPENDIX 8.3: EPMA DATA OF IGDLUTALIK AND TASEQ NORDITES.

Sample	EHG4	EHG7	EHG10	EHG13	EHG15	EHG EPOXY
n	*8*	*23*	*12*	*33*	*10*	*13*
Weight percent oxides						
SiO_2	45.2(5)	43(1)	44.2(6)	43(1)	43.2(8)	44(1)
ZnO	8.6(3)	4.2(8)	4.7(5)	4.2(6)	4.4(6)	4.2(8)
FeO	0.2(1)	2.7(8)	2.4(2)	2.7(7)	2.5(7)	2.8(9)
MnO	0.09(4)	0.8(3)	0.6(1)	0.8(4)	0.7(2)	0.7(2)
MgO	0.10(4)	-	-	-	-	-
La_2O_3	9(1)	5(3)	5(3)	5(3)	6.4(6)	6.1(6)
Ce_2O_3	11.0(8)	13(2)	14(2)	13(2)	14(1)	13(1)
Nd_2O_3	1.1(5)	3(4)	3(2)	3(3)	2.0(9)	1.9(9)
Pr_2O_3	0.6(3)	1.1(8)	1.1(4)	1.0(6)	0.9(3)	0.9(3)
SrO	9.8(6)	5(3)	6(1)	5(3)	5(3)	5(3)
BaO	1.0(6)	9(6)	6(2)	9(6)	7(6)	9(7)
CaO	1.5(1)	0.3(2)	0.4(1)	0.3(2)	0.4(2)	0.3(2)
Na_2O	12.0(2)	11.4(6)	11.3(2)	11.1(5)	11.2(4)	11(1)
Total	100.10	99.18	99.40	98.46	98.75	99.09
Atoms per formula unit						
Si	5.99	5.99	6.03	6.01	5.99	6.02
Zn	0.84	0.43	0.47	0.43	0.45	0.43
Fe^{2+}	0.02	0.32	0.27	0.31	0.29	0.32
Mn	0.01	0.09	0.07	0.09	0.08	0.09
Mg	0.02	-	-	-	-	-
La	0.44	0.27	0.26	0.28	0.33	0.31
Ce^{3+}	0.53	0.68	0.69	0.68	0.72	0.68
Nd	0.05	0.15	0.15	0.14	0.10	0.09
Pr	0.03	0.05	0.06	0.05	0.05	0.04
Sr	0.75	0.37	0.50	0.39	0.43	0.37
Ba	0.05	0.52	0.32	0.48	0.41	0.50
Ca	0.21	0.04	0.06	0.05	0.06	0.04
Na	3.07	3.06	3.01	3.00	3.02	3.04

APPENDIX 8.4: EMPIRICAL FORMULAS BASED ON CHECMICAL DATA FROM APPENDIX 8.3

Samples	**Empirical formula**
EHG4	$Na_{3.07}(Sr_{0.75}Ca_{0.20}Ba_{0.05})_{\Sigma 1.01}(Ce_{0.53}La_{0.44}Nd_{0.05}Pr_{0.03})_{\Sigma 1.05}(Zn_{0.43}Fe_{0.02}Mg_{0.02}Mn_{0.01})_{\Sigma 0.90}Si_{5.99}O_{17}$
EHG7	$Na_{3.06}(Ba_{0.52}Sr_{0.37}Ca_{0.04})_{\Sigma 0.93}(Ce_{0.67}La_{0.27}Nd_{0.14}Pr_{0.05})_{\Sigma 1.14}(Zn_{0.43}Fe_{0.32}Mn_{0.09})_{\Sigma 0.84}Si_{5.99}O_{17}$
EHG10	$Na_{3.01}(Sr_{0.50}Ba_{0.32}Ca_{0.06})_{\Sigma 0.88}(Ce_{0.69}La_{0.26}Nd_{0.15}Pr_{0.06})_{\Sigma 1.16}(Zn_{0.47}Fe_{0.27}Mn_{0.07})_{\Sigma 0.81}Si_{6.03}O_{17}$
EHG13	$Na_{3.00}(Ba_{0.48}Sr_{0.39}Ca_{0.05})_{\Sigma 0.92}(Ce_{0.68}La_{0.28}Nd_{0.14}Pr_{0.05})_{\Sigma 1.15}(Zn_{0.43}Fe_{0.31}Mn_{0.09})_{\Sigma 0.83}Si_{6.01}O_{17}$
EHG15	$Na_{3.02}(Sr_{0.43}Ba_{0.41}Ca_{0.06})_{\Sigma 0.89}(Ce_{0.72}La_{0.33}Nd_{0.10}Pr_{0.05})_{\Sigma 1.19}(Zn_{0.45}Fe_{0.29}Mn_{0.07})_{\Sigma 0.82}Si_{5.99}O_{17}$
EPOXY	$Na_{3.04}(Ba_{0.50}Sr_{0.37}Ca_{0.04})_{\Sigma 0.91}(Ce_{0.69}La_{0.31}Nd_{0.09}Pr_{0.04})_{\Sigma 1.13}(Zn_{0.42}Fe_{0.32}Mn_{0.09})_{\Sigma 0.83}Si_{6.02}O_{17}$

APPENDIX 8.5: ATOMIC COORDINATES AND DISPLACEMENT PARAMETERS FOR IGDLUTALIK NORDITE (EXP. 420)

Atom	*x*	*y*	*z*	U_{ani}	U_{11}	U_{22}	U_{33}	U_{23}	U_{13}	U_{12}
Na1	0.000000	0.000000	0.500000	0.0163(3)	0.0189(6)	0.0095(5)	0.0205(5)	0.0030(4)	-0.0097(4)	-0.0020(4)
Na2	0.06964(6)	-0.9926(1)	0.17155(3)	0.0197(2)	0.0328(5)	0.0136(4)	0.0126(3)	0.0014(2)	-0.0016(3)	-0.0034(3)
Sr	0.250000	0.000000	0.52333(2)	0.00756(6)	0.0072(1)	0.0076(1)	0.0079(1)	0.000	0.000	0.00004(7)
Zn	0.250000	-0.500000	0.66956(2)	0.00734(8)	0.0068(1)	0.0098(1)	0.0053(1)	0.000	0.000	0.0001(1)
Ce	0.250000	0.000000	0.31960(2)	0.00606(4)	0.00578(6)	0.00609(6)	0.00631(6)	0.000	0.000	0.00036(4)
Si1	0.09856(3)	-0.46342(8)	0.56506(2)	0.00652(8)	0.0068(2)	0.0066(2)	0.0061(2)	-0.0002(1)	-0.0005(1)	0.0002(1)
Si2	0.10235(3)	-0.46064(8)	0.27419(2	0.00635(8)	0.0059(2)	0.0067(2)	0.0064(2)	-0.0001(1)	-0.0006(1)	0.0003(1)
Si3	0.11203(3)	0.45484(8)	0.41881(2)	0.00618(8)	0.0063(2)	0.0069(2)	0.0053(2)	-0.0002(1)	0.0005(1)	0.0006(1)
O1	-0.00530(8)	-0.3393(2)	0.58228(5)	0.0098(2)	0.0074(5)	0.0098(5)	0.0123(5)	-0.0003(4)	0.0013(4)	0.0000(4)
O2	0.17078(8)	-0.3011(2)	0.60975(5)	0.0102(2)	0.0102(5)	0.0106(5)	0.0097(5)	-0.0005(4)	-0.0037(4)	0.0001(4)
O3	0.11865(8)	0.6433(2)	0.48588(5)	0.0090(2)	0.0123(5)	0.0087(4)	0.0060(5)	-0.0004(3)	0.0004(4)	-0.0004(4)
O4	0.10259(8)	-0.7677(2)	0.56776(5)	0.0113(2)	0.0139(6)	0.0078(5)	0.0123(5)	0.0009(4)	-0.0008(4)	0.0003(4)
O5	0.000000	-0.3572(3)	0.250000	0.0117(3)	0.0074(7)	0.0094(7)	0.0184(8)	0.000	-0.0044(6)	0.000
O6	0.17699(8)	-0.2896(2)	0.23274(5)	0.0093(2)	0.0097(5)	0.0097(5)	0.0085(5)	-0.0001(4)	0.0019(4)	-0.0007(4)
O7	0.11898(8)	0.6500(2)	0.35308(5)	0.0092(2)	0.0126(5)	0.0091(5)	0.0059(5)	0.0003(3)	-0.0005(4)	-0.0020(4)
O8	0.11439(8)	-0.7642(2)	0.27257(5)	0.0115(2)	0.0136(6)	0.0081(5)	0.0128(5)	-0.0009(4)	-0.0024(4)	0.0017(4)
O9	0.18573(8)	0.2277(2)	0.41822(5)	0.0104(2)	0.0106(5)	0.0116(5)	0.0092(5)	-0.0006(4)	0.0000(4)	0.0036(4)

APPENDIX 8.6: ATOMIC COORDINATES AND DISPLACEMENT PARAMETERS FOR IGDLUTALIK NORDITE (EXP. 422)

Atom	*x*	*y*	*z*	U_{ani}	U_{11}	U_{22}	U_{33}	U_{23}	U_{13}	U_{12}
Na1	0.000000	-0.500000	0.500000	0.0170(2)	0.0202(4)	0.0096(3	0.0212(4)	0.0029(3)	-0.0099(3)	-0.0017(2)
Na2	0.07003(5)	-0.49238(9)	0.17153(2)	0.0196(2)	0.0319(4)	0.0138(3)	0.0132(3)	0.0013(2)	-0.0019(2)	-0.0035(2)
Sr1	0.250000	0.500000	0.52346(2)	0.00800(5)	0.00785(7)	0.00768(7)	0.00848(7)	0.000	0.000	0.00003(5)
Ca1	0.250000	0.500000	0.52346(2)	0.00800(5)	0.00785(7)	0.00768(7)	0.00848(7)	0.000	0.000	0.00003(5)
Zn1	0.250000	0.000000	0.66959(2)	0.00796(6)	0.0078(1)	0.0100(1)	0.00612(9)	0.000	0.000	-0.00002(6)
Ce1	0.250000	0.500000	0.31959(2)	0.00646(3)	0.00650(4)	0.00621(4)	0.00666(4)	0.000	0.000	0.00040(3)
Ca2	0.250000	0.500000	0.31959(2)	0.00646(3)	0.00650(4)	0.00621(4)	0.00666(4)	0.000	0.000	0.00040(3)
Si1	0.09851(2)	0.03660(6)	0.56508(2)	0.00689(6)	0.0077(1)	0.0066(1)	0.0064(1)	-0.00026(9)	-0.00047(9)	0.0003(1)
Si2	0.10234(2)	0.03950(6)	0.27420(2)	0.00660(6)	0.0065(1)	0.0067(1)	0.0066(1)	-0.00022(9)	-0.00058(9)	0.00036(9)
Si3	0.11201(2)	0.95458(6)	0.41883(2)	0.00680(6)	0.0074(1)	0.0072(1)	0.0058(1)	-0.00001(9)	0.00068(9)	0.0005(1)
O1	-0.00525(5)	0.1607(2)	0.58230(4)	0.0102(1)	0.0076(3)	0.0108(4)	0.0123(3)	-0.0006(3)	0.0014(3)	-0.0001(3)
O2	0.17083(5)	0.1991(1)	0.60981(4)	0.0103(1)	0.0107(3)	0.0101(3)	0.0101(3)	-0.0009(3)	-0.0038(3)	0.0000(3)
O3	0.11844(5)	0.1432(1)	0.48585(4)	0.0095(1)	0.0129(4)	0.0090(3)	0.0065(3	-0.0005(2)	0.0010(3)	-0.0002(3)
O4	0.10247(6)	-0.2674(2)	0.56762(4)	0.0117(1)	0.0153(4)	0.0075(3)	0.0125(3)	0.0004(3)	-0.0012(3)	0.0002(3)
O5	0.000000	0.1427(2)	0.250000	0.0122(2)	0.0085(5)	0.0102(5)	0.0178(5)	0.000	-0.0040(4)	0.000
O6	0.17692(5)	0.2107(1)	0.23278(4)	0.0096(1)	0.0103(3)	0.0096(3)	0.0089(3)	-0.0006(3)	0.0024(3)	-0.0007(3)
O7	0.11891(5)	1.1499(1)	0.35307(4)	0.0096(1)	0.0136(4)	0.0087(3)	0.0064(3)	0.0005(2)	-0.0006(3)	-0.0022(3)
O8	0.11452(6)	-0.2636(1)	0.27266(4)	0.0119(1)	0.0144(4)	0.0081(3)	0.0131(3)	-0.0012(3)	-0.0031(3)	0.0012(3)
O9	0.31429(5)	1.2722(2)	0.41826(4)	0.0109(1)	0.0109(4)	0.0117(3)	0.0101(3)	0.0008(3)	-0.0002(3)	0.0037(3)

APPENDIX 8.7 ATOMIC COORDINATES AND DISPLACEMENT PARAMETERS FOR TASEQ NORDITE (EXP. 430)

Atom	*x*	*y*	*z*	U_{ani}	U_{11}	U_{22}	U_{33}	U_{23}	U_{13}	U_{12}
Na1	0.000000	0.500000	0.500000	0.0268(9)	0.033(2)	0.021(1)	0.027(1)	-0.003(1)	-0.012(1)	0.002(1)
Na2	0.0677(2)	0.5097(3)	0.67249(8)	0.0314(7)	0.050(1)	0.026(1)	0.0179(9)	0.0007(6)	-0.0033(7)	-0.0033(8)
Sr1	0.250000	0.500000	0.52461(2)	0.0157(1)	0.0151(2)	0.0189(2)	0.0132(2)	0.000	0.000	0.0002(1)
Ba1	0.250000	0.500000	0.52461(2)	0.0157(1)	0.0151(2)	0.0189(2)	0.0132(2)	0.000	0.000	0.0002(1)
Zn1	0.250000	0.000000	0.67141(3)	0.0162(3)	0.0154(4)	0.0227(5)	0.0106(4)	0.000	0.000	0.0007(3)
Fe1	0.250000	0.000000	0.67141(3)	0.0162(3)	0.0154(4)	0.0227(5)	0.0106(4)	0.00	0.000	0.0007(3)
Ce1	0.250000	0.500000	0.31891(2)	0.0151(1)	0.0152(2)	0.0176(2)	0.0124(2)	0.000	0.000	-0.0005(1)
Si1	0.09634(8)	0.9676(2)	0.56594(5)	0.0160(2)	0.0165(5)	0.0190(5)	0.0126(5)	0.0007(4)	-0.0003(4)	-0.0011(4)
Si2	0.10167(8)	0.9590(2)	0.27460(5)	0.0154(2)	0.0155(5)	0.0188(5)	0.0120(5)	0.0005(3)	0.0011(3)	-0.0005(4)
Si3	0.11132(8)	0.0465(2)	0.41858(5)	0.0157(2)	0.0161(5)	0.0199(5)	0.0112(5)	-0.0006(3	0.0007(4)	-0.0007(4)
O1	0.0055(2)	0.1629(6)	0.4178(1)	0.0192(6)	0.017(1)	0.023(1)	0.017(1)	0.0005(10)	0.001(1)	-0.002(1)
O2	0.1684(2)	0.8098(6)	0.6106(1)	0.0217(6)	0.023(1)	0.025(1)	0.017(1)	0.003(1)	-0.006(1)	-0.003(1)
O3	0.1178(2)	0.8643(5)	0.4865(1)	0.0181(6)	0.022(1)	0.022(1)	0.010(1)	0.0007(9)	0.001(1)	-0.0003(11)
O4	0.0979(2)	0.2694(6)	0.5693(1)	0.0213(6)	0.028(2)	0.017(1)	0.019(1)	-0.0002(10)	-0.002(1)	-0.001(1)
O5	0.000000	0.8565(8)	0.250000	0.0203(8)	0.014(2)	0.021(2)	0.026(2)	0.000	-0.006(2)	0.000
O6	0.1765(2)	0.7860(5)	0.2341(1)	0.0189(6)	0.019(1)	0.024(1)	0.014(1)	-0.0003(10)	0.001(1)	-0.001(1)
O7	0.1174(2)	0.8496(5)	0.3535(1)	0.0185(6)	0.023(1)	0.021(1)	0.011(1)	-0.001(1)	0.001(1)	0.002(1)
O8	0.1152(2)	0.2598(5)	0.2721(1)	0.0217(6)	0.025(1)	0.020(1)	0.019(1)	0.001(1)	-0.003(1)	-0.004(1)
O9	0.1849(2)	0.2706(6)	0.4163(1)	0.0200(6)	0.019(1)	0.026(1)	0.015(1)	0.002(1)	-0.001(1)	-0.005(1)

APPENDIX 8.8: ATOMIC COORDINATES AND DISPLACEMENT PARAMETERS FOR TASEQ NORDITE (EXP. 431)

Atom	*x*	*y*	*z*	U_{ani}	U_{11}	U_{22}	U_{33}	U_{23}	U_{13}	U_{12}
Na1	0.000000	0.500000	0.500000	0.0254(6)	0.031(1)	0.0174(9)	0.027(1)	-0.0038(7)	-0.0137(8)	0.0019(7)
Na2	0.0671(1)	0.5104(2)	0.67249(5)	0.0284(5)	0.049(1)	0.0208(7)	0.0157(6)	0.0009(4)	-0.0041(5)	-0.0031(6)
Sr1	0.250000	0.500000	0.52469(2)	0.01285(9)	0.0134(1)	0.0135(1)	0.0117(1)	0.000	0.000	0.00012(9)
Ba1	0.250000	0.500000	0.52469(2)	0.01285(9)	0.0134(1)	0.0135(1)	0.0117(1)	0.000	0.000	0.00012(9)
Zn1	0.250000	0.000000	0.67170(2)	0.0131(2)	0.0135(3)	0.0172(3)	0.0085(3)	0.000	0.000	0.0006(2)
Fe1	0.250000	0.000000	0.67170(2)	0.0131(2)	0.0135(3)	0.0172(3)	0.0085(3)	0.000	0.000	0.0006(2)
Ce1	0.250000	0.500000	0.31864(2)	0.01166(8)	0.0129(1)	0.0125(1)	0.0096(1)	0.000	0.000	-0.00056(8)
Si1	0.09574(6)	0.9682(1)	0.56596(4)	0.0126(2)	0.0145(4)	0.0129(3)	0.0103(3)	0.0011(2)	-0.0002(3)	-0.0009(3)
Si2	0.10168(5)	0.9586(1)	0.27464(4)	0.0122(2)	0.0130(4)	0.0130(3)	0.0107(3)	0.0001(2)	-0.0008(2)	-0.0007(3)
Si3	0.11097(5)	0.0472(1)	0.41845(3)	0.0122(2)	0.0137(4)	0.0139(3)	0.0089(3)	-0.0003(2)	0.0003(2)	-0.0007(3)
O1	0.0058(1)	0.1639(4)	0.41777(9)	0.0166(4)	0.0165(9)	0.0171(9)	0.0161(9)	0.0001(7)	0.0011(7)	-0.0006(7)
O2	0.1677(1)	0.8119(4)	0.61105(9)	0.0182(4)	0.021(1)	0.019(1)	0.0146(9)	0.0024(7)	-0.0047(8)	-0.0022(8)
O3	0.1176(1)	0.8681(4)	0.48678(8)	0.0160(4)	0.021(1)	0.0172(9)	0.0096(8)	0.0015(7)	0.0005(7)	-0.0002(8)
O4	0.0966(1)	0.2701(4)	0.56955(9)	0.0192(4)	0.026(1)	0.015(1)	0.0162(9)	-0.0009(7)	-0.0018(8)	-0.0022(8)
O5	0.000000	0.8590(5)	0.250000	0.0182(6)	0.013(1)	0.017(1)	0.024(1)	0.000	-0.005(1)	0.000
O6	0.1759(1)	0.7864(4)	0.23411(9)	0.0160(4)	0.017(1)	0.0176(9)	0.0135(8)	0.0006(7)	0.0013(7)	0.0013(8)
O7	0.1169(1)	0.8506(4)	0.35351(8)	0.0153(4)	0.021(1)	0.0155(9)	0.0092(8)	-0.0003(7)	-0.0001(7)	0.0011(8)
O8	0.1154(1)	0.2591(4)	0.27178(9)	0.0192(4)	0.024(1)	0.0151(9)	0.0178(9)	0.0026(7)	-0.0036(8)	-0.0029(8)
O9	0.1846(1)	0.2710(4)	0.41598(9)	0.0177(4)	0.018(1)	0.019(1)	0.0156(9)	0.0009(7)	-0.0001(8)	-0.0043(8)

APPENDIX 8.9: ATOMIC COORDINATES AND DISPLACEMENT PARAMETERS FOR TASEQ NORDITE (EXP. 478)

Atom	*x*	*y*	*z*	U_{ani}	U_{11}	U_{22}	U_{33}	U_{23}	U_{13}	U_{12}
Na1	0.000000	0.500000	0.500000	0.0209(8)	0.026(1)	0.012(1)	0.024(1)	-0.001(1)	-0.0117(9)	0.003(1)
Na2	0.0687(1)	0.4897(4)	0.17218(7)	0.0237(5)	0.038(1)	0.0157(9)	0.0171(8)	-0.0018(7)	-0.0017(6)	0.0054(9)
Sr1	0.250000	0.500000	0.52454(2)	0.0102(1)	0.0089(2)	0.0105(2)	0.0112(2)	0.000	0.000	0.0003(2)
Ba1	0.250000	0.500000	0.52454(2)	0.0102(1)	0.0089(2)	0.0105(2)	0.0112(2)	0.000	0.000	0.0003(2)
Zn1	0.250000	0.000000	0.67125(3)	0.0105(2)	0.0088(4)	0.0143(3)	0.0084(3)	0.000	0.000	0.0004(4)
Fe1	0.250000	0.000000	0.67125(3)	0.0105(2)	0.0088(4)	0.0143(3)	0.0084(3)	0.000	0.000	0.0004(4)
Ce1	0.250000	0.500000	0.31889(2)	0.0089(1)	0.0079(1)	0.0091(1)	0.0098(1)	0.000	0.000	-0.0008(1)
Si1	0.09641(7)	0.9666(2)	0.56576(4)	0.0102(2)	0.0104(5)	0.0106(5)	0.0095(4)	0.0007(4)	-0.0007(3)	-0.0013(4)
Si2	0.10192(7)	0.9587(2)	0.27459(4)	0.0091(2)	0.0084(5)	0.0086(5)	0.0101(4)	0.0009(3)	-0.0015(3)	-0.0006(4)
Si3	0.11129(7)	0.0466(2)	0.41850(4)	0.0092(2)	0.0104(5)	0.0090(4)	0.0083(4)	0.0003(4)	0.0003(3)	-0.0010(3)
O1	0.0053(2)	0.8370(5)	0.5823(1)	0.0130(5)	0.010(1)	0.013(1)	0.016(1)	-0.001(1)	0.001(1)	0.001(1)
O2	0.1684(2)	0.8085(5)	0.6103(1)	0.0143(5)	0.014(1)	0.016(1)	0.013(1)	0.003(1)	-0.004(1)	-0.001(1)
O3	0.1177(2)	-0.1349(5)	0.4866(1)	0.0129(5)	0.016(1)	0.012(1)	0.010(1)	0.003(1)	0.002(1)	0.001(1)
O4	0.0979(2)	1.2690(5)	0.5692(1)	0.0162(6)	0.023(1)	0.010(1)	0.015(1)	0.001(1)	-0.003(1)	0.001(1)
O5	0.000000	0.8583(7)	0.250000	0.0150(8)	0.006(2)	0.016(2)	0.023(2)	0.000	-0.004(1)	0.000
O6	0.1760(2)	0.7862(5)	0.2342(1)	0.0117(5)	0.010(1)	0.013(1)	0.013(1)	0.0004(11)	0.001(1)	0.000(1)
O7	0.1177(2)	0.8508(5)	0.3535(1)	0.0116(5)	0.016(1)	0.011(1)	0.008(1)	0.001(1)	0.001(1)	0.002(1)
O8	0.1152(2)	0.2604(5)	0.2721(1)	0.0151(6)	0.019(1)	0.009(1)	0.017(1)	0.002(1)	-0.003(1)	-0.002(1)
O9	0.1850(2)	0.2704(5)	0.4167(1)	0.0141(5)	0.015(1)	0.013(1)	0.014(1)	0.0005(11)	-0.001(1)	-0.005(1)

APPENDIX 8.10: SELECTED BOND DISTANCES IN IGDLUTALIK NORDITE (EXP. 420)

Exp. 420	Distance (Å)		Distance (Å)
***A*-site**		***Z*-site**	
A-O(1)	2.394(1)x2	*Z*-O(2)	1.937(1)x2
A-O(3)	2.530(1)x2	*Z*-O(6)	1.961(1)x2
A-O(4)	2.327(1)x2		
Ave	2.417	Ave	1.949
***B*-site**		***T(1)* -site**	
B-O(1)	2.688(1)	*T(1)* -O(1)	1.661(1)
B-O(2)	2.432(1)	*T(1)*-O(2)	1.601(1)
B-O(4)	2.443(1)	*T(1)*-O(3)	1.683(1)
B-O(5)	2.639(1)	*T(1)*-O(4)	1.577(1)
B-O(6)	2.492(1)		
B-O(7)	3.320(1)		
B-O(8)	2.407(1)		
B-O(8')	3.102(1)		
Ave	2.690	Ave	1.630
***X*-site**		***T(2)* -site**	
X-O(2)	2.577(1)x2	*T(2)* -O(5)	1.637(1)
X-O(3)	2.743(1)x2	*T(2)* -O(6)	1.614(1)
X-O(4)	2.591(1)x2	*T(2)* -O(7)	1.677(1)
X-O(9)	2.560(1)x2	*T(2)* -O(8)	1.581(1)
Ave	2.618	Ave	1.627
***Y*-site**		***T(3)*-site**	
Y-O(6)	2.509(1)x2	*T(3)* -O(1)	1.647(1)
Y-O(7)	2.697(1)x2	*T(3)* -O(3)	1.648(1)
Y-O(8)	2.481(1)x2	*T(3)* -O(7)	1.648(1)
Y-O(9)	2.457(1)x2	*T(3)* -O(9)	1.583(1)
Ave	2.536	Ave	1.631

APPENDIX 8.11: SELECTED BOND DISTANCES IN TASEQ NORDITE (EXP. 430 AND 478)

Exp. 430	Distance (Å)		Distance (Å)	Exp. 478	Distance (Å)		Distance (Å)
***A*-site**		***Z*-site**		***A*-site**		***Z*-site**	
A-O(1)	2.400(2)x2	*Z*-O(2)	1.961(3)x2	*A*-O(1)	2.396(3)x2	*Z*-O(2)	1.962(2)x2
A-O(3)	2.572(2)x2	*Z*-O(6)	1.982(3)x2	*A*-O(3)	2.568(3)x2	*Z*-O(6)	1.986(2)x2
A-O(4)	2.315(2)x2			*A*-O(4)	2.311(2)x2		
Ave	2.429	Ave	1.971	Ave	2.425	Ave	1.974
***B*-site**		***T(1)*-site**		***B*-site**		***T(1)*-site**	
B-O(1)	2.693(2)	*T(1)*-O(1)	1.662(3)	*B*-O(1)	2.687(3)	*T(1)*-O(1)	1.654(3)
B-O(2)	2.469(2)	*T(1)*-O(2)	1.599(3)	*B*-O(2)	2.450(3)	*T(1)*-O(2)	1.596(3)
B-O(4)	2.440(2)	*T(1)*-O(3)	1.693(3)	*B*-O(4)	2.432(3)	*T(1)*-O(3)	1.683(2)
B-O(5)	2.641(2)	*T(1)*-O(4)	1.575(3)	*B*-O(5)	2.656(3)	*T(1)*-O(4)	1.577(3)
B-O(6)	2.524(2)			*B*-O(6)	2.512(3)		
B-O7	3.319(4)			*B*-O(7)	3.332(4)		
B-O(8)	2.414(2)			*B*-O(8)	2.409(3)		
B-O(8')	3.118(4)			*B*-O(8')	3.122(4)		
Ave	2.702	Ave	1.632	Ave	2.700	Ave	1.627
***X*-site**		***T*(2)-site**		***X*-site**		***T(2)*-site**	
X-O(2)	2.631(3)x2	*T(2)*-O(5)	1.645(2)	*X*-O(2)	2.620(3)x2	*T(2)*-O(5)	1.641(2)
X-O(3)	2.805(3)x2	*T(2)*-O(6)	1.625(3)	*X*-O(3)	2.803(2)x2	*T(2)*-O(6)	1.613(3)
X-O(4)	2.668(3)x2	*T(2)*-O(7)	1.681(3)	*X*-O(4)	2.663(3)x2	*T(2)*-O(7)	1.677(2)
X-O(9)	2.633(3)x2	*T(2)*-O(8)	1.582(3)	*X*-O(9)	2.623(2)x2	*T(2)*-O(8)	1.584(2)
Ave	2.684	Ave	1.633	Ave	2.678	Ave	1.629
***Y*-site**		***T(3)*-site**		***Y*-site**		***T(3)*-site**	
Y-O(6)	2.490(3)x2	*T(3)*-O(1)	1.653(3)	*Y*-O(6)	2.488(1)x2	*T(3)*-O(1)	1.651(3)
Y-O(7)	2.739(3)x2	*T(3)*-O(3)	1.652(3)	*Y*-O(7)	2.735(1)x2	*T(3)*-O(3)	1.650(2)
Y-O(8)	2.502(3)x2	*T(3)*-O(7)	1.652(3)	*Y*-O(8)	2.496(1)x2	*T(3)*-O(7)	1.646(2)
Y-O(9)	2.461(3)x2	*T(3)*-O(9)	1.585(3)	*Y*-O(9)	2.464(1)x2	*T(3)*-O(9)	1.581(3)
Ave	2.548	Ave	1.635	Ave	2.546	Ave	1.632

APPENDIX 8.12: SXRD SETTINGS FOR EXPERIMENTS COMPLETED FOR THIS STUDY

Experiment	Exp 420 Mo	Exp 422 Mo
Sample	EHG 4	EHG 4
Crystal dimensions (mm)	Min: 0.025 Med: 0.038 Max:0.104	Min: 0.026 Med: 0.060 Max:0.120
Resolution (Å)	0.70, Hemisphere.	0.68, Hemisphere.
Detector distance (mm)	45.00	40.00
Exposure time (s)	26	10
Scan width (º)	0.30	0.30
Redundancy	7	7

Experiment	Exp 430 Mo	Exp 431 Mo	Exp 478 A Mo
Sample	EHG 13	EHG 13	EHG SXRD
Crystal dimensions (mm)	Min: 0.047 Med: 0.070 Max:0.107	Min: 0.013 Med: 0.024 Max:0.059	Min: 0.009 Med: 0.027 Max:0.038
Resolution (Å)	0.70, Hemisphere.	0.75, Hemisphere.	0.70, Hemisphere.
Detector distance (mm)	50.00	50.00	45.00
Exposure time (s)	25	46	105
Scan width (º)	0.30	0.30	0.30
Redundancy	3	4	3

Top row contains the Igdlutalik experiments, bottom row the Taseq experiments.

Appendix 8.13: Excell spreadsheet. Chemical and trace element data on nordites and the accessory minerals that was used for this thesis. ICPMS data used were MDL filtered.

Appendix. 8.14-18: CIF files containing the structural data on nordites analyzed for this thesis.